

THE ZURICH ENVIRONMENTAL STUDY (*ZENS*) OF GALAXIES IN GROUPS ALONG THE COSMIC WEB. I. WHICH ENVIRONMENT AFFECTS GALAXY EVOLUTION?[†]

C. MARCELLA CAROLLO^{1,*}, ANNA CIBINEL¹, SIMON J. LILLY¹, FRANCESCO MINIATI¹, PEDER NORBERG⁵, JOHN D. SILVERMAN², JACQUELINE VAN GORKOM³, EWAN CAMERON¹, ALEXIS FINOGUENOV⁴, ANTONIO PIPINO¹, CRAIG S. RUDICK¹, TING LU¹, YINGJIE PENG¹

SUBMITTED TO APJ

ABSTRACT

The *Zurich Environmental Study (ZENS)* is designed to compare the dependence of $z = 0$ galaxy structural and stellar populations diagnostics at constant stellar mass on four measures of the environment of galaxies, namely: (1) the mass of the host group halos; (2) the projected distance from the center of the halo; (3) the rank of galaxies as central or satellites within their host groups; and (4) the filamentary large-scale structure (LSS) density on which the groups reside. The complete *ZENS* sample contains 1630 $b_J < 19.45$ galaxies in $141 \sim 10^{12.5-14} M_\odot$ 2dFGRS 2PIGG galaxy groups within a narrow redshift bin centered at $z = 0.0585$. In this paper, we outline the motivation for the survey and describe novel approaches to quantify the environments of galaxies in different ways. We introduce a set of self-consistency checks to define the group centers and to rank galaxies as centrals or satellites, and describe an Nth-nearest-neighbor approach to determine the LSS density field using groups, weighted by their total masses, as tracers. We publish in this paper the *ZENS* catalogue of galaxy and group properties, which combines the environmental diagnostics presented here with parametric and non-parametric structural and Spectral Energy Distribution (SED) measurements described in subsequent papers. In a suite of follow-up articles we will use the *ZENS* catalogue to investigate which measures of environment most strongly affect the properties of different galaxy populations. In this paper, we highlight the following: (i) For $\sim 40\%$ of $< 10^{13.5} M_\odot$ groups there is no self-consistent identification of a central galaxy and as many as $\sim 10 - 20\%$ of groups may be dynamically young systems; (ii) The main properties of central galaxies in the relaxed and unrelaxed groups are similar indicating that central galaxies are not regulated by their environment but exclusively by their stellar mass; (iii) Satellites with $M > 10^{10} M_\odot$ in relaxed and unrelaxed groups, as well as central galaxies, have similar size, color and (specific) star formation rate distributions, but at lower galaxy masses, however, satellites are ~ 0.1 mag bluer in unrelaxed groups. This may possibly indicate that physical processes that occur in dynamically-relaxed group halos are important to quench star formation in low mass satellites.

Subject headings: surveys — galaxies: groups — galaxies: evolution — galaxies: structure — galaxies: photometry

1. INTRODUCTION

The study of the effect of the environment on the evolution of galaxies is beset by a number of difficulties that have made it hard to define a single coherent picture and to isolate the main physical processes. It has been clear for many years that both the mass and the environment of a galaxy affect its evolution and its appearance today. Since the pioneering work of e.g., Oemler (1974), Dressler (1980), Postman & Geller (1984), many studies have highlighted clear trends between different observa-

tional diagnostics of evolution such as color or morphology and both galactic mass and environment (e.g. Balogh et al. 1999; Goto et al. 2003; Blanton et al. 2005; Zehavi et al. 2002; Weinmann et al. 2006b, 2009; Croton et al. 2005; Park et al. 2007; Kovač et al. 2010; Peng et al. 2010, 2012; Wetzel et al. 2011; Calvi et al. 2012; Woo et al. 2012), but the detailed phenomenology, as well as physical understanding, remain unclear. This can be traced to several complicating factors or difficulties.

First, there are a number of galactic properties that are relevant to define its evolutionary state. Galaxy evolution may be traced by changes in the star-formation rates (SFRs) of galaxies (e.g. Lilly et al. 1996; Madau et al. 1996; Chary & Elbaz 2001; Rodighiero et al. 2010; Wetzel et al. 2011; Woo et al. 2012), leading to differences in the integrated stellar populations, and therefore in the colors of galaxies (e.g. Masters et al. 2010; Bundy et al. 2010; perhaps modified by the effects of dust; e.g. Labbé et al. 2005; Williams et al. 2009; Wolf et al. 2009). Galaxy evolution may also be manifested by changes in the morphologies of galaxies, both in terms of the overall structural morphology of bulge-to-disk ratios and the structural properties of each component (Brinchmann & Ellis 2000; Carollo et al. 2007; Kovač et al. 2010; Oesch

* E-mail: marcella@phys.ethz.ch

¹ Institute for Astronomy, ETH Zurich, CH-8093 Zurich, Switzerland

² Institute for the Physics and Mathematics of the Universe (IPMU), University of Tokyo, Kashiwa-shi, Chiba 277-8568, Japan

³ Department of Astronomy, Columbia University, New York, NY 10027, USA

⁴ Max-Planck-Institut für extraterrestrische Physik, D-84571 Garching, Germany

⁵ Institute for Computational Cosmology, Department of Physics, Durham University, South Road, Durham DH1 3LE, UK

[†] Based on observations collected at the European Southern Observatory, La Silla Chile. Program ID 177.A-0680

et al. 2010; Feldmann et al. 2011; Skibba et al. 2011; Calvi et al. 2012; Cooper et al. 2012; Raichoor et al. 2012, among others) and also in the appearance of features such as spiral arms or bars. Color and morphology clearly broadly correlate within the nearby galaxy population, but with a significant and poorly understood scatter (Strateva et al. 2001). Morphology and color may reflect different aspects of a single evolutionary sequence, or may reflect the outcome of quite different physical processes that may conceivably occur either synchronously or asynchronously. Many previous studies have focused on just one or other of this color-morphology duality. A comprehensive picture is likely to require the simultaneous treatment of all such physically relevant properties.

Second, with both mass and environment, it is not clear exactly *which* mass or environment is likely to be the most relevant for centrals, i.e., galaxies which appear to dominate their haloes, and satellites, i.e. galaxies which orbit another more massive galaxy within a single dark matter halo (e.g. De Lucia et al. 2011; Haas et al. 2012; Muldrew et al. 2012). Observationally, the existing stellar mass of a galaxy is the most easily accessible, but the physical driver of the evolution could be the mass of the dark matter halo of a galaxy, or, in the case of satellite galaxies, the mass of the dark matter halo in which the galaxy resides, leading to an environment-like measure of mass. Similarly, the environment that could influence the evolution of a galaxy could reflect either very local effects, e.g. the location of a galaxy in a dark matter halo, or the interaction with nearby neighbors through the mass of the dark matter halo (as above), or the broader environment beyond the halo, as defined by the cosmic web of filaments and voids. Clearly some of the definitions of environment are closely linked to the mass of a galaxy, especially for galaxies which dominate their dark matter haloes. Even for galaxy stellar mass we could imagine some direct crosstalk between it and environment if the stellar mass function of galaxies was itself dependent on environment (Bundy et al. 2006; Baldry et al. 2006; Bolzonella et al. 2010; Kovač et al. 2010), necessitating the careful isolation of these two variables.

A recent analysis in the Sloan Digital Sky Survey (SDSS; York et al. (2000)) of the three-way relationships between color, stellar mass and environment, the latter defined simply in terms of a 5th-nearest galaxy-neighbor density, reveals some interesting simplicities within the galaxy population (Peng et al. 2010). Not least, the effects of environment and stellar mass on the fraction of galaxies that are observed to be red (the red fraction) are straightforwardly separable in the sense that the chance that a given galaxy is red is the product of two functions, one of mass independent of environment, and the other of environment, independent of mass. This led Peng et al. to identify two separate physical processes, termed mass-quenching and environment-quenching. A conclusion of this analysis was that for galaxy stellar masses below $\sim 10^{10} M_{\odot}$ the effects of the environment dominate, while above $\sim 10^{11} M_{\odot}$ the galaxy population is dominated by the effects of merging, which again is environmentally determined. The differential effects of galactic stellar mass and environment can be most clearly seen in the $\sim 10^{10-11} M_{\odot}$ galaxy population. Peng et al. (2012) extended their original formalism to the central-satellite dichotomy of galaxies, using a large group catalogue (Yang

et al. 2005, 2007). Although the characteristics of mass- and environment-quenching were identified, their physical origin remains uncertain.

Also unclear remains whether morphological transformations anticipate or lag behind the spectrophotometric transformations which shift blue, star forming galaxies onto the red sequence of bulge-dominated systems (e.g. Arnouts et al. 2007; Faber et al. 2007; Pozzetti et al. 2010; Feldmann et al. 2010, 2011). Many processes can lead to the disruption of disks and quenching of star formation, e.g., galaxy mergers or tidal interactions (e.g. Park et al. 2007, and references therein), ram pressure stripping of cold gas (Gunn & Gott 1972; Feldmann et al. 2011, but see also Rasmussen et al. 2008) or strangulation of the galactic system by removal of hot and warm gas, necessary to fuel star formation (Larson 1980; Balogh & Morris 2000; Font et al. 2008; Rasmussen et al. 2012). In a hierarchical picture, a gaseous disk can be re-accreted around pre-made spheroids at relatively late epochs. This evolutionary path is observed to happen in high-resolution cosmological hydrodynamical simulations (Springel & Hernquist 2005; Feldmann et al. 2010).

The intermediate-mass scales of galaxy groups, which are the most common environments of $\sim L^*$ galaxies in the local Universe (Eke et al. 2004a), have a reputation for being the place where environmental drivers of galaxy evolution should be at their peak efficiency. With an in-spiral timescale of dynamical friction that varies in proportion to σ^3/ρ , with σ and ρ the dark matter halo velocity dispersion and density, respectively, galaxy tidal interactions and mergers should take place on a cosmological short timescale in group potentials with relatively low velocity dispersion, unlike the most massive galaxy clusters where the velocity dispersion is much higher. Also, with ram pressure efficiency varying as $\rho_{\text{igm}} v^2$, with ρ_{igm} and v respectively the density of the intergalactic/intragroup medium (IGM) and relative velocity of the galaxy toward the IGM, galaxies may well begin to lose their gas already at intermediate environmental densities typical of galaxy groups (Rasmussen et al. 2006, 2008). Resulting internal dynamical instabilities may also contribute to galaxian evolution, e.g., by fuelling star formation and supermassive black holes in the centers of galaxies (see e.g. Di Matteo et al. 2007; Hopkins et al. 2008 for a theoretical perspective, and Genzel et al. 1998; Kewley et al. 2006; Smith et al. 2007; Silverman et al. 2011 for some observational evidences) and establishing feedback loops that affect whole galaxies (Croton et al. 2006).

These considerations motivate the present study, termed *ZENS* (the Zurich Environmental Study), where we use a statistically complete sample of 1630 galaxies brighter than $b_J = 19.45$, known to be members of 141 nearby groups spanning the mass range between $\sim 10^{12.5} M_{\odot}$ and $\sim 10^{14} M_{\odot}$. The *ZENS* sample is complete at stellar masses above $10^{10} M_{\odot}$ for passively evolving galaxies with old stellar populations, and above $10^{9.2} M_{\odot}$ for star forming galaxies. In *ZENS* we aim at simultaneously (1) characterizing the present evolutionary state of galaxies in as broad a way as possible, using both diagnostics based on stellar populations and structural morphology, and (2) studying as broad a range of environments as possible and characterizing the environments in a number of ways that sample different physi-

cal scales, and include a careful distinction between central and satellite galaxies. Specifically, in our study we directly compare, at fixed galaxy stellar mass, the dependence of key galactic populations diagnostics on the large-scale environmental (over)density (δ_{LSS}), on the mass of the host group halo (M_{GROUP}), on the location of galaxies within their group halos (the latter expressed in terms of projected distance from the halo center, r/r_{200} , with r_{200} the characteristic size of the group) maintaining a central-satellite distinction when possible and relevant.

The *ZENS* sample is extracted from the 2-degree Field Galaxy Redshift Survey (2dFGRS; Colless et al. 2001), which contains nearly 225,000 redshifts for galaxies with $14 < b_J < 19.45$ and a median redshift $z \sim 0.11$, with a redshift completeness of $85 \pm 5\%$. In combination with a dynamic range of five magnitudes at each redshift, the 2dFGRS is the ideal basis for constructing a homogeneous catalogue of nearby galaxies in a wide range of environments. We have followed up the *ZENS* sample with B and I deep WFI imaging at the ESO/2.2m to derive, for all galaxies in the sample, detailed properties of substructure such as bulges, disks, bars and tidal tails. The wealth of data on the *ZENS* groups enables us to define very carefully the nature of the group, including its likely dynamical state (relaxed or unrelaxed), to do a careful group-by-group identification of the most likely dominant member, to derive accurate photometric and structural measurements for galactic subcomponents (disks, bulges and bars) all analyses unaffected by distance, size, magnitude, mass, type and other biases, which often complicate the interpretation of comparisons of independent studies published in the literature.

In this first paper in the *ZENS* series:

(i) We describe the *ZENS* design and database (Section 2);

(ii) We present our definitions and calculations of the four environmental parameters δ_{LSS} , M_{GROUP} , r/r_{200} plus the central-satellite distinction (Section 3). Specifically, in this section we detail the approaches that we adopt to identify central and satellite galaxies and thus the centers of the groups, and to measure a large-scale structure (over)density proxy which, at relatively low group masses, provides a measurement which is independent of the richness and mass of the host group halos. We furthermore quantify how random and systematic errors in the computation of each environmental parameter affect the studied trends of galaxy properties with such environment;

(iii) We publish the *ZENS* catalogue (Section 4)⁸ which lists, for every galaxy in the sample, the environmental parameters derived in this paper, as well as structural (from Cibinel et al. 2012a, Paper II) and spectrophotometric measurements (from Cibinel et al. 2012b, Paper III). The structural measurements are corrected for magnitude-, size-, concentration-, ellipticity-, and PSF-dependent biases;

(iv) We discuss our classification of groups in dynamically ‘relaxed’ and ‘unrelaxed’ systems (Section 5), and

briefly investigate whether their galaxy members, both central and satellites, differ in fundamental structural (size), star formation (specific star formation rate, sSFR) and surface density of star formation rate (Σ_{SFR}) and optical ($B - I$) properties. Finally,

(v) we summarize our main points in Section 6.

In Appendices A, B, C, D and E we present details on, respectively, (a) the impact on our study of the 2dFGRS magnitude limits in the *ZENS* fields, (b) the impact of ‘missed’ galaxies, either by the 2dFGRS, or by the new B and I ESO 2.2m/WFI imaging for the *ZENS* sample, (c) data reduction and photometric calibration of these WFI data, (d) 2PIGG incompleteness in group-membership, and (e) additional tests on the robustness of our fiducial LSS density estimates and the comparison with traditional N-neighbor-galaxies estimators, and, finally, (f) the *Readme* file of the published catalog.

For the relevant cosmological parameters we assume the following values: $\Omega_m = 0.3$, $\Omega_\Lambda = 0.7$ and $h = 0.7$. Unless otherwise stated, group masses and luminosities are given in units of M_\odot and L_\odot , i.e., we incorporate the value $h = 0.7$ in the presentation of our results. All magnitudes are in the AB system. These choices are also adopted in Cibinel et al. 2012a,b (which present respectively the structural and photometric measurements included in the catalogue associated with this paper), as well as in Lu et al. (2012, Paper IV, where we analyze the impact of local and LSS environments on the star formation and morphological properties of satellites); in Rudick et al. (2012, Paper V, where we study the effects of environment on different scales separately for the bulge and disk components of galaxies); in Pipino et al. (2012, Paper VI, where we investigate the structural and star formation properties of central-satellite and satellite-satellite mergers compared with non-merging systems of similar stellar mass in similar environmental conditions); in Rudick et al. (2012b, Paper VII, where we study environmental trends in the radial stellar profiles of the outer disks); in Cibinel et al. (2012c, Paper VIII, where we discuss the relevance of different environment in triggering secular evolution through bar instabilities in galactic disks); and in Carollo et al. (2012b, Paper IX, where we show the environmental dependences of sizes, surface mass densities, and star formation properties separately for satellites and centrals, and for their disk and bulge components).

2. THE ZURICH ENVIRONMENTAL STUDY (ZENS)

2.1. Design and Sample Specifications

The entire *ZENS* sample of 141 galaxy groups was selected from the 2dFGRS Percolation-Inferred Galaxy Group catalogue (2PIGG, Eke et al. 2004a), which is based on a friends-of-friends (Huchra & Geller 1982) percolation algorithm thoroughly tested on realistic mock galaxy catalogues generated from cosmological N-body simulations. We refer to Eke et al. (2004a) for the details of the group finding algorithm and the procedures adopted for the identification of the groups. The 2PIGG catalogue covers the 1500 square degrees of the 2dFGRS and provides one of the largest homogeneous samples of galaxy groups currently available, with around 7000 groups with ≥ 4 catalogued members and spanning a wide range in luminosity, from $\sim 10^{10} L_\odot$ up to

⁸ Currently the catalogue contains all measurements for the ‘first-epoch’ 769 galaxies in 79 groups that we have analyzed to date, and some of the measurements for the galaxies members of the remaining 62 groups. The *ZENS* catalogue will be soon augmented with the data for the galaxies in these 62 groups.

$\sim 10^{12} L_{\odot}$, and dynamical mass from a few $10^{12} M_{\odot}$ up to clusters of mass $10^{15} M_{\odot}$ (Eke et al. 2004b). The catalogue is selected from a volume of $\sim 250,000 (\text{Mpc h}^{-1})^3$, and it is so large that one not only has information on the groups themselves from the 2dFGRS data (e.g., velocity dispersions, spatial positions of members, mass, density, compactness etc.), but also on their proximity to large clusters, filaments, and voids of the large-scale structure web. The 2PIGG catalogue is representative of the Universe as a whole, and contains a large number of groups that are close enough to allow detailed studies of the galaxy members. It is thus ideal for undertaking the study of the nearby galaxy properties as a function of the environment, and in particular, for directly comparing how galaxy properties and key galaxy population diagnostics depend respectively on group mass, on the location of galaxies within their host groups, and on the location of the host groups relative to the large scale filamentary structure (i.e. on the local density of the cosmic web). The 2dFGRS fields are located well above the Milky Way disk, minimizing the effect of extinction from Galactic dust (typically 0.1 mag in the B-band).

The *ZENS* groups were randomly extracted from the complete sample of 185 2PIGG groups (excluding few groups falling in very incomplete fields of the survey) to be in the narrow redshift bin $0.05 < z < 0.0585$ and to have at least 5 confirmed galaxy members in the 2dFGRS. The *ZENS* sample provides a statistically complete and representative census of the nearby galaxy population inhabiting these environments. The very narrow redshift range of the *ZENS* sample was chosen to optimize several issues: (i) The 2dFGRS magnitude limits translate at this redshift to luminosities between $[M^* - 2]$ to $[M^* + 3]$ (Norberg et al. 2002), meaning that the existing redshift catalogue already samples all of the luminosity function of massive galaxies and straddles well the break or bimodality in galaxy properties around M^* (Kauffmann et al. 2003); (ii) This redshift range is located just below the peak in $N(z)$ in 2PIGG, and thus ideally samples the targeted range of group mass $\sim 10^{12.5-14} M_{\odot}$. (iii) Likewise, the groups fully cover the entire range of large-scale structure environments, with some groups residing in very dense regions and others residing in much lower density environments, allowing us to study the effects of the large-scale structure on group and galaxy evolution. (iv) At this redshift the group selection is robust and less affected by the peculiar velocities of the galaxies than is the case at lower redshifts. (v) Finally, deep, ground-based imaging with typical seeing $\sim 1''$ is well suited for the determination of morphologies, substructure units such as bars, bulges and disks, and presence and properties of faint structures. It is also directly relatable to Hubble Space Telescope $\ll 1''$ -resolution images of the $z > 0.5$ Universe (with a relative angular diameter distance of a factor 8), and therefore provides an ideal benchmark for a direct comparison with HST images of galaxies in high- z groups (e.g. Knobel et al. 2009; Kovač et al. 2010). A summary of the properties of the *ZENS* groups is given in Table 1 and Figure 1.

2.2. Impact of the 2dFGRS selection function on *ZENS*

2.2.1. Impact of the 2dFGRS redshift incompleteness and of field-to-field scatter in the 2dFGRS magnitude limits

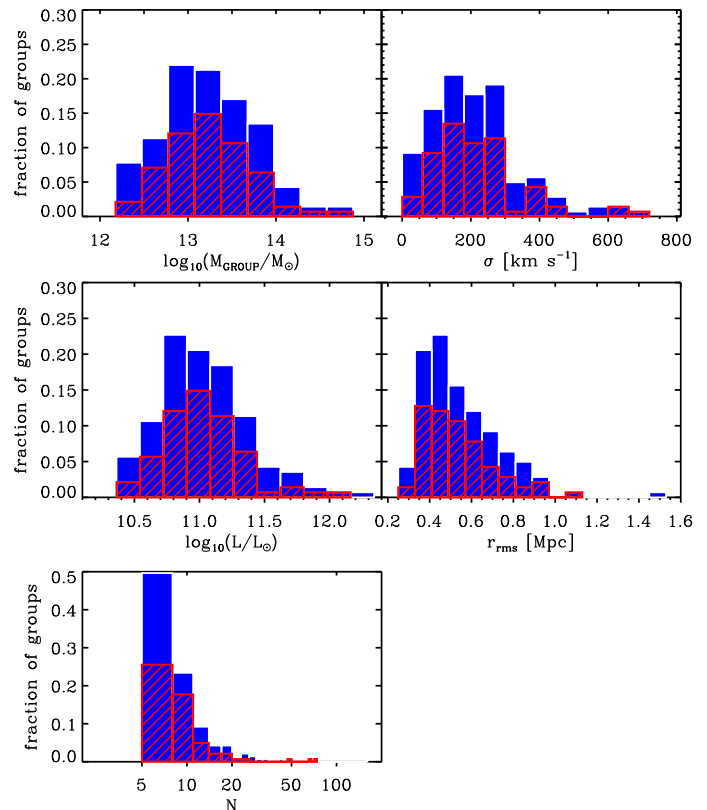


Figure 1. Distributions of main properties for the 141 *ZENS* groups (filled histograms). Dashed curves show the distributions for the 79 ‘first-epoch’ groups for which the WFI *ZENS* images have been reduced and analyzed to date. These are fully representative of the entire *ZENS* sample. From left to right and top to bottom we plot the distributions of *ZENS* group masses (derived as described in Section 3.1), velocity dispersions and luminosities, and also the distributions of projected r.m.s. galaxy separations within the groups and of number of group member galaxies.

The depth and completeness of the 2dFGRS are not uniform over the sky for a number of reasons (Colless et al. 2001): the 2dFGRS parent catalogue (APM survey, Maddox et al. 1990) was recalibrated and the extinction corrections were revised after the survey limit of $b_j = 19.45$ was originally set; moreover the number of successful or repeated observations varies with position on the sky. We quantify in Appendix A the impact of the original 2dFGRS magnitude limits in our targeted fields. These limits translate into a minimum mass at which *ZENS* is complete; this corresponds to $10^{10} M_{\odot}$ for passively evolving galaxies with old stellar populations, and to $10^{9.2} M_{\odot}$ for galaxies with star forming SEDs. A detailed description of the derivation of galaxy stellar masses and of the mass completeness limits of *ZENS* is given in Paper III.

We also note that, unless explicitly stated otherwise, all statistical analysis that we present in this and in the following *ZENS* papers refer to quantities corrected for spectroscopic incompleteness of the 2dFGRS.

2.2.2. Sample completeness tested on the SDSS

We investigated the resulting incompleteness in the *ZENS* group sample, originating from the catalogue limitations described above. To this end we searched the

SDSS DR7 spectroscopic catalogue (Abazajian et al. 2009) for galaxies within up to $\pm 30\%$ of the redshift distribution of a given *ZENS* group, not present however in the parent 2dFGRS catalogue. The details of this comparison are given in Appendix B.1. There are many aspects of our analyses that could in principle be affected by any such incompleteness, i.e., the estimates for the group masses, the determination of the group centers (and thus radial trends with group-centric distance), and the related separation into central and satellite galaxies. The results of our tests, presented in the Appendix, indicate however that our main results are not severely affected by significant biases due to incompleteness in the parent 2dFGRS catalogue.

2.3. New *B* and *I* data with the ESO/2.2m Wide Field Imaging Camera

ZENS capitalizes on the wealth of data and measurements already available from the original 2dFGRS analyses and other surveys (e.g. GALEX, 2MASS and SDSS). In order to achieve accurate measurements for the structural (Cibinel et al. 2012a) and stellar population properties (Cibinel et al. 2012b) of galactic subcomponents, we furthermore acquired new deep *B* (*BB#B/123_ESO878*) and *I* (*BB#I/203_ESO879*) images with the WFI at the MPG/ESO 2.2m telescope. The data were taken in several observing runs over the period 2005-2009. Following a pilot-project time allocation in 2005, most of the observations were carried out as service-mode observations in the context of the ESO Large Program 177.A-0680. For a combination of weather and technical issues, the service-mode observations were distributed over several runs during the period 2006-2008. The last two observing runs were carried out in visitor-mode in 2009, achieving a final sample of 141 groups randomly extracted from the original complete sample of 185 targets.

To date we have completed the data reduction for 79 target groups out of the 141 in the total *ZENS* sample. These first-epoch 79 groups host a total of 837 catalogued galaxy members brighter than the magnitude limit of the 2dFGRS survey, 769 of which within our WFI pointings (see Appendix B). For these galaxies we have derived accurate structural measurements (sizes, bulge-disk decompositions, bar sizes and strengths, non-parametric diagnostics such as concentration, Gini, asymmetry etc. as well as a quantitative, robust morphological classification which corrects for seeing, inclination and dust effects; see Paper II) and photometric measurements (e.g., colors, specific and total SFRs, stellar masses, for the whole galaxies, as well as for bulges and disks, including corrections for inclination, dust and fiber-area effects; see Paper III). We will soon augment the published *ZENS* catalogue with similar measurements for the galaxies members of the remaining 62 *ZENS* groups. In Appendix C we provide details on the observing runs, the raw data properties, the data reduction procedures and the photometric calibration for the 79 *ZENS* groups on which we base our current analysis (as well as the analyses of the first-epoch *ZENS* papers II-VIII that are mentioned in the introduction).

3. FOUR ENVIRONMENTS IN COMPARISON WITH ONE ANOTHER

With the goal of identifying *which* environment affects galactic evolution at different galaxy mass scales, we quantify four environmental diagnostics that will enable us to search for differential trends with these environments in different galactic populations. The four environments are, respectively: (1) the mass of the host group halo, (2) the distance of a galaxy from the center of its group halo, (3) the average LSS density at the position of the host group, determined by the underlying filamentary structure of the cosmic web, and (4) the central versus satellite dichotomy, considered here to be also an environmental condition that galaxies experience in their life within a bound common halo.

3.1. Environment number one: The mass of the Host Group Halo

The 2PIGG catalogue from which we have extracted the *ZENS* sample lists the velocity dispersions σ returned by the friends-of-friends algorithm which was used to construct the catalogue, and the radii of the groups (reported in Table 1), defined as the weighted r.m.s. of the projected separations between the nominal 2PIGG center and the remaining group members. Eke et al. (2004a) and Eke et al. (2004b) discuss in detail the tests performed to ascertain the robustness of these estimates, which were optimized to best reproduce the global properties of the 2dFGRS mock catalogues (Eke et al. 2004a).

Dynamical halo masses computed as $M_{dyn} = 5 \frac{\sigma^2 r_{rms}}{G}$ are however affected by large uncertainties, especially for groups with a relatively low number of members, due to redshift errors which in the 2dFGRS are typically $\sim 85 \text{ km s}^{-1}$. In contrast, group total (stellar) luminosities can be measured with a higher accuracy even in poor groups. Using mock catalogues, Eke et al. (2004b) calibrated the observed group total luminosities into total group masses, providing robust estimates for the halo mass-to-light ratios (Υ_{b_j}) needed to convert the luminosities into total halo masses M_{GROUP} . We adopt such luminosity-based halo masses as our fiducial estimates for the matter content of the *ZENS* groups.

Specifically, following the prescription of Eke et al. (2004b), we computed the observed group luminosity as the weighted sum of the luminosities of the individual galaxy members L_{i,b_j} , i.e., $L_{GROUP,OBS} = \sum_i^N w_i L_{i,b_j}$, with N the number of member galaxies in the group and w_i the weights used in the construction of the 2PIGG catalogue that account for the 2dFGRS redshift incompleteness. Apparent (Vega) b_j magnitudes were converted to absolute magnitudes by applying the mean $k + e$ correction as given in equation 2.4 of Eke et al. (2004b), $k + e = \frac{z+6z^2}{1+8.9z^{5/2}}$. This observed luminosity was corrected into total luminosity (L_{GROUP}) by integrating a Schechter function to zero luminosity, namely by dividing $L_{GROUP,OBS}$ by the incomplete Gamma function $\Gamma(\alpha+2, L_{min}/L_*)/\Gamma(\alpha+2)$. In the above formula (α, L_*) are the slope and cut-off luminosity of the Schechter function, and L_{min} is the luminosity corresponding to the magnitude limit of the 2dFGRS survey at the considered position in the sky. The correction was done by keeping the slope and L_* fixed for all groups and assuming the values $\alpha = -1.18$ and $M_* = -19.725$, obtained by Eke et al. (2004b) from a global Schechter function for the 2dFGRS galaxies. Our fiducial total

halo masses M_{GROUP} were finally obtained using eq. 4.4 in Eke et al. (2004b) for the mass-to-light ratio: $\log Y_{b_j} = 2.28 + 0.4 \tanh[1.9(\log L_{GROUP} - 10.6)]$.

3.1.1. Sources and Effect of Errors on our Fiducial Group Masses

The conversion of group luminosity into dark matter halo mass outlined above is affected by several factors, in addition to errors in the relevant galactic measurements (such as redshifts and luminosities). The most important additional contributions to the uncertainty in the conversion come from (i) errors in group membership, either by “missing” group members above the galaxy luminosity completeness cut in the survey, or by including interloper galaxies which are not physically associated with the given group; (ii) peculiarities in the groups’ luminosity functions; and (iii) the intrinsic uncertainty/scatter in group mass-to-light ratio relation, partly due to uncertainties in the physics underlying this conversion. These sources of error on the group masses are not easy to eliminate, and thus we try to assess their impact on our analyses.

3.1.1.1. Erroneous group membership assignments: Interlopers and ‘missing’ galaxies— How sensitive are our halo mass estimates to the spurious inclusion or exclusion of member galaxies from a given group? The most obvious source of such kind of error is a non-optimal performance of the friends-of-friends algorithm used to generate the 2PIGG catalogue. To address this issue, we searched the parent 2dFGRS catalogue for galaxies which in principle could have been physically associated with a 2PIGG group, but were not included in that group by the 2PIGG algorithm. In particular, using similar criteria to those used to search for missed galaxies in the SDSS (Section 2.2.2 and Appendix B.1), we searched the 2dFGRS catalogue for galaxies within $\pm 30\%$ of the redshift window of our *ZENS* groups, lying within a circular projected areas of radius equal to 1.5 times the r.m.s. radius of the group⁹, and which were not associated with the given group by the 2PIGG algorithm. For those groups for which our centers differed from the original 2PIGG centers, the choice of using our own choice/definition for the centers also enables us to simultaneously test the impact of this definition on the resulting group membership.

Following these criteria we found a total of 26 ‘extra’ 2dFGRS candidate galaxy members for 11 of the 79 first-epoch *ZENS* groups. We present in Appendix B.3 details on the spatial and velocity distributions of these new candidates in relation to the galaxies which are identified as group members in the 2PIGG catalogue, as well as the distributions of fiducial halo masses for the groups which may miss these extra candidates.

These potential extra members are found for relatively massive *ZENS* groups with $M_{GROUP} \gtrsim 10^{13} M_{\odot}$. Including these potential galaxy members in the computation of the group masses has therefore a small effect at these mass scales, typically within 0.1 dex. Only for two groups the difference between the fiducial group mass and the recalculated mass is larger than this value (of order 0.2–0.3 dex). We therefore conclude that missing 2dFGRS

galaxies in the 2PIGG associations is not a dominant source of error in the computation of the fiducial *ZENS* group masses.

In contrast, at the typical redshift and mass scale of the *ZENS* groups, the level of contamination from interlopers is estimated to be between 20–40%, depending on the mass of the group (see Figure 2 of Eke et al. 2004a). Interlopers are thus a substantial source of error in the estimate of the group masses. As we have not a priori knowledge on which galaxies could be false members, we approach this problem in a statistical manner. From each group we remove, in 3000 bootstrap realizations, a random 20–40% of the member galaxies (both including, and, in a separate set of tests, excluding, the possible extra candidates discussed above), and each time recalculate the mass of the groups from the luminosity function, as outlined in Section 3.1. Note that for groups with low numbers of galaxies this is equivalent to spanning all the possible combination of rejected galaxies. For groups with $N_{gal} > 15$ this is not the case anymore; however, given the large number of bootstrap sample we employ in the analysis, the derived distributions will be representative of the complete mass range. This bootstrap approach provides us, for each group, with a distribution of masses for each bootstrap configuration, and a median of this distribution. The results are shown in Figure 2. The symbols in the plot are the medians, in different bins of group mass, of the distributions of differences, normalized to the fiducial mass of a group (as determined in Section 3.1), between the fiducial mass of that group (‘original’) and that in a given bootstrap realization (‘resampled’). The shaded area shows the 1σ scatter around the plotted medians, obtained from generating 3000 random realizations for the mass of a group according to the bootstrap distribution of masses for that group.

Given that for the vast majority of groups there are no extra candidates, the new masses are obviously smaller than the original ones. The presence of spurious members causes an overestimation of the group mass which is on average of order 15% and in most of the cases less than 40%. As expected, the variation is a function of the group mass, and becomes less important in high mass group with a high number of galaxies.

3.1.1.2. Comparison with independent group catalogues for the 2dFGRS— Another question we ask is of how sensitive are the halo mass estimates, as inferred in Section 3.1, to the details of the algorithm adopted for identification of the groups. To learn about this issue in a ‘post-processing’ approach, we cross-matched the *ZENS* sample, extracted from the 2PIGG catalogue, with the independent 2dFGRS group catalogue of Yang et al. (2005). In this catalogue the basic identification of potential groups also follows a friends-of-friends algorithm, but the final group membership – hence properties – are iteratively refined, starting from the initial friends-of-friends estimates, by assuming that groups at any redshift are described by a NFW density profile (Navarro et al. 1997) and that the phase space distribution of galaxies is similar to that of dark matter particles. Furthermore, the Yang et al. 2dFGRS catalogue imposes a minimum redshift completeness of 80%. The parent 2dFGRS catalogue adopted by Yang et al. hence excludes galaxies

⁹ The circular areas were centered on the central galaxy for the 79 first-epoch groups, or on the 2PIGG original center for the remainder groups.

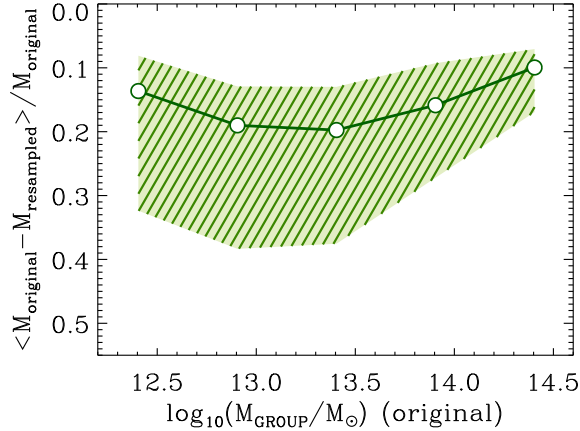


Figure 2. Results of the test performed to assess the effect of interloper galaxies on the group halo mass estimates. The global effect is an overestimate of typically $\sim 20\%$, up to $\sim 40\%$ at low masses. The test was performed by removing, for each group, between 20 - 40% of the member galaxies (also including potential extra galaxies, as discussed in Section 3.1.1.1), and recomputing the halo mass for each resulting group configuration. The symbols represent the medians of the distributions of differences, normalized to the fiducial mass of a group (as determined in Section 3.1), between the fiducial mass of that group (‘original’) and the mass in a given bootstrap realization (‘resampled’); the different points are obtained in the corresponding bins of group mass of width 0.5 dex. The shaded area shows the typical scatter around the median value (solid line).

(the sample used is 25% smaller than the one in 2PIGG), which means that only 123 of our *ZENS* sample groups can be compared with the group catalogue of these authors. Note that not all galaxies in a *ZENS* group are necessarily associated to a group in the Yang et al. catalogue. In 21 of these 123 groups only one galaxy is found in the Yang et al. catalogue.

In practice, for any given group in the *ZENS* sample, we searched in the Yang et al. catalogue to which of its groups the *ZENS* member galaxies were assigned, and we associated the most massive of the Yang et al. groups so identified to the given *ZENS* group.

We show in Figure 3 the comparison between the corresponding group masses in the two catalogues. As some of the groups are fragmented in the Yang et al. catalogue into single galaxies (see Figure 4), we consider for the comparison only the *ZENS* groups which are associated with a group which contains at least 40% of its members.

The masses of the Yang et al. groups matching the *ZENS* groups are typically smaller than the fiducial *ZENS* masses as estimated in Section 3.1. An inspection of the two cross-matched catalogues shows that, in most cases, the *ZENS* groups are fragmented into smaller subgroups in the Yang et al. catalogue. This is shown in Figure 4, which plots, for each of the 73 of our 79 first-epoch groups that appear in both catalogues, the position of the nominal 2PIGG member galaxies with respect to the ‘central galaxy’ (see Section 3.2.1), and with colors the members of the Yang et al. groups. Factor that contribute to these systematic differences include the attempt to take into account, in the Yang et al. catalogue, of the effects of interlopers discussed above, and also, however, missing galaxies in the input 2dFGRS catalogue

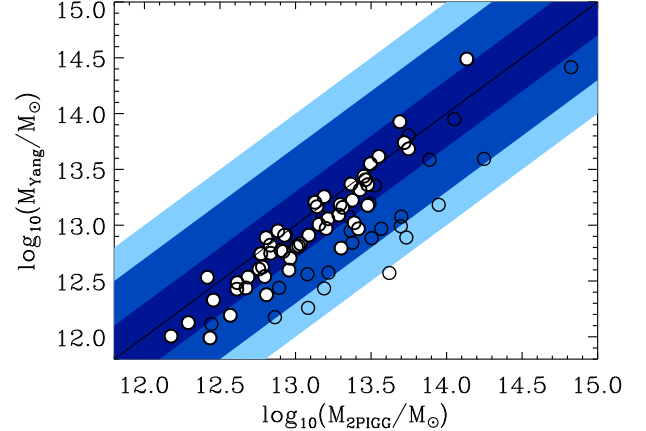


Figure 3. Comparison between the *ZENS* group masses as originally defined by the 2PIGG catalogue and the mass of the cross-matched groups in the Yang et al. (2005) catalogue. The latter are defined as the most massive groups in this catalogue which is associated to each *ZENS* group. The shaded areas show a factor of two (dark-color strip), five (intermediate) and ten (light-color strip) difference in mass. Groups which are fragmented into more than one group in the Yang et al. catalogue are shown with empty points. Note that not all galaxies in *ZENS* group are necessarily associated to groups in the Yang et al. catalogue. Groups which are associated to a single galaxy in the Yang et al. group catalogue or are fragmented into sub groups containing less than 40% of the 2PIGG members are not shown.

that they adopt, as discussed before.

The problem of correctly identifying interlopers is of course a general one; therefore, the fragmentation of the 2PIGG groups in the Yang et al. compilation not necessarily leads to a cleaner definition of the bound structures. This is illustrated in Figure 5, where we plot the velocities of the galaxies in the Yang et al. catalogue with respect to the group mean redshift and the velocity of the nominal 2PIGG group members. Clearly the original 2PIGG groups are split arbitrarily in distinct sub-components by the other algorithm: galaxies that are assigned to allegedly distinct groups in the Yang et al. catalogue have often positions and velocities fully within the extremes in these quantities shown by the galaxies that are assigned to a single group by the 2PIGG algorithm.

Important is however that, despite the differences between the two cross-matched catalogues, for 75% of the groups the difference in their mass estimates is smaller than a factor of two. This uncertainty is comparable with the error in total group mass that we estimated in Section 3.1.1.3, and does not affect our study of galaxy properties as a function of (also) group mass over about two order of magnitudes in the latter.

3.1.1.3. How well do group halo masses inferred from integration of luminosity functions approximate the true halo masses? — Existing physical trends in galaxy properties with group mass may be smeared across different group mass bins and even washed out by the relatively large random and systematic errors in the estimates of the group masses. To quantify the uncertainties introduced by the specific algorithm of Section 3.1, that we adopted for computing the group masses, we used the Millennium

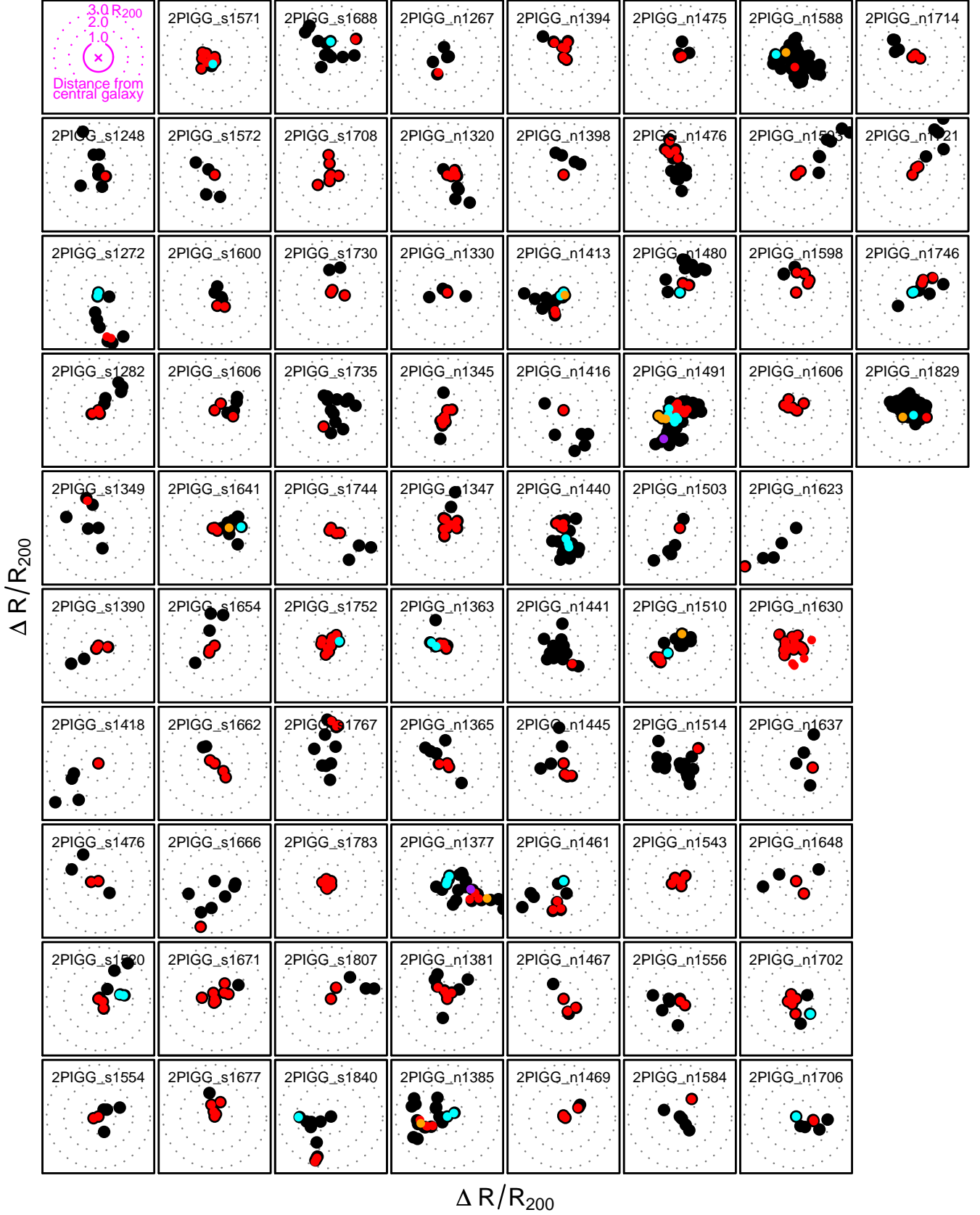


Figure 4. For each of the 73 of the 79 first-epoch *ZENS* groups which have at least one matching group in the Yang et al. group catalogue, we show the spatial distribution, with respect to the identified central galaxy, of the nominal 2PIGG members (black dots) and, superimposed in a different color, of galaxies that are identified as members of different groups in the Yang et al. catalogue. Symbols that are left in black do not belong to any group in the Yang et al. compilation. Galaxies of the same color are linked into the same group in the Yang et al. catalogue.

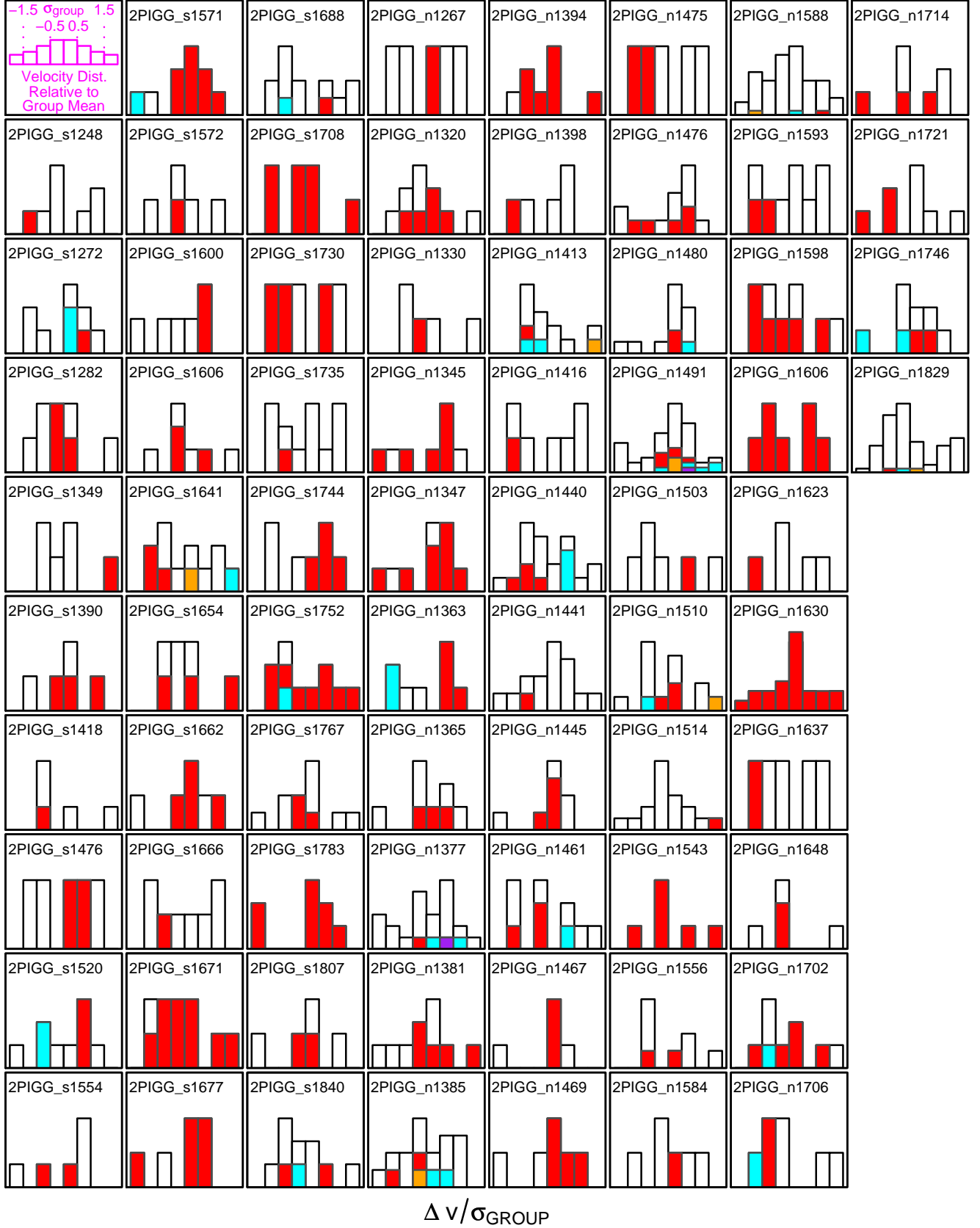


Figure 5. For each of the 73 of the 79 first-epoch *ZENS* groups which have at least one matching group in the Yang et al. group catalogue, we show the distribution of velocities relative to the group redshift for the 2PIGG member galaxies (black histograms). Superimposed in a different color, using the identical color scheme as in Figure 4, we show the corresponding histograms for galaxies that are identified as members of different groups in the Yang et al. catalogue. As in Figure 4, a given color is used for galaxies that are linked into the same group in the Yang et al. catalogue.

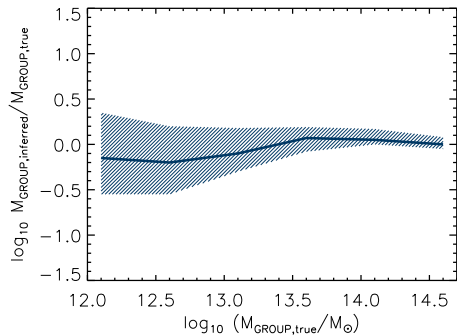


Figure 6. Relation between inferred halo mass, estimated from the total group luminosity as discussed in Section 3.1, and input (‘true’) dark matter halo mass from the DeLucia & Blaizot (2007) semi-analytic model. The shaded area show the scatter around the median relation (solid line) obtained in a thousand random realizations.

simulation (Lemson & Virgo Consortium 2006) with the semi-analytic model of De Lucia & Blaizot (2007). The model is not specifically designed to match the 2dFGRS properties and selection function; nonetheless, it enables us to gain useful insight on the limitations of our analysis.

Details of the model are given in the original reference. The dark matter component is taken from the Millennium simulation (Springel et al. 2005b); details of the baryon physics are added in the fashion that is customary in semi-analytic modeling of galaxy evolution. Recipes for gas cooling, star-formation, AGN and supernovae feedback are included. The typical baryonic resolution of the adopted models corresponds to a galaxy mass of $\sim 3 \times 10^9 M_\odot$, smaller than the limiting mass of completeness for *ZENS* galaxies.

For each halo in the volume of mass above $10^{12.2} M_\odot$ we computed the total 2dFGRS b_j luminosity of the host galaxies above the survey limit of $b_j = 19.45$. A thousand random realizations were obtained, sampling each halo with 80% of the galaxies, to simulate the spectroscopic completeness of our sample. The ‘inferred’ halo mass was obtained adopting the same approach that we used for the *ZENS* groups (see Section 3.1).

The comparison between ‘true’ dark matter halo masses, and halo masses inferred from the extrapolation of the group luminosity function, is shown in Figure 6. The shaded area in Figure 6 shows the scatter around the median relation in the thousand realizations. The average trend tracks the 1:1 relation above $M_{\text{GROUP}} \sim 10^{13.5} M_\odot$ with a modest scatter $< 10\%$. At lower group masses, the data tend to underestimate the true values on average at the $\sim 20\%$ level, with a scatter up to $40\% - 50\%$. Not surprisingly, the scatter in the relation decreases with increasing mass of the group.

These uncertainties are comparable with the errors in the inferred group total luminosities as a function of number of member galaxies shown in Figure 3 of Eke et al. (2004b).

3.1.1.4. Summary: Impact of the uncertainties on group masses on trends of galaxy properties with halo mass — The

tests above indicate that our fiducial group mass estimates suffer from a global uncertainty of about 0.3 dex, which we thus consider to be the typical error on these estimates. We therefore ask what maximum trends in galaxy properties with group mass could remain undetected in our sample, due to this level of uncertainty in the measurements of group masses. In other words, how strong a dependence of a given quantity on halo mass could disappear in our data, due to the uncertainty in our practical realization of the group masses? We address this question by computing how much the observed slope of a measured trend can change with respect to the ‘true’ one, also given the statistical size of the *ZENS* sample.

We consider the two cases in which the observed property is either a fractional quantity (for example, the fraction of quiescent satellite galaxies analyzed in our Paper IV) or a non-fractional quantity (for example, the colors of bulges and disks of satellite and central galaxies, as studied in our Paper V). We consider for this test a sample of groups of size equal to the 79 first-epoch *ZENS* groups, having the same group mass distribution of the *ZENS* sample. The results are similar when the whole sample of 141 groups is considered. We split the sample in two bins of group mass separated at $10^{13.4} M_\odot$, which is what we often will do in our analyses. We impose as an initial condition the same number of galaxies in the low- and high- group mass bins as we have in the real *ZENS* sample.

For the case of a fractional quantity, we assume that each group has a total number of galaxies n_i of which k_i have a given property, producing a fraction f_i of galaxies in that group with this characteristic. As a starting point we assume that the mass of the group is known without errors, and that all groups in the low (high) group mass bin have initially the same $f_{i,Low}$ ($f_{i,High} = f_{i,Low} + \delta_f$, with δ_f the ‘intrinsic’ difference in the two group mass bins). This determines the *slope* $\alpha_f = \delta_f / \Delta \log_{10} M$ of the relationship between the fractional quantity under study and the group mass. For simplicity, in the analysis, we set $\Delta \log_{10} M = 1$, so the values of α_f vary between zero and one. We calculate the global input fractions f_{Low} and f_{High} of all galaxies in the low and high mass bins, which gives the assumed ‘input’ (i.e., true) slope of the relation. A thousand realizations of the sample are then obtained by perturbing the initial group masses with logarithmic random Gaussian errors, for several initial $f_{i,Low}$ spanning the range $[0, 0.9]$. Due to the errors, groups in the high group mass bin will move into the low group mass bin and vice versa. The observed fractions \hat{f}_{Low} and \hat{f}_{High} are computed for each realization of the error-perturbed sample, and the resulting new slopes are estimated.

In Figure 7 we show the comparison between the input (true) slope $\alpha_{f,input}$ with the output, error-affected slopes $\alpha_{f,observed}$. This enables us to assess the impact of the errors on group masses on our capability of measuring the input, true slope of any trend with group mass that we will seek to measure. In the figure, the two shaded areas correspond to realizations with 0.1 dex (dark color) and 0.3 dex (dashed area) perturbation amplitudes, respectively; these realizations bracket the minimum and maximum resulting slopes for a given value of the input slope. The solid line is the median relation for the typical

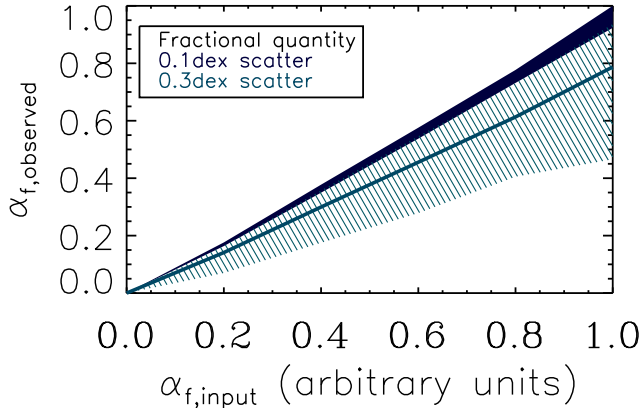


Figure 7. Effect of errors in the group masses on the measured slope $\alpha_{f,observed}$ of the relationship with group mass of a given fractional property (e.g., fraction of passive galaxies, etc.). Plotted are the effects of a 0.1 dex (dark area) and 0.3 dex (dashed area), assuming Gaussian errors for the group masses. The median relation for the typical case of a 0.3 dex error is highlighted as a solid line; this implies a correction factor of order ~ 1.3 to recover the intrinsic slope $\alpha_{f,input}$ of a trend with group mass, from the slope $\alpha_{f,observed}$ that is measured using the *ZENS* dataset. The uncertainty on a flat relationship, i.e., $\alpha_{f,observed} = 0$ is ~ 0.05 .

0.3 dex uncertainty in *ZENS* group masses.

As expected, the effect of the errors on the group masses is to lead to an underestimation of the slope of any relationship of fractional galaxy properties with this environmental quantity.¹⁰ Nevertheless, the *ZENS* data enable us to detect even moderate trends with group mass. A median ‘correction factor’ can be estimated from this test, i.e., $\alpha_{f,input} \sim 1.3 \times \alpha_{f,observed}$, with an uncertainty of order ~ 0.05 for a flat relationship with $\alpha_{f,observed} \sim 0$.

To establish the error on trends with group mass for non-fractional quantities, we assume that all groups in the low group-mass bins have an initial distribution of such quantity with a certain mean value, equal to $\langle q_{nf,Low} \rangle$, and a standard deviation equal to $\sigma_{nf} = 0.3$. The groups in the high group mass bin have an initial distribution of values with the same dispersion as the low mass groups, but centered at $\langle q_{nf,High} \rangle = \delta_{nf} + \langle q_{nf,Low} \rangle$, with $\alpha_{nf} = \delta_{nf} / \Delta \log_{10} M$ the slope of the relationship between the non-fractional quantity under study and group halo mass. We exemplify this case in Figure 8 by setting $\langle q_{nf,Low} \rangle = 0$ and exploring a range of $\langle q_{nf,High} \rangle$ from 0 to 1 in arbitrary units. Again we set $\Delta \log_{10} M = 1$, so that the slope will vary between zero and one as well. Starting from the given initial condition, we perturb the group masses with 0.1 and 0.3 dex Gaussian errors, and recalculate the average values, deviations and difference of the measurements between the low and high groups mass bins, as above. Figure 8 shows that observed slope $\alpha_{nf,observed}$ is typically ~ 1.4 times flatter than the true slope $\alpha_{nf,input}$. Also,

¹⁰ As an additional a-posteriori check entirely and self-consistently based on our data, in some analyses we also assess the impact on trends with group mass of a 0.3 dex Gaussian error on the latter by computing a large number of simulated realizations of the given observed trend, each realization differing from the true observed trend by the addition of a random error on M_{GROUP} sampled from the Gaussian (see e.g., Paper IV, for the utilization of this approach). This test returns results consistent with those discussed in this Section.

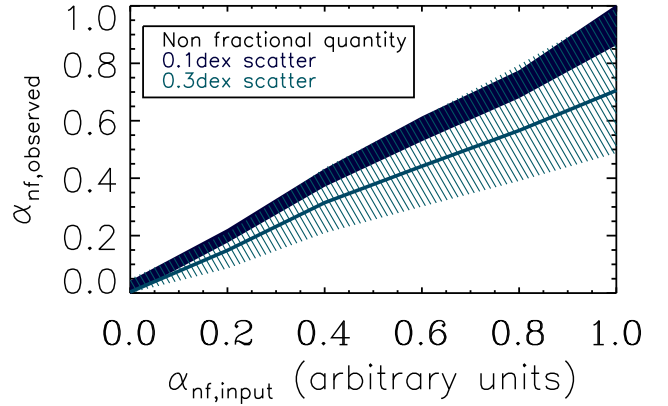


Figure 8. As in Figure 7, but for the case in which the studied property is not a fractional quantity. In this case, the errors on the group masses flatten the intrinsic slope of the relationship of this quantity with halo mass of a factor of order ~ 1.4 . The uncertainty on a flat relationship, i.e., $\alpha_{nf,observed} = 0$ is ~ 0.1 .

an observed $\alpha_{nf,observed} \sim 0$ may hide an intrinsic slope of $\sim 10\%$.

These tests give us a benchmark for interpreting correctly the trends with group mass that we explore in *ZENS*.

3.2. Environments number two and number three: Galaxy distance from the group center and the central/satellite dichotomy

Galaxies may suffer environmental effects as they plunge into, or as they orbit the dark matter halos of their host groups. Also, central and satellite galaxies are expected to experience different physical conditions through their evolution with cosmic time (Somerville & Primack 1999; Simha et al. 2009). Ideally we would want to know the precise location and velocity vector of each galaxy within the three-dimensional potential of its host group halo, relative to the characteristic size of the halo, e.g., the R_{200} radius at which the density in the halo is a factor 200 higher than the density of the Universe at the redshift of the structure. A valuable proxy for this is given by the projected distance of the galaxy from the assumed center of the group: this is the quantity that we use in our studies to explore the dependence of galaxy properties on the location of galaxies within their host groups.

While simulations easily assign the rank of central or satellite to a galaxy in a common halo, with real data determining the group centers and, related to this, separating galaxies into central and satellite galaxies, is not without challenges. We therefore adopt an operational definition, and subsequently establish the impact on the final results of our choice.

To separate central galaxies, assumed to sit on the center of the groups, from satellite galaxies, assumed to orbit the central galaxies within the group potentials, previous literature has typically adopted galaxy luminosity (e.g. Weinmann et al. 2006b; Skibba 2009; Hansen et al. 2009) or stellar mass (e.g. van den Bosch et al. 2008; Guo et al. 2009; Kimm et al. 2009, the latter in some cases in addition to luminosity, e.g., Peng et al. 2012). For our sample, the 2PIGG catalogue (Eke et al. 2004a) provides a

group center determined with an iterative approach: the weighted mean position of the member galaxies is calculated, and the most distant galaxy subsequently rejected until only two galaxies are left, at which point the center of the given group is associated with the galaxy with either the larger ‘weight’ that models the local incompleteness of the 2dFGRS data, or, for identical weights, the larger flux.

In our work we scrutinize three different definitions for the center of a group, i.e., the 2PIGG centers, the geometric center of stellar mass, and the (center of the) galaxy with the highest stellar mass, respectively. Ultimately we opted for the latter definition as our fiducial estimate for the group center and central galaxy of a group; however, we imposed that the resulting central galaxy should satisfy a consistency requirement for it being also at the spatial and velocity center of the group. Furthermore, in determining which galaxy had the highest mass, we considered not only the mass estimates provided by the ‘best-fit’ templates to the observed galactic SEDs, but also the errors in these estimates. We discuss in detail below (Section 3.2.1) our procedure for identifying the central galaxies and the centers of the groups.

In order to derive an estimate for the characteristic radii R_{200} , given the uncertainties in the group velocity dispersions mentioned above, we used our fiducial total group masses and derived $\hat{R}_{200} = \left(\frac{GM_{GROUP}}{10H(z)^2} \right)^{1/3}$, with $H(z) = H_0 \sqrt{\Omega_M(1+z)^3 + \Omega_\Lambda}$ the Hubble constant at the given redshift. Note that we use the measured values of M_{GROUP} , which are assumed to be proportional to the M_{200} values; for this reason we have distinguished $\hat{R}_{200} \neq R_{200}$. For simplicity, however, we will drop the \hat{R}_{200} notation, but it should be kept in mind that a conversion factor is needed to rescale our size measurements to the formal R_{200} values.

3.2.1. A non-trivial challenge: Which is the central and which are the satellites?

Inspecting the properties that our *ZENS* groups and their central galaxies would have, if we used solely luminosities or nominal best-fit stellar masses for the identification of such centrals and centers, highlights some shortfalls in all those definitions. For example, Peng et al. (2012) combine a requirement on luminosity with a requirement on stellar mass to determine the central galaxies in their SDSS group sample, to minimize the effects of recent star formation or dust reddening in the identification of the centrals; these effects can be substantial in a luminosity-based approach, especially by introducing stellar mass dependent biases. It is clear however that the identification of ‘the most massive galaxy’ is affected by random and systematic errors in the derivation of galaxy stellar masses; these errors are not customarily included in the identification of the central galaxies.

A result of these shortfalls is that the alleged central galaxies that are identified based on a (luminosity or even a) best-fit stellar mass criterion often lie at the projected spatial or kinematic outskirts of the groups of which they are supposed to be the centers. We have tested that this consideration holds in both the two of the most used clustering-based group catalogs of Yang et al. (2007) (for the SDSS) and Eke et al. (2004a) (for the 2dFGRS). For

example, identifying the group center with the nominal most massive galaxies, we find that roughly 50% of the *ZENS* groups suffer from this unphysical ‘displacement’ of their own alleged centers. Other authors have addressed the issue of contamination and/or incompleteness in samples of central vs. satellite galaxies, at least in terms of establishing a global statistical effects (without however applying an active correction to their final analysis). For example, Weinmann et al. 2009 tested their grouping algorithm against SDSS mock catalogs, and found a contamination of $\sim 30\%$ of centrals in their sample of satellites and vice versa.

In our study we implemented a procedure for improving the identification of the central galaxies, which also gives insight on the origin of central vs. satellite contaminations. In detail, we scrutinized the properties of the nominal most massive galaxies for each group in our sample, and we retained them as their ‘centrals’ only if they were compatible, within the errors on the stellar mass estimates, with being the most massive galaxies in their groups, *and* furthermore resulted in self-consistent solutions in the (projected) spatial and (line-of-sight) velocity domains. That is to say, for a galaxy to be a good central in a group halo, it must be its most massive inhabitant *and* must be compatible with the inferred spatial *and* velocity centroids of this halo. For cases in which the galaxy with the highest formal best fit stellar mass did not satisfy simultaneously these criteria, we either found an alternative galaxy within the group which provided such self-consistent solution, or flagged the groups as ‘unrelaxed’, in order to keep in our analyses the information that, for these systems, none of their member galaxies satisfied all conditions for being genuine ‘central’ galaxies.

Quantitatively, we implemented these criteria by requesting that not only (i) the central galaxy be the most massive member of the group ‘within the errors’ of our stellar mass estimates, but also that (ii) its projected location lies within the inner circular area centered on the stellar-mass-weighted geometric center of the group, and enclosed within a radius $0.5R_{200}$; and (iii) its inferred line-of-sight velocity lies within one standard deviation of the median of the velocity distribution for that group.

We started the procedure highlighted above by assuming as fiducial stellar masses for the *ZENS* galaxies the best-fit (i.e., minimum χ^2) masses that result from fitting, with the code *ZEBRA+* (Feldmann et al. 2006; Oesch et al. 2010), a large library of synthetic models to the galaxy SEDs¹¹. The adoption of these fiducial stellar masses leads to the identification of a nominal central galaxy, i.e., the galaxy member in a group which has the highest fiducial best-fit stellar mass. We then checked the spatial and velocity location of these nominal centrals. For each of the 79 first-epoch *ZENS* groups, we show in Figure 9 the location of the member galaxies

¹¹ The stellar masses for the *ZENS* galaxies were derived by combining the *B* and *I* WFI photometry with the available multi-wavelength archival photometry (SDSS *u,g,r,i,z* (Abazajian et al. 2009), the 2MASS *J, H, K*, (Skrutskie et al. 2006) and the GALEX NUV and FUV magnitudes see Paper III for details on the procedure adopted to derive and calibrate the stellar masses. Note that, in our *ZENS* analyses, we adopt for the definition of galaxy stellar mass the integral of the star formation rate, i.e., we do not include the mass ‘returned’ to the gas through stellar evolution processes.

relative to the mass-weighted geometric group centers; in each panel, the radial scale is set by our estimate of R_{200} for the given halo. The nominal most massive member of each group is indicated with a yellow point. Light and dark blue points represent galaxies with masses respectively within a factor of two and four of the nominal most massive galaxy. Less massive group members are shown as black dots. For each of the groups, the corresponding velocity distributions are shown in Figure 10. Here each panel presents the relative line-of-sight velocity distribution about the median of the distribution, with the scale set by its dispersion. The position in velocity of each individual galaxy is indicated with an arrow, using the same color-coding as in Figure 9 for the nominal most massive member of each group, for galaxies with nominal stellar masses within a factor of two and four from the nominal most massive galaxy, and for lower mass galaxies (respectively yellow, light and dark blue, and black).

In about 50% of the first-epoch *ZENS* groups, the nominal centrals were confirmed to be fully consistent, both spatially and in velocity terms, with lying at the bottom of the potential well of their host groups. We thus confirmed these galaxies to be genuine centrals, and identified with them the centers of the groups. The yellow points/curves identifying these central galaxies in Figures 9 and 10 (and 11, see below) are highlighted in green for these groups. In the remaining $\sim 50\%$ of groups, however, the nominal centrals were either at the spatial periphery of their group halos, or appeared to be ‘shooting away’ from them. We thus asked whether this might be due to uncertainties in our stellar mass estimates for the galaxy members (see Paper III).

To address this issue we capitalized on the availability of the entire posterior probability distributions (PPDs) for the stellar masses. These PPDs are presented in Figure 11. Specifically, each panel in this figure shows the PPDs of the stellar masses for the few top-massive galaxies in each of the first-epoch 79 *ZENS* groups. For each of the plotted galaxies, the PPDs are obtained by connecting 21 sampling points spanning the 1 to 99% quantiles. In each panel, the horizontal scale is logarithmic in mass and covers the range between one-tenth (leftmost value) to three times (rightmost value) the nominal highest mass; the PPD for this nominal highest mass galaxy is highlighted again in yellow. Also the remaining colors are as in Figures 9 and 10, i.e., light and dark blue curves indicate galaxies with nominal (best fit) stellar masses within a factor of two and four, respectively, of the nominal highest mass for that group. Note that in several groups there are galaxies, with nominal masses within a factor $\sim 2 - 4$ from the nominal highest mass, which would thus be classified as ‘satellites’, which however have, according to their PPDs, a substantial probability that their stellar masses are actually larger than the nominal highest stellar mass of the nominal central.

For the groups in which the nominal (best fit) most massive galaxy failed to pass the projected-spatial criterion and/or the line-of-sight velocity criterion to be a genuine central galaxy, we thus searched for an alternative viable central by requiring that this (i) satisfies both the spatial and velocity criteria; (ii) has a nominal stellar mass within a factor of four from the nominal highest mass for that group, and (iii) has a $\geq 10\%$ probability, as defined by the overlapping area with the PPD of the

most massive member, to exceed the minimum mass in the PPD of this dominant galaxy. We found six *ZENS* groups for which such viable alternative centrals could be identified, which we adopted as the correct central galaxies in these groups. These alternative centrals are highlighted with orange contours to the relevant symbols in Figures 9, 10 and 11.

For the remaining 35 groups of the first-epoch sample, this iterative procedure failed to identify a galaxy member which satisfied the set criteria for being a genuine central galaxy. For these groups the nominal most massive galaxy was thus retained as the nominal central, but we flagged these groups so as to be able to estimate the impact of their inclusion in analyses that rely either on a central/satellite separation, or on the knowledge of the group center. These ‘dubious’ centrals are highlighted with red contours to the symbols in Figures 9, 10 and 11.

3.2.2. Sources and effects of errors on our fiducial centrals and group centers

The fiducial centers and centrals defined as above are correct within a certain statistical uncertainty: In addition to introducing uncertainties in the estimate of the total masses of the groups, as discussed in Section 3.1.1.1, the presence of interlopers and the absence of genuine group members from the 2PIGG lists (which define the groups in our sample), can also affect the identification of the central galaxy and thus the identification of the center of the groups. We discuss this issue more in detail in Appendix B. Here we highlight that, based on our own test of comparison between the 2dFGRS catalogue and the SDSS spectroscopic and photometric catalogues (Abazajian et al. 2009), we expect that these effects should lead to the mis-identification of the central galaxies in at most $\sim 10\%$ of the cases (or less). The dominant source of error in the identification of centrals and satellites remains the association of galaxies with a given group through the 2PIGG algorithm. We will discuss the impact of such an uncertainty in each individual analysis that relies on either a central-satellite split, or on the identification of the group centers.

3.3. Environment number four: The backbone density field of the Large Scale Structure

A major achievement of recent large spectroscopic redshift surveys, and large multi-wavelength imaging surveys with accurate photometric redshifts, has been enabling the determination of a proxy density field produced by the large-scale structure (LSS). The projected overdensity at a position θ in celestial coordinates, and at a given redshift z , is defined as $\delta_{LSS} = \frac{\rho(\theta, z) - \rho_m}{\rho_m}$, with $\rho(\theta, z)$ the comoving projected the density of the tracers of the density field, and ρ_m the mean projected density calculated over the global survey area at the given redshift. Several approaches have been used to derive LSS density fields e.g., by measuring the density within a fixed volume (e.g. Hogg et al. 2003; Blanton et al. 2005; Wilman et al. 2010); through Voronoi-Delaunay techniques (Gerke et al. 2005; Romano-Díaz & van de Weygaert 2007; Knobel et al. 2009); and with adaptive approaches in which the density is calculated out the distance to a N^{th} nearest neighboring galaxy (e.g. Gómez

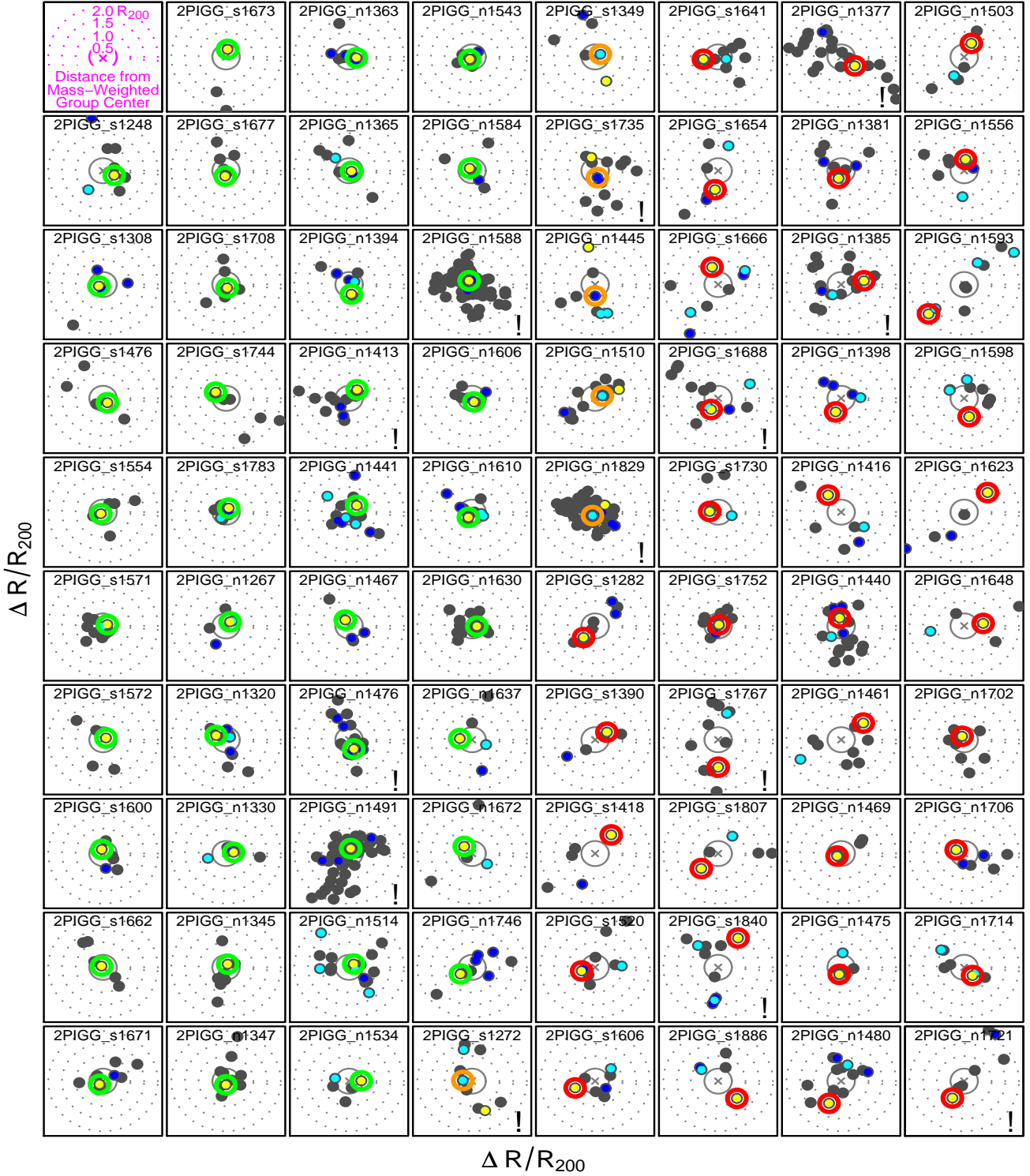


Figure 9. The spatial distributions of galaxies in each of the 79 first-epoch *ZENS* groups. Each panel presents the (projected) radial distribution around the mass-weighted geometric center in each group, with the scale set by our estimate of R_{200} for that halo. Concentric line-circles mark galactocentric distances of 0.5, 1.0, 1.5, and $2.0R_{200}$, respectively, to the mass-weighted center of the groups (marked by grey crosses, not always visible). Yellow symbols indicate the nominal most massive member of each group, based on our fiducial definition of stellar mass of a galaxy, i.e., the best-fit stellar mass obtained by fitting a large number of synthetic templates, spanning a large range of star formation histories, to the observed galaxy SED. Light and dark blue symbols represent galaxies with nominal stellar masses within a factor of two and four, respectively, from the nominal highest mass in the group. Green and orange circles around the symbols for the galaxies assumed to be the centrals identify groups which we have labeled as ‘relaxed’; red circles identify ‘unrelaxed’ groups. Green identifies groups in which, based on spatial and velocity considerations, the nominal most massive galaxy in the group is confirmed to be the central galaxy. Orange identifies groups in which the nominal most massive galaxy is not consistent in the spatial and/or velocity domain with being the center of the group, but another galaxy member in the group (i) has an integrated probability $\geq 10\%$ to have a stellar mass higher than the nominal most massive galaxy, and (ii) also satisfies the spatial and velocity criteria described in the text. These alternative most massive galaxies, highlighted in orange, are assumed to be the central galaxies of their host groups. The groups marked with a “!” are those for which the WFI pointings did not cover their entire extent; some galaxy members located at the group outskirts have been missed, but these are low mass galaxies, unlikely to be the centrals. In general, missed galaxies do not impact the analyses of the central galaxies (see Appendix B for details).



Figure 10. The line-of-sight velocity distributions of galaxies in the 79 first-epoch *ZENS* groups. Each panel presents the velocity distribution relative to the median redshift of the group; the eight bins from left to right indicate velocities equal to $-2, -1.5, -1.0, -0.5, 0, 0.5, 1, 1.5$, and 2 the value of σ_{GROUP} , respectively (i.e., the velocity scale is normalized to the velocity dispersion of each individual group). The velocities of individual galaxies are shown with an arrow, using the color-coding as in Figure 9.

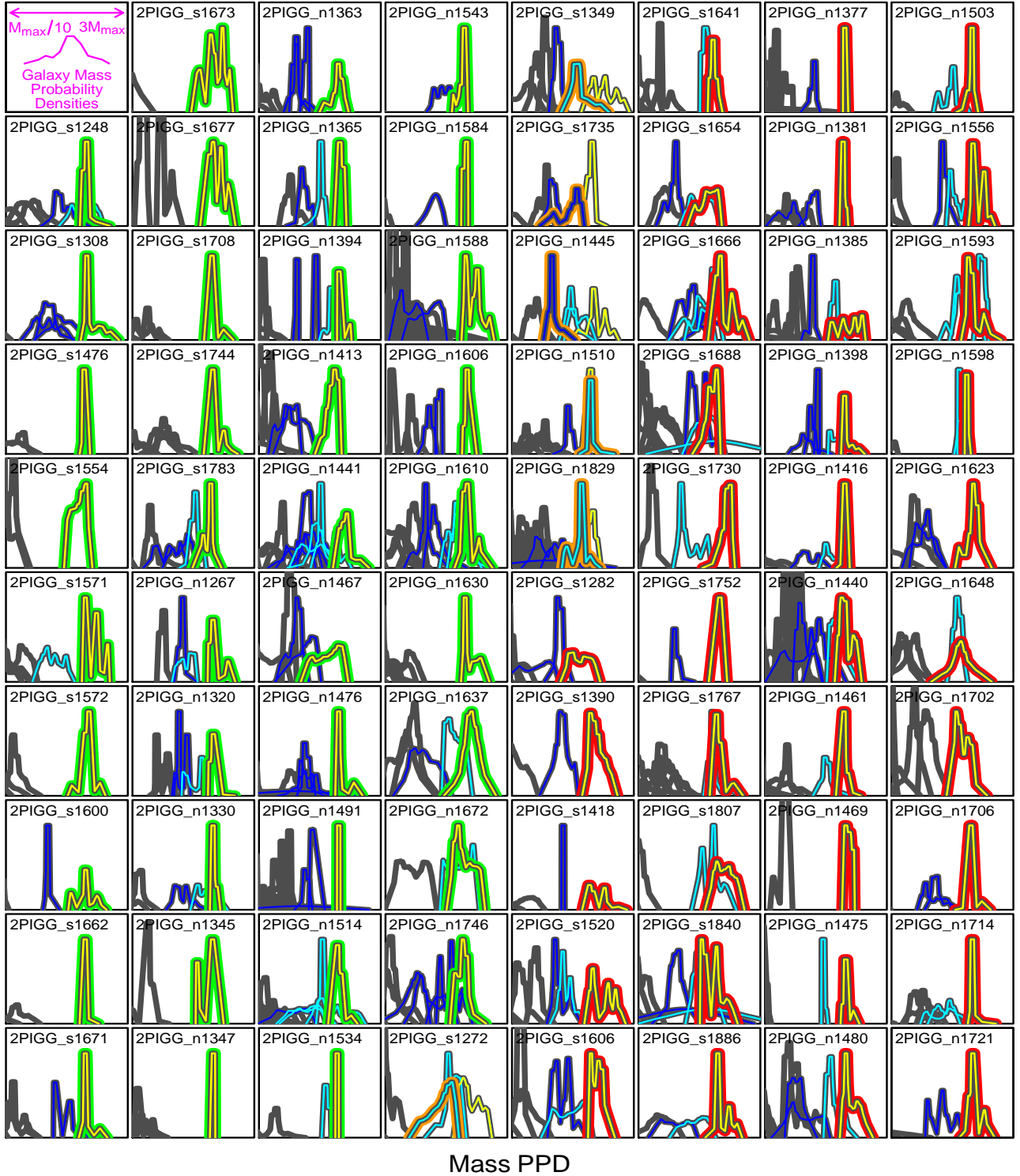


Figure 11. The posterior probability distributions (PPDs) of galaxy stellar masses for the top few most massive galaxies in each of the 79 first-epoch *ZENS* groups. The PPDs are derived by connecting 21 sample points spanning the 1 to 99% quantiles for the stellar masses obtained by fitting a large set of synthetic templates to the observed galaxy SEDs. The horizontal scale is logarithmic in mass and ranges from one-tenth to three times the nominal (best fit) mass of the most massive member. The color-coding is as in Figures 9 and 10. Gaussian PPDs are assumed for galaxies which do not have WFI *B*– and *I*– band images (due to the limited coverage of the WFI pointings); for these, the stellar mass is inferred from the $r_F - M$ relation (see text). The widths of the Gaussian correspond to 1.5 times the observed scatter in this relation.

et al. 2003; Balogh et al. 2004; Baldry et al. 2006; Kovač et al. 2010b).

All these methods have their virtues and shortfalls, as extensively discussed in the previous literature. The N th-nearest galaxy neighbors is often preferred to the ‘fixed volume’ approach because the latter washes out information on scales of order of the adopted volume; however, it has the strong disadvantage that it shifts its physical meaning from density ‘within a halo’ to density ‘between halos’ for galaxies which reside in groups of richness straddling across the chosen value of ‘ N ’ (see also Peng et al. 2012 for a discussion on the correlation between N -nearest galaxy neighbor overdensity and group membership). More generally, as discussed also by Haas et al. (2012) all the above-mentioned methods contain a built-in correlation with halo mass, which hampers separating the effects on galaxies of the LSS from those of the host halos. To achieve an environmental LSS that is insensitive to halo mass, these authors construct a density field based on dimensionless galaxy luminosities/masses and distances.

In our study we use a different approach to minimize a correlation by-construction between halo mass and LSS density field. Specifically, we adopt the N^{th} nearest method; however, as tracers of the LSS density field, we use the groups themselves (treated as point masses of mass M_{GROUP}), instead of their member galaxies. Thus, $\rho(\theta, z) = \sum_i^N w_i / (\pi d_N^2)$ with N is the chosen number of nearest (point-mass) groups, which we set to 5, d_N the comoving distance to the N^{th} neighbor group and w_i the weights, which we set equal to M_{GROUP} . For each group, the search for neighboring groups was restricted within a redshift interval of $dz = \pm 0.01$; a minimum luminosity was set for the groups or isolated galaxies equal to the total (i.e. integrated to zero) luminosity of a single $b_j = 19.1$ galaxy at redshift $z = 0.07$. The entire 2PIGG catalogue, supplemented by all remaining galaxies in the 2dFGRS (treated as groups with one galaxy member), was used to derive this N th-nearest group neighbors overdensity field δ_{LSS} . Halo masses for isolated galaxies were calculated following the same procedure adopted for the groups; a correction to total luminosity was applied, which assumes that these isolated galaxies have companions fainter than the survey magnitude limit (see Section 3.1). We note that densities calculated at the edges of the 2dFGRS area are biased as a consequence of the limited area of the survey. To correct for this effect we followed the approach of Kovač et al. (2010b), and divided the computed density for the fraction of the area enclosed within d_N which is covered by the 2dFGRS pointings.

While the fiducial δ_{LSS} estimates that we use in our analyses are based on the 5th nearest neighbor groups, we also computed 3rd- and 10th- nearest group estimates and checked that our main results do not depend on which of these representations of the LSS density field we use. The comparison between these three estimates is shown in Appendix D, where we also discuss for completeness a comparison of our fiducial δ_{LSS} , which uses the groups as point-mass tracers of the LSS, with the standard N th-nearest neighbors density field that uses as tracers the individual member galaxies.

Note that, by construction, in our analysis all galaxies

belonging to a given group are characterized by the same value of LSS overdensity δ_{LSS} .

The final distribution of δ_{LSS} values for the *ZENS* groups (and thus galaxies within the groups) is presented in the left panel of Figure 12 as dashed histogram, and compared to the complete parent samples of 2PIGG groups in the redshift range $0.035 < z < 0.075$ (solid histogram). Not surprisingly the *ZENS* sample is shifted towards high density regions compared to the global distributions of 2PIGG groups, which extend down to smaller associations of two members only (and thus shifted relative to the whole 2dFGRS catalogue which includes isolated galaxies). Note that our fiducial estimate of δ_{LSS} does not produce the tail at very high overdensities that is observed when the individual galaxies are used as tracers in N th-nearest neighbor calculations of the LSS density field (see Appendix D), a tail which is mostly due to small inter-galaxy separations *within* massive halos with richness larger than the adopted ‘ N ’ value.

To enable comparisons with the global galaxy population (in addition to relative comparisons within the *ZENS* sample), we split the distribution of δ_{LSS} sampled by the entire 2PIGG catalogue in four quartiles (one to four in order of increasing density), and label the *ZENS* groups as residing in *low* LSS environments those groups whose local overdensity is not higher than the value characterizing the first quartile of the global 2PIGG distribution (dashed vertical line in the left panel of Figure 12). Similarly, we label as residing in *high* LSS density regions those *ZENS* groups with a local overdensity larger than the threshold defining the fourth quartile (solid line in the left panel of Fig. 12). The remaining groups are labeled to reside in regions of the LSS of *intermediate* density. As indicated in Table 1, applying these criteria results in 8% (6%), 37% (29%) and 55% (64%) of *ZENS* groups being located respectively in low, intermediate and high density environments (the numbers in parenthesis give the fractions for the 79 first-epoch groups).

Note that, as shown in the right panel of Figure 12, the δ_{LSS} values that we have adopted to describe the underlying density of the cosmic web do correlate with the mass of the groups. Given the approach that we have used to compute δ_{LSS} , this is however mostly a reflection of the fact that the more massive groups inhabit, by definition, high density regions of the Universe (which tend to be highly clustered). However, groups with masses below $M \sim 10^{13.5} M_{\odot}$ are found over a very wide range of LSS environments (as sampled by our δ_{LSS} measurements). At these masses, we can therefore compare the properties of groups of similar halo masses which live in different LSS environments, and thus to identify trends induced by the LSS environment separately from those induced by the group halo mass.

3.3.1. Sources and effects of errors on our LSS (over)density estimates

3.3.1.1. Inclusion or exclusion of isolated galaxies in the 2dFGRS — In the calculation of the fiducial δ_{LSS} values that we adopt in our analysis we included all 2dFGRS galaxies which are not associated with any of the 2PIGG groups (i.e., also the ‘isolated’ galaxies in the 2dFGRS catalogue). We checked however whether the LSS density field that we measure at the location of the *ZENS* groups depends on whether these isolated galaxies are

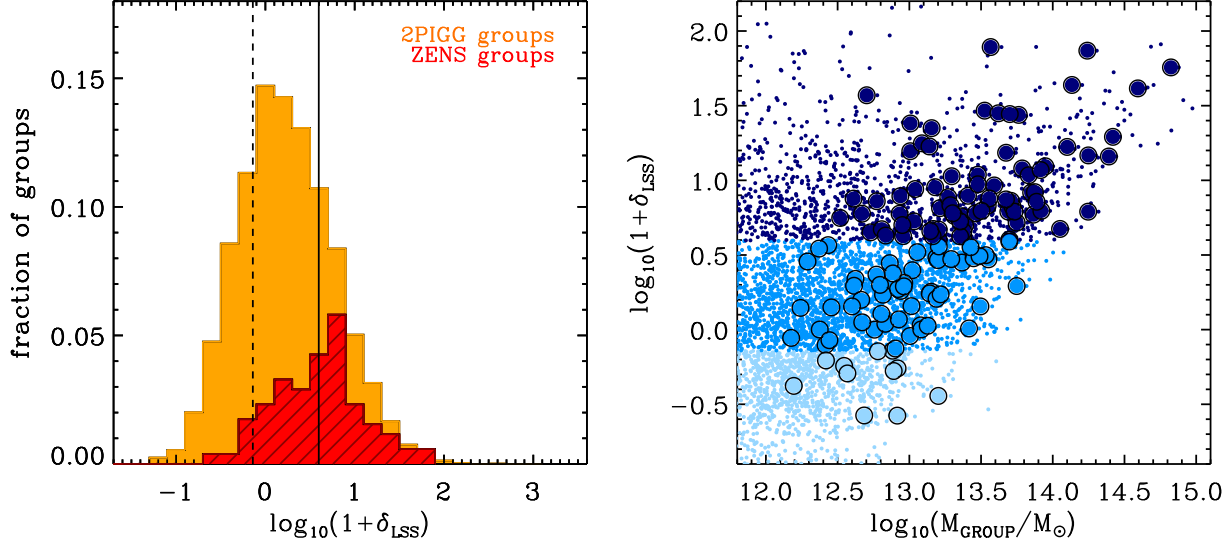


Figure 12. *Left:* The distribution of the fiducial δ_{LSS} overdensities calculated with the 5-th nearest *group* neighbor approach described in Section 3.3. All galaxies in a given *ZENS* group have the same value of overdensity, corresponding to that of their host group. The dashed histogram is for the *ZENS* sample and the solid histogram is for all 2PIGG groups in the redshift range $0.035 < z < 0.075$. The dashed and solid lines highlight the first and fourth quartile of the latter distribution, respectively. *Right:* The fiducial LSS overdensity values δ_{LSS} , based on the 5th nearest *group* neighbor approach described in Section 3.3, as a function of group mass M_{GROUP} , calculated as described in Section 3.1. The three shades of blue highlight, from fainter to darker blue, groups in low (lowest quartile), intermediate and high (highest quartile) LSS densities (relative to the global distribution derived for all 2PIGG groups in the $0.035 < z < 0.075$ redshift range, which are shown as small points with the same color scheme). High mass groups naturally live in high LSS regions; below $\sim 10^{13.5} M_{\odot}$, however, groups with similar masses occupy a wide range of LSS environments (as estimated by the δ_{LSS} field).

included or excluded in the computation of the (Nth-nearest-group-neighbor-based) LSS density field. We show in Appendix D that the use of one or another of these two alternative realizations of the LSS densities shifts a group at most to an adjacent density quartile of the global distribution of densities in $> 90\%$ of the cases, with no major impact on our *comparative* analyses between environments.

3.3.1.2. The choice of N — We also investigated the impact of the size of the projected aperture (i.e., the value of ‘ N ’ in the Nth-nearest group neighbor algorithm) adopted to filter the distribution of the density tracers. In Appendix D we show that, in contrast with Nth-nearest neighbor computations which use the galaxies as the tracers of the LSS density field, our adoption of the groups themselves as tracers of the LSS density results in much weaker differences with the use of $N=3, 5$ or 10 .

4. THE *ZENS* CATALOG: ENVIRONMENTAL, STRUCTURAL AND PHOTOMETRIC MEASUREMENTS

For the 769 galaxies in the 79 first-epoch groups, we have measured a number of structural (Paper II) and photometric (Paper III) diagnostics.

In particular, we have quantified galaxy structure both non-parametrically, through measurements of concentration, Gini coefficient, $M20$, smoothness, as well as parametrically, through single-Sersic and double-component (Sersic bulge plus exponential disk) analytical fits to the two-dimensional surface brightness distributions. Furthermore, we have used an isophotal analysis to quantify the strength of bars. All structural measurements, including bulge and disk parameters, have been corrected in order to eliminate biases that depend not only on see-

ing/PSF, but also on magnitude, size, concentration and axis ratio. We have furthermore employed the corrected structural measurements, including the bulge-to-total ratios, to define a *quantitative* morphological classification, also validated by visual inspection of each galaxy in the sample, into elliptical, early-, intermediate- and late-type disk, and irregulars.

The photometric measurements for the galaxies as a whole include colors (total, and at various galactocentric distances); radial color gradients from analytical fits to the galaxy surface brightness profiles and the scatter around these gradients; total stellar masses and star-formation rates (and dust reddening), through fitting synthetic stellar population models to the near-UV to near-IR galaxy SEDs. Furthermore, through inspection of $(NUV - I) - (B - I)$ and $(FUV - NUV) - (NUV - B)$ color-color diagrams, we have disentangled dust-reddened galaxies from red, quiescent galaxies, and used this additional information to robustly classify galaxies into star-forming or ‘intermediate’ star-forming, or quiescent systems. We have also derived estimates for stellar masses separately for the disk and bulge components of galaxies, from the $B - I$ colors of these sub-galactic components derived from the two-component surface brightness fits.

We publish electronically the *ZENS* catalogue, containing all structural and spectrophotometric *ZENS* measurements for these 769 galaxies, together with the environmental diagnostics discussed above and listed in Table 1. We will augment in the future the *ZENS* catalogue so as to include the measurements for the galaxies in the remaining 62 groups whose measurements are underway. The *readme file* of the *ZENS* catalogue is given

for convenience in Appendix E.

5. GROUPS WITH OR WITHOUT A CENTRAL GALAXY: DEFINITION OF ‘RELAXED’ AND ‘UNRELAXED’ GROUPS

In Section 3.2.1 we saw that a total of 44 first-epoch *ZENS* groups, whose centrals are highlighted in either green (38) or orange (6) in Figures 9, 10 and 11, host a galaxy member which satisfies simultaneously the three criteria that we require in order to be a genuine central, i.e., having highest stellar mass within the errors, and being consistent with being the center of the group both in the spatial and velocity domains. The fact that in these groups the most massive galaxies have been able to establish their rank within their group potentials suggests a state of dynamical relaxation for their host groups. Dynamically ‘relaxed’ systems show indeed a well-defined center for the potential, and are a golden sample to extend to low (i.e., smaller than cluster) mass scales studies of galaxy properties as a function of group-centric distance.

In the remaining 35 first-epoch *ZENS* groups no galaxy member in the nominal 2PIGG group associations satisfies simultaneously the three criteria above to be a genuine central. For these groups we highlight in red in Figures 9, 10 and 11, the symbols for their nominal centrals, as a reminder that these, adopted as such on the basis of their nominal highest stellar masses, show a ‘displacement’ from the groups spatial and/or velocity centers. We label these groups as ‘unrelaxed’, to contrast them to the well-behaved, relaxed groups discussed above. Figure 13 shows the distribution of total group masses for these unrelaxed groups, comparatively with the distribution of group masses for the entire *ZENS* sample; this shows that unrelaxed groups span a large range of masses, from low to relatively high ones.

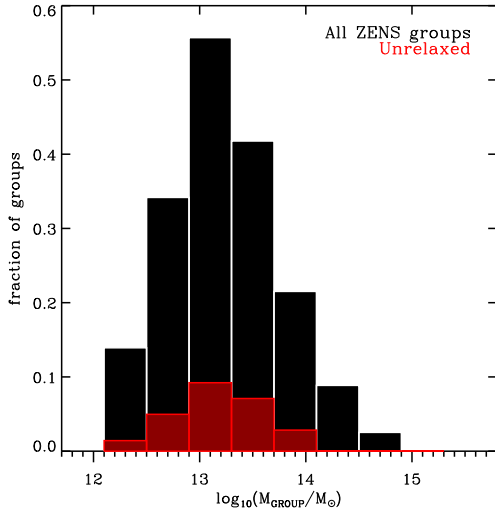


Figure 13. The red histogram shows the distribution of M_{GROUP} for the 79 first-epoch groups which are classified as ‘unrelaxed’ according to the criteria described in Sections 3.2.1 and 5. The black histogram is distribution for the complete *ZENS* sample of groups. Both curves are normalized to the total number of *ZENS* groups.

We expect a physical origin to contribute to our inability to identify a bulletproof central galaxy in the ‘unre-

laxed’ groups in the *ZENS* sample. Non-physical factors may also however contribute to preventing us from identifying the real central galaxy in some of these groups. The main sources of error are again related to interlopers in group membership, incompleteness in the parent 2dFGRS database and/or the inherent limitations of the 2PIGG group-finding algorithm (see Section 2.2, Section 3.2.2, and Appendix B). Based on the tests that we have conducted to understand the impact of interlopers and missing galaxies in the identification of central galaxies (3.2.2), we expect that $\sim 20 - 25\%$ of groups may appear as ‘unrelaxed’ due to these catalogue failures. The fraction that we observed is however substantially higher, of order $\sim 40 - 50\%$. We thus estimate that, in at least $\sim 10 - 15\%$ of groups in the *ZENS* sample, the displaced centrals are a genuine smoking gun for an unsettled dynamical state. This may result from the accretion of individual galaxies by the group potential and/or of group-group merger events.

We briefly investigate below whether and how the central and satellite galaxy populations in ‘relaxed’ and ‘unrelaxed’ groups display differences that can help understanding the co-evolution of galaxies and their host group halo potentials. First however we perform another test, to firm our estimates for the fraction of genuinely unrelaxed groups in the *ZENS* sample.

5.1. Testing the dynamical state of groups with a sub-clustering analysis

As a complementary method for testing the dynamical state of the *ZENS* groups we searched for substructures in position and velocity space, following the approach described in Dressler & Shectman (1988). In the original test, for each group, a local mean velocity (\bar{v}_{local}) and velocity dispersion (σ_{local}) around each member is calculated by using the N th nearest neighbors galaxies in the group, plus the galaxy on which the search is centered. The quantity $\delta^2 = \frac{(N+1)}{\sigma^2} [(\bar{v}_{\text{local}} - \bar{v})^2 + (\sigma_{\text{local}} - \sigma)^2]$ parameterizes the deviation of this subset of galaxies from the group global velocity and dispersion, with \bar{v} and σ the group mean velocity and total dispersion. Under Gaussian assumption and in the absence of substructures within the groups, the sum of the δ parameters of all galaxies in a group (Δ_{tot}) will be close to the number of its members. As discussed in Dressler & Shectman (1988) a non-Gaussian distribution of galaxies velocities can bias the result also in the absence of real substructures. For these reasons, the test is repeated for a number of Monte Carlo realizations, in which the position of the galaxies are held fixed, but the velocities are randomly redistributed between the group members. Any intrinsic correlation among velocities will be thus erased and these Monte Carlo samples can be used to quantify the probability that a value of Δ_{tot} larger than the one observed can originate from a random distribution.

To optimize the test for the *ZENS* groups, which have typically much lower richness than the clusters for which the test was devised, we applied the following modification to the original formulation: we chose an N which depends to the group richness to calculate \bar{v}_{local} and σ_{local} ; specifically, we adopted $N = 0.4 \times N_{\text{members}}$. This accounts for the fact that the *ZENS* groups span a wide richness range, from $N_{\text{members}} = 5$ to $N_{\text{members}} \simeq$

100. Following the above prescription, we generated 500 Monte Carlo simulations for each *ZENS* group and identified groups having significant sub-clustering as those in which less than 20% of the Monte Carlo simulations result in a Δ_{tot} greater than the group Δ_{tot} .

Out of the 44 ‘relaxed’ groups in which we can identify a central galaxy according to the criteria described in section 3.2.1, $\sim 15\%$ (i.e., 7 groups) are found to have distinct subunits in this clustering analysis. There is therefore a good agreement between the two approaches that we have considered for establishing the dynamical state of the group. In contrast, only $\sim 25\%$ (9 groups) of 35 ‘unrelaxed’ groups are also dynamically unrelaxed according to the Δ statistics. No evidence for substructure is found for the remaining majority of them, again hinting at an absolute fraction of groups that are genuinely dynamically young of order $\sim 10 - 15\%$.

5.2. A quick exploration of centrals and satellites properties in relaxed and unrelaxed groups

We briefly investigate how some key galactic properties of central or satellite galaxies in relaxed groups compare with those of similar galaxies in unrelaxed groups. To perform this comparison, we consider two bins of stellar mass, i.e., $10^{9.3}M_{\odot} < M < 10^{10}M_{\odot}$ and $10^{10}M_{\odot} < M < 10^{10.7}M_{\odot}$. Only satellites populate the ‘low-mass’ bin in our sample; in the ‘high-mass’ bin both satellites and centrals are fairly represented. We use the measurements published in Cibinel et al. 2012a,b to search for differences in galaxy half-light radii $r_{1/2}$, specific star formation rates (sSFRs), surface densities of star formation rate (Σ_{SFR}) and $(B - I)$ colors. SFR and $sSFR$ for galaxies in which the best-fit template result in very low $SFR < 10^{-4}M_{\odot}yr^{-1}$ are set to $SFR = 10^{-4}M_{\odot}yr^{-1}$ and $sSFR = 10^{-14}M_{\odot}yr^{-1}$, respectively. The results are shown in Figure 14.

The figure shows, from left to right, the distribution of $r_{1/2}$, $sSFR$, Σ_{SFR} and $(B - I)$ for central (red/orange) and satellite (dark/light blue) galaxies in our low (top) and high (bottom) bins of stellar mass. To avoid introducing biases due to different distributions of group masses between relaxed and unrelaxed groups (see Figure 13), only groups with $M_{GROUP} < 10^{13.5}M_{\odot}$ are considered in this analysis.

We find a global similarity of central and satellite properties at high masses, $10^{10}M_{\odot} < M < 10^{10.7}M_{\odot}$. Some rather large-sized centrals appear in relaxed groups, which seem to be absent in the unrelaxed potentials; these systems are however flagged in Cibinel et al 2012a to have large errors associated with the measurements of their $r_{1/2}$. We therefore do not interpret the appearance of this population in the relaxed groups as significant.

We see a modest signal in our data for satellites of low mass ($10^{9.3}M_{\odot} < M < 10^{10}M_{\odot}$) in unrelaxed groups to be on average 0.07 magnitude bluer than galaxies of similar rank and mass in relaxed groups; the probability that the two distributions differ is slightly marginal in our data, at the level of $\sim 92\%$. We note that we do not detect a similar effect in the sSFR (or Σ_{SFR}) diagrams. This could be due to dilution of signal due to intrinsic uncertainties in the SFR values derived from SED fits. Another possibility is that the redder median color of galaxies in unrelaxed groups is at least partially a reflec-

tion of a higher fraction of dusty star forming galaxies relative to the fraction of these objects in relaxed groups (20% versus 10% of all galaxies, respectively). Star forming and quiescent galaxies constitute 92% and 82% of galaxies in unrelaxed and relaxed groups, and dusty star forming systems are 22% and 15% of these populations, respectively. Most probably both these factors contribute to smearing the signal in the sSFR distributions.

Despite the relatively modest significance in our data of the trend of galaxy $(B - I)$ with dynamical state of the group, we highlight it to raise the possibility that such trend may be stronger between bona fide merging and virtualized groups, and may be diluted in our sample, in which we estimate that the classification of a group as unrelaxed might be due, of order a half of the times, to the incompleteness issues discussed above. The trend, taken at face value, supports the following scenario, which we adopt as a working hypothesis, that we will investigate further in the future:

(1) Central galaxies do not know generally whether they live in relaxed or unrelaxed potentials, i.e., their properties are most likely defined only by their mass.

(2) Satellites at high masses are either unaffected by the group environment, or they may suffer transformations as they enter the potential of a relatively small group, with further group-group mergers not having any additional impact on their properties (see also De Lucia et al. (2011)).

(3) Low-mass satellites have their star formation quenched by processes acting in relaxed group potentials. This is further substantiated by other analyses of the *ZENS* sample that we present in papers IV-VIII, and is in agreement with some independent studies that also point at satellite-quenching by physical processes that are enabled by physical mechanisms acting within virtualized halos.

In future analyses we will ensure that including or excluding the unrelaxed groups from the analysis of any given specific diagnostic will not impact our main conclusions, or will explicitly comment on this if it will.

6. SUMMARY AND CONCLUDING REMARKS

Motivated by the picture that both the mass of a galaxy, and its immediate and distant environment, may impact how the galaxy evolves and its redshift zero properties, and by the uncertainty on which mass and which environment are the relevant ones to galactic life, we undertake the *ZENS* project, which uses new and archival multi-wavelength data for a statistically complete sample of 1630 galaxies brighter than $b_J = 19.45$ which are members of $141 \sim 10^{12.5-14.5}M_{\odot}$, $z = 0.0585$ groups. The emphasis of *ZENS* is to explore the dependence of key galactic populations diagnostics on the large-scale environment, on the mass of the host group halo, on the location of galaxies within their group halos, and on the central/satellite rank of a galaxy within its host group halo. The *ZENS* sample is extracted from the 2PIGG catalogue of the 2dFGRS.

In this first paper, introducing the project, we have described improved algorithm adopted to define the group centers, to rank galaxies as centrals or satellites in their host groups, and to separate the effects on galaxies of groups mass and LSS density. Specifically:

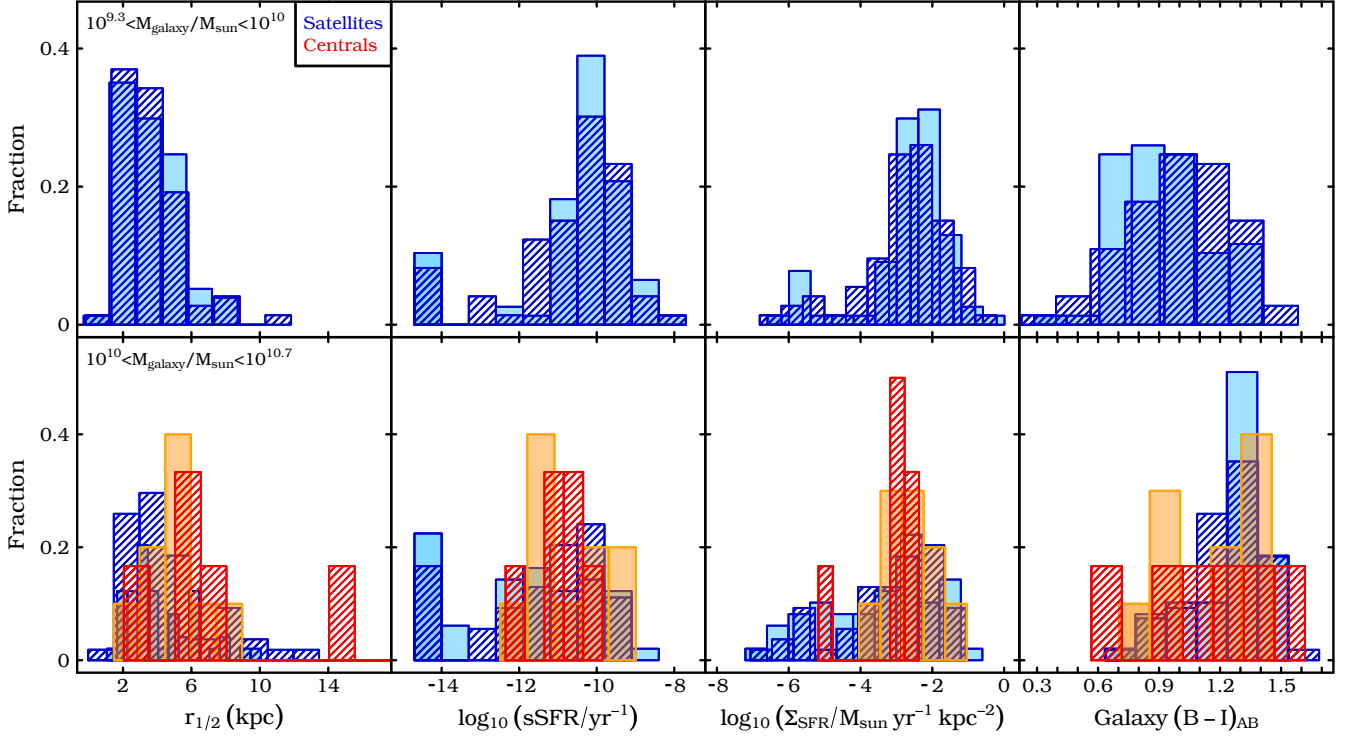


Figure 14. From left to right, the figure shows the distribution of galaxy half-light radii, specific star-formation rates, star-formation rate surface densities and $(B - I)$ colors for central (red) and satellite (blue) galaxies in two bins of stellar mass (top and bottom rows, as indicated in the figure). Dark hatched histograms are for galaxies in relaxed groups, light filled histogram are for galaxies in unrelaxed groups. To match the distribution of halo masses of the unrelaxed sample and avoid spurious effects in the comparison between relaxed and unrelaxed groups due to differences in the distributions of group masses between these two families (see Figure 13), only groups with $M_{GROUP} < 10^{13.5} M_{\odot}$ are considered in this figure.

(i) We have introduced a three-faceted self-consistency criterion for identifying central galaxies. These must, simultaneously, be the most massive galaxies in the group within the errorbars estimated for the galaxy stellar masses, and must be consistent with being the spatial and dynamical centers of the host groups.

(ii) We have adopted a Nth-nearest *group*-neighbors computation to estimate the LSS density underlying the groups which, especially at group masses $M_{GROUP} < 10^{13.5} M_{\odot}$, is independent of group mass/richness and enables us to study separately the effects on galaxies of these two environments.

Furthermore, we have used simulations, also based on semi-analytic models of galaxy evolution, to quantify the intrinsic uncertainties in the trends of galaxy properties with the environmental parameters, that are propagated from the random and systematic errors in these parameters.

We have found that at least 60% of groups are dynamically-relaxed systems with a well-identifiable central galaxy that satisfy the stringent criterion above – and thus a well-defined center of the group. These groups enable a robust investigation of galaxy properties with group-centric distance down to the smallest group masses sampled in *ZENS*. In the remaining $\sim 40\%$ of groups there is no galaxy which satisfies the required criteria to be the central – and the center of the group potential well. We estimate however that in a substantial fraction of these ‘unrelaxed’ groups the lack of identification of a self-consistent central galaxy has its roots in the incomplete spectroscopic and photometric coverage of the

2PIGG and 2dFGRS surveys, respectively.

Therefore, our classification into dynamically-relaxed and -unrelaxed systems should be read as indicating the important fact that the alleged central galaxies and thus the centers in these groups should be handled with care. This is what we do in our study, by checking that results that depend on these quantities stand unchanged when these ‘unrelaxed’ groups are excluded from the analyses. We also stress that these problems in the identification of the real central galaxies in the groups are likely present in all currently available catalogs of galaxy groups, and that are possibly unavoidable; they can affect analyses of central versus satellite galaxies and studies of galaxy trends with group-centric distance which neglect correcting for (or even quantifying all together) these biases.

On the other hand, it is also important to stress that a non-negligible fraction of groups in the *ZENS* sample, of order $\sim 10 - 15\%$, is likely to be made of genuinely dynamically young, possibly merging groups. We caution against the significance in our data of differential trends in properties of centrals and satellites in relaxed and unrelaxed groups, but push forward an interpretation for such trends, which we assume and propose as a working hypothesis, because they may indeed result from dilution of real effects between relaxed and genuine merging groups. These trends and their interpretation are as follows: At constant stellar mass, central galaxies in relaxed and unrelaxed groups have similar properties, which we interpret as evidence as indicating that central galaxies owe their properties to their own mass content. If at all affected by the group environment, massive satel-

lites are most transformed as they enter the potential of a group, with successive mergers between their host group with other groups not impacting anymore the satellite properties. In contrast, low mass satellites appear to be ‘reddened’ by physical processes that take place in relaxed potential well, although at least part of this reddening may be due not to quenching but to an excess of dusty star forming systems in unrelaxed relative to relaxed groups.

Finally, we publish the *ZENS* catalogue which combines the environmental diagnostics computed in this article with the structural and spectrophotometric galactic measurements described in Cibinel et al. (2012ab).

We have so far used the first-epoch *ZENS* catalogue of 769 galaxies in the 79 first-epoch groups to study, respectively, in the diverse environments probed with *ZENS*: variations in galaxy concentration at constant mass and Hubble type (Cibinel et al. 2012a, Paper II); galaxy color gradients and color maps (Cibinel et al. 2012b, paper III); variations at constant stellar mass and Hubble types in the passive fractions of satellite galaxies (Lu et al. 2012, Paper IV); colors of bulge and disk components of satellite galaxies (Rudick et al. 2012, Paper V); variations in central-satellite and satellite-satellite merger fractions, and in structural and star formation properties of merging galaxies compared with non-merging systems of similar stellar mass (Pipino et al. 2012, Paper VI); differences in sizes, surface mass densities, and star formation properties separately for satellites and centrals (Carollo et al. 2012, Paper VII); and variations in the fractions of barred disks for different morphological and spectral types (Cibinel et al. 2012, Paper VIII). These and other *ZENS* analyses underway, which monitor simultaneously all physically relevant galaxy and environmental properties, push towards a picture where galactic transformations are driven by the ‘immediate surroundings’ environment that galaxy experience during the hierarchical assembly of mass with cosmic time.

ACKNOWLEDGMENTS

A.C., E.C., T.L. and C.R. acknowledge support from the Swiss National Science Foundation. This publication makes use of data from ESO Large Program 177.A-0680, and data products from the Two Micron All Sky Survey, which is a joint project of the University of Massachusetts and the Infrared Processing and Analysis Center/California Institute of Technology, funded by the National Aeronautics and Space Administration and the National Science Foundation. *GALEX (Galaxy Evolution Explorer)* is a NASA Small Explorer mission. The Millennium Simulation databases used in this paper and the web application providing online access to them were constructed as part of the activities of the German Astrophysical Virtual Observatory.

REFERENCES

- Abazajian, K. N., Adelman-McCarthy, J. K., Agüeros, M. A., et al. 2009, *ApJS*, 182, 543
 Arnouts, S., et al. 2007, *A&A*, 476, 137
 Baldry, I. K., Balogh, M. L., Bower, R. G., et al. 2006, *MNRAS*, 373, 469
 Balogh, M. L., Morris, S. L., Yee, H. K. C., Carlberg, R. G., & Ellingson, E. 1999, *ApJ*, 527, 54
 Balogh, M. L., & Morris, S. L. 2000, *MNRAS*, 318, 703
 Balogh, M., et al. 2004, *MNRAS*, 348, 1355
 Bertin, E., & Arnouts, S. 1996, *A&AS*, 117, 393
 Blanton, M. R., Eisenstein, D., Hogg, D. W., Schlegel, D. J., & Brinkmann, J. 2005, *ApJ*, 629, 143
 Bolzonella, M., et al. 2010, *A&A*, 524, A76
 Brinchmann, J., & Ellis, R. S. 2000, *ApJ*, 536, L77
 Bundy, K., Ellis, R. S., Conselice, C. J., et al. 2006, *ApJ*, 651, 120
 Bundy, K., et al. 2010, *ApJ*, 719, 1969
 Calvi, R., Poggianti, B. M., Fasano, G., & Vulcani, B. 2012, *MNRAS*, 419, L14
 Cardelli, J. A., Clayton, G. C., & Mathis, J. S. 1989, *ApJ*, 345, 245
 Carollo, C. M., Scarlata, C., Stiavelli, M., Wyse, R. F. G., & Mayer, L. 2007, *ApJ*, 658, 960
 Carollo, C. M. et al. 2012, in prep. (Paper IX)
 Chary, R., & Elbaz, D. 2001, *ApJ*, 556, 562
 Cibinel, A. Carollo, C. M. et al. 2012a, *ApJ*, submitted. (Paper II)
 Cibinel, A., Carollo, C. M. et al. 2012b, *ApJ*, submitted (Paper III)
 Cibinel, A., Carollo, C. M. et al. 2012c, in prep. (Paper VIII)
 Cole, S., et al. 2005, *MNRAS*, 362, 505
 Colless, M., et al. 2001, *MNRAS*, 328, 1039
 Cooper, M. C., Griffith, R. L., Newman, J. A., et al. 2012, *MNRAS*, 419, 3018
 Croton, D. J., Springel, V., White, S. D. M., et al. 2006, *MNRAS*, 365, 11
 Croton, D. J., et al. 2005, *MNRAS*, 356, 1155
 De Lucia, G., Weinmann, S., Poggianti, B., Aragon-Salamanca, A., & Zaritsky, D. 2011, *arXiv:1111.6590*
 De Lucia, G., & Blaizot, J. 2007, *MNRAS*, 375, 2
 Di Matteo, P., Combes, F., Melchior, A.-L., & Semelin, B. 2007, *A&A*, 468, 61
 Dressler, A. 1980, *ApJ*, 236, 351
 Dressler, A., & Shectman, S. A. 1988, *AJ*, 95, 985
 Eke, V. R., Baugh, C. M., Cole, S., et al. 2004a, *MNRAS*, 348, 866
 Eke, V. R., Frenk, C. S., Baugh, C. M., et al. 2004b, *MNRAS*, 355, 769
 Faber, S. M., Willmer, C. N. A., Wolf, C., et al. 2007, *ApJ*, 665, 265
 Feldmann, R., Carollo, C. M., Porciani, C., et al. 2006, *MNRAS*, 372, 565
 Feldmann, R., Carollo, C. M., Mayer, L., Renzini, A., Lake, G., Quinn, T., Stinson, G. S., & Yepes, G. 2010, *ApJ*, 709, 218
 Feldmann, R., Carollo, C. M., & Mayer, L. 2011, *ApJ*, 736, 88
 Font, A. S., Bower, R. G., McCarthy, I. G., et al. 2008, *MNRAS*, 389, 1619
 Fukugita M. et al., 1995, *PASP*, 107, 945
 Genzel, R., Lutz, D., Sturm, E., et al. 1998, *ApJ*, 498, 579
 Gerke, B. F., et al. 2005, *ApJ*, 625, 6
 Gómez, P. L., et al. 2003, *ApJ*, 584, 210
 Goto T. et al., 2003, *MNRAS*, 346, 601
 Gunn, J. E., & Gott, J. R., III 1972, *ApJ*, 176, 1
 Guo, Y., et al. 2009, *MNRAS*, 398, 1129
 Haas, M. R., Schaye, J., & Jeesson-Daniel, A. 2012, *MNRAS*, 419, 2133
 Hambly N. C. et al., 2001, *MNRAS*, 326, 1279
 Hansen, S. M., Sheldon, E. S., Wechsler, R. H., & Koester, B. P. 2009, *ApJ*, 699, 1333
 Hatton, S., Devriendt, J. E. G., Ninin, S., Bouchet, F. R., Guiderdoni, B., & Vibert, D. 2003, *MNRAS*, 343, 75
 Hogg, D. W., et al. 2003, *ApJ*, 585, L5
 Hopkins, P. F., Hernquist, L., Cox, T. J., & Kereš, D. 2008, *ApJS*, 175, 356
 Huchra, J. P., & Geller, M. J. 1982, *ApJ*, 257, 423
 Kauffmann, G., Heckman, T. M., White, S. D. M., et al. 2003, *MNRAS*, 341, 33
 Kewley, L. J., Geller, M. J., & Barton, E. J. 2006, *AJ*, 131, 2004
 Kimm, T., Somerville, R. S., Yi, S. K., et al. 2009, *MNRAS*, 394, 1131
 Knobel C. et al., 2009, *ApJ*, 697, 1842
 Kovač, K., et al. 2010, *ApJ*, 718, 86
 Kovač, K., et al. 2010b, *ApJ*, 708, 505
 Kron, R. G. 1980, *ApJS*, 43, 305
 Labbé, I., Huang, J., Franx, M., et al. 2005, *ApJ*, 624, L81
 Landolt A. U, 1992, *ApJ*, 104, 340

- Larson R., 1980, *ApJ*, 237, 692
- Lemson, G., & Virgo Consortium, t. 2006, arXiv:astro-ph/0608019
- Lilly, S. J., Le Fevre, O., Hammer, F., & Crampton, D. 1996, *ApJ*, 460, L1
- Lu, T., et al. 2012, in prep. (Paper IV)
- Madau, P., Ferguson, H. C., Dickinson, M. E., et al. 1996, *MNRAS*, 283, 1388
- Maddox, S. J., Efstathiou, G., Sutherland, W. J., & Loveday, J. 1990, *MNRAS*, 243, 692
- Masters, K. L., Mosleh, M., Romer, A. K., et al. 2010, *MNRAS*, 405, 783
- Muldrew, S. I., Croton, D. J., Skibba, R. A., et al. 2012, *MNRAS*, 419, 2670
- Navarro, J. F., Frenk, C. S., & White, S. D. M. 1997, *ApJ*, 490, 493
- Norberg P. et al., 2002, *MNRAS*, 336, 907
- Oemler, A., Jr. 1974, *ApJ*, 194, 1
- Oesch, P. A., Carollo, C. M., Feldmann, R., et al. 2010, *ApJ*, 714, L47
- Oke, J. B. 1974, *ApJS*, 27, 21
- Park, C., Choi, Y.-Y., Vogeley, M. S., et al. 2007, *ApJ*, 658, 898
- Peng, Y.-j., et al. 2010, *ApJ*, 721, 193
- Peng, Y., Lilly, S. J., Renzini, A., & Carollo, M. 2012, arXiv:1106.2546
- Pipino, A. et al. 2012, *ApJ*, in prep. (Paper VI)
- Postman M. and Geller M. J., 1984, *ApJ*, 281, 95
- Pozzetti, L., Bolzonella, M., Zucca, E., et al. 2010, *A&A*, 523, A13
- Raichoor, A., Mei, S., Stanford, S. A., et al. 2012, *ApJ*, 745, 130
- Rasmussen J. et al., 2006, *MNRAS*, 370, 453
- Rasmussen, J., Ponman, T. J., Verdes-Montenegro, L., Yun, M. S., & Borthakur, S. 2008, *MNRAS*, 388, 1245
- Rasmussen, J., Bai, X.-N., Mulchaey, J. S., et al. 2012, *ApJ*, 747, 31
- Rodighiero, G., Vaccari, M., Franceschini, A., et al. 2010, *A&A*, 515, A8
- Romano-Díaz, E., & van de Weygaert, R. 2007, *MNRAS*, 382, 2
- Rudick, C. S. et al. 2012, in prep. (Paper V)
- Rudick, C. S. et al. 2012b, in prep. (Paper VII)
- Schlegel, D. J., Finkbeiner, D. P., & Davis, M. 1998, *ApJ*, 500, 525
- Silverman, J. D., Kampczyk, P., Jahnke, K., et al. 2011, arXiv:1109.1292
- Simha, V., Weinberg, D. H., Davé, R., et al. 2009, *MNRAS*, 399, 650
- Skibba, R. A. 2009, *MNRAS*, 392, 1467
- Skibba, R. A., Masters, K. L., Nichol, R. C., et al. 2011, arXiv:1111.0969
- Skrutskie, M. L. et al., 2006, *AJ*, 131, 1163
- Smith, B. J., Struck, C., Hancock, M., et al. 2007, *AJ*, 133, 791
- Somerville, R. S., & Primack, J. R. 1999, *MNRAS*, 310, 1087
- Springel, V., & Hernquist, L. 2005, *ApJ*, 622, L9
- Springel, V., White, S. D. M., Jenkins, A., et al. 2005b, *Nature*, 435, 629
- Strateva I., et al., 2001, *ApJ*, 122, 1861
- van den Bosch, F. C., Aquino, D., Yang, X., et al. 2008, *MNRAS*, 387, 79
- Weinmann, S. M., van den Bosch, F. C., Yang, X., & Mo, H. J. 2006b, *MNRAS*, 366, 2
- Weinmann, S. M., Kauffmann, G., van den Bosch, F. C., Pasquali, A., McIntosh, D. H., Mo, H., Yang, X., & Guo, Y. 2009, *MNRAS*, 394, 1213
- Wetzel, A. R., Tinker, J. L., & Conroy, C. 2011, arXiv:1107.5311
- Williams, R. J., Quadri, R. F., Franx, M., van Dokkum, P., & Labbé, I. 2009, *ApJ*, 691, 1879
- Wilman, D. J., Zibetti, S., & Budavári, T. 2010, *MNRAS*, 406, 1701
- Wolf, C., Aragón-Salamanca, A., Balogh, M., et al. 2009, *MNRAS*, 393, 1302
- Woo, J., Dekel, A., Faber, S. M., et al. 2012, arXiv:1203.1625
- Yang, X., Mo, H. J., van den Bosch, F. C., & Jing, Y. P. 2005, *MNRAS*, 356, 1293
- Yang, X., Mo, H. J., van den Bosch, F. C., et al. 2007, *ApJ*, 671, 153
- York, D. G., Adelman, J., Anderson, J. E., Jr., et al. 2000, *AJ*, 120, 1579
- Zehavi I. et al., 2002, *ApJ*, 571, 172

Table 1
Coordinates, properties and LSS environment of the *ZENS* groups.

name	RA (B1950)	DEC (B1950)	z	r_{rms} (Mpc)	\hat{R}_{200} (Mpc)	σ (km s ⁻¹)	L_{GROUP} (10 ¹⁰ L _⊙)	N_m	M_{GROUP} (10 ¹² M _⊙)	$\log(1 + \delta_{LSS})$	Env.
² 2PIGG-s1248*	23:41:34.53	-26:44:18.8	0.05188	0.362	0.340	600.7	4.990	8	4.683	0.78	4
² 2PIGG-s1272*	23:37:55.83	-30:07:02.9	0.05079	0.784	0.465	247.6	8.602	9	11.98	0.03	2
² 2PIGG-s1282*	23:43:44.24	-27:40:01.7	0.05038	0.446	0.356	148.8	5.414	8	5.363	0.65	4
² 2PIGG-s1308*	23:59:16.70	-35:45:24.3	0.05143	0.338	0.328	287.4	4.678	5	4.211	0.34	3
² 2PIGG-s1313	23:43:59.64	-28:17:42.9	0.05020	0.454	0.445	57.2	7.976	6	10.49	0.40	3
⁵ 2PIGG-s1325	22:28:47.25	-27:04:44.6	0.05066	0.222	0.363	42.0	5.624	5	5.719	-0.00	2
⁵ 2PIGG-s1334	23:31:22.74	-30:08:48.2	0.05157	0.785	0.840	301.9	26.53	23	70.70	0.92	4
² 2PIGG-s1349*	23:53:45.32	-25:48:25.1	0.05122	0.272	0.236	132.0	2.378	6	1.564	-0.38	1
² 2PIGG-s1390*	22:11:20.62	-26:12:44.0	0.05192	0.481	0.449	261.7	8.102	5	10.78	0.73	4
² 2PIGG-s1418*	02:29:19.43	-25:23:58.9	0.05275	0.349	0.271	264.8	3.218	5	2.374	0.00	2
⁵ 2PIGG-s1454	01:16:41.52	-31:21:13.0	0.05270	0.373	0.288	161.5	3.653	5	2.861	0.15	2
⁵ 2PIGG-s1459	22:39:44.52	-25:22:48.2	0.05294	0.380	0.283	58.3	3.529	5	2.717	0.57	3
⁵ 2PIGG-s1471	23:42:25.65	-26:54:06.7	0.05276	0.721	0.689	255.4	17.49	15	39.06	0.97	4
² 2PIGG-s1476*	00:38:10.18	-28:16:13.4	0.05366	0.395	0.325	172.1	4.610	5	4.116	0.29	3
⁵ 2PIGG-s1481	23:18:56.30	-30:30:23.4	0.05360	0.243	0.410	24.9	6.969	7	8.280	-0.26	1
² 2PIGG-s1520*	23:59:28.18	-35:09:38.0	0.05434	0.603	0.505	219.3	9.951	9	15.46	0.48	3
⁵ 2PIGG-s1538	00:33:27.53	-31:31:14.4	0.05447	0.254	0.366	43.4	5.724	5	5.894	0.37	3
² 2PIGG-s1554*	22:05:41.02	-24:16:55.8	0.05610	0.448	0.598	286.9	13.41	6	25.64	0.90	4
² 2PIGG-s1571*	02:34:50.63	-25:36:33.5	0.05676	0.286	0.501	330.8	9.835	10	15.14	0.95	4
² 2PIGG-s1572*	01:36:09.86	-26:20:05.3	0.05534	0.312	0.308	160.8	4.173	5	3.510	-0.24	1
¹ 2PIGG-s1600*	02:44:28.07	-28:15:32.1	0.05561	0.208	0.438	90.8	7.810	6	10.11	-0.04	2
⁵ 2PIGG-s1601	22:41:13.88	-32:54:00.8	0.05634	0.650	0.466	169.7	8.653	10	12.11	0.00	2
² 2PIGG-s1606*	02:10:42.52	-26:56:25.8	0.05700	0.353	0.515	405.0	10.29	7	16.37	0.81	4
⁵ 2PIGG-s1609	23:01:09.93	-33:24:56.6	0.05461	0.636	0.849	171.4	27.29	12	73.36	0.77	4
⁵ 2PIGG-s1613	22:50:31.74	-33:19:03.5	0.05552	0.306	0.279	52.3	3.433	5	2.607	-0.10	2
⁴ 2PIGG-s1614	22:22:29.12	-25:38:30.9	0.05676	0.658	0.746	447.0	20.59	18	49.80	0.60	4
⁵ 2PIGG-s1632	02:36:41.35	-27:09:22.1	0.05704	0.367	0.538	335.3	11.10	9	18.69	0.89	4
⁵ 2PIGG-s1635	00:14:10.01	-27:25:22.2	0.05578	0.549	0.579	189.1	12.64	11	23.27	0.45	3
² 2PIGG-s1641*	22:25:29.09	-30:31:27.6	0.05515	0.679	0.675	644.6	16.85	12	36.91	1.89	4
² 2PIGG-s1654*	22:26:06.85	-25:32:23.8	0.05568	0.558	0.425	116.5	7.408	7	9.214	0.31	3
³ 2PIGG-s1659	22:29:12.65	-25:39:07.8	0.05655	0.510	0.244	279.0	2.580	5	1.743	0.15	2
⁵ 2PIGG-s1661	01:55:37.94	-27:40:31.3	0.05650	0.393	0.253	211.3	2.802	5	1.951	0.46	3
² 2PIGG-s1662*	22:05:07.47	-29:11:55.6	0.05616	0.667	0.492	206.0	9.512	6	14.30	1.35	4
² 2PIGG-s1665	02:35:48.88	-26:54:17.1	0.05701	0.900	0.885	284.2	30.06	13	83.24	0.80	4
² 2PIGG-s1666*	23:56:22.08	-34:08:53.4	0.05649	0.752	0.415	150.1	7.100	8	8.551	0.78	4
⁵ 2PIGG-s1670	01:03:41.10	-34:29:55.1	0.05708	0.323	0.379	289.6	6.092	5	6.554	0.23	3
² 2PIGG-s1671*	22:21:10.37	-30:15:31.1	0.05671	0.469	0.618	210.1	14.26	10	28.34	0.51	3
² 2PIGG-s1673*	02:31:18.64	-26:40:47.4	0.05619	0.500	0.302	n.a.	4.008	5	3.296	0.75	4
² 2PIGG-s1677*	22:15:49.09	-26:48:48.5	0.05630	0.392	0.630	99.6	14.78	6	30.03	1.04	4
² 2PIGG-s1688*	22:03:50.60	-24:22:35.0	0.05510	1.163	0.665	398.0	16.34	13	35.19	0.83	4
² 2PIGG-s1691	23:49:42.16	-34:05:28.6	0.05635	0.570	0.616	175.1	14.16	9	28.04	0.48	3
⁵ 2PIGG-s1696	01:52:32.06	-28:23:38.3	0.05780	0.305	0.384	423.0	6.227	5	6.804	0.04	2
⁵ 2PIGG-s1704	02:07:03.44	-26:55:54.6	0.05707	0.244	0.487	138.0	9.349	8	13.87	0.24	3
² 2PIGG-s1708*	22:17:33.50	-32:56:16.8	0.05675	0.441	0.667	90.6	16.47	7	35.61	0.47	3
⁵ 2PIGG-s1721	23:57:13.34	-33:46:02.4	0.05754	0.775	0.450	169.4	8.188	6	10.99	0.94	4
⁵ 2PIGG-s1729	01:37:38.25	-28:12:32.3	0.05662	0.689	0.601	52.2	13.54	5	26.07	0.01	2
² 2PIGG-s1730*	02:09:44.75	-25:58:15.7	0.05746	0.371	0.399	215.4	6.659	5	7.646	-0.14	1
² 2PIGG-s1735*	23:57:15.26	-34:44:59.1	0.05663	0.770	0.670	185.6	16.60	13	36.04	0.88	4
² 2PIGG-s1744*	22:05:50.68	-24:52:57.9	0.05664	0.642	0.439	216.4	7.829	7	10.15	1.20	4
⁵ 2PIGG-s1749	01:49:55.62	-28:45:38.2	0.05692	0.377	0.285	60.0	3.578	6	2.773	-0.07	2
² 2PIGG-s1752*	22:18:23.02	-26:15:32.7	0.05773	0.351	0.775	194.4	22.37	11	56.01	0.72	4
⁵ 2PIGG-s1762	01:56:00.40	-30:49:20.9	0.05711	0.358	0.343	n.a.	5.094	5	4.846	-0.57	1
² 2PIGG-s1767*	02:10:38.51	-26:39:21.3	0.05735	0.855	0.511	242.0	10.16	11	16.03	0.60	4
² 2PIGG-s1783*	22:14:30.38	-37:14:49.1	0.05833	0.256	0.741	208.9	20.37	8	49.00	0.79	4
⁵ 2PIGG-s1786	00:59:46.79	-28:41:06.9	0.05758	0.301	0.482	109.6	9.180	8	13.43	0.03	2
² 2PIGG-s1793	23:46:48.92	-31:03:35.2	0.05728	0.717	0.339	n.a.	4.998	5	4.694	0.05	2
⁵ 2PIGG-s1798	00:56:46.93	-26:44:43.0	0.05761	0.459	0.510	142.8	10.12	6	15.93	-0.44	1
⁵ 2PIGG-s1799	01:12:14.90	-34:12:01.3	0.05819	0.438	0.653	199.5	15.83	13	33.50	1.47	4
⁵ 2PIGG-s1802	23:38:30.06	-31:22:09.2	0.05794	0.335	0.578	136.4	12.60	7	23.16	0.76	4
² 2PIGG-s1807*	03:27:32.73	-31:44:00.3	0.05814	0.681	0.377	121.0	6.020	5	6.423	0.67	4
² 2PIGG-s1840*	22:20:27.71	-29:21:01.2	0.05825	0.799	0.583	132.0	12.81	10	23.79	0.63	4
³ 2PIGG-s1863	22:20:57.32	-29:48:30.4	0.05806	0.410	0.422	114.2	7.333	6	9.047	0.63	4
² 2PIGG-s1886*	03:16:48.81	-30:35:18.7	0.05805	0.481	0.456	87.0	8.349	5	11.37	0.52	3
⁴ 2PIGG-s1935	22:25:04.97	-30:49:51.5	0.05802	1.867	1.770	554.6	200.9	159	667.0	1.76	4
³ 2PIGG-n1267*	13:55:38.14	-04:26:56.6	0.05024	0.264	0.410	371.2	6.951	5	8.241	-0.58	1
¹ 2PIGG-n1320*	10:15:21.93	-01:07:51.4	0.05076	0.497	0.631	157.6	14.78	10	30.04	0.97	4
¹ 2PIGG-n1330*	10:25:04.34	-02:48:39.1	0.05044	0.287	0.440	n.a.	7.843	5	10.19	1.38	4

Table 1 — *Continued*

	name	RA (B1950)	DEC (B1950)	z	r_{rms} (Mpc)	\hat{R}_{200} (Mpc)	σ (km s $^{-1}$)	L_{GROUP} ($10^{10} L_{\odot}$)	N_m	M_{GROUP} ($10^{12} M_{\odot}$)	$\log(1 + \delta_{LSS})$	Env.
¹	2PIGG-n1345*	10:06:15.29	-04:15:10.6	0.05140	0.367	0.545	61.2	11.32	8	19.33	0.83	4
¹	2PIGG-n1347*	09:57:13.93	-05:02:28.0	0.05214	0.534	0.624	167.7	14.46	10	29.00	0.78	4
³	2PIGG-n1363*	12:03:15.25	-02:41:48.6	0.05207	0.289	0.402	221.0	6.727	8	7.781	-0.28	1
¹	2PIGG-n1365*	10:26:06.57	-00:53:25.5	0.05153	0.483	0.510	170.8	10.08	8	15.81	0.47	3
¹	2PIGG-n1377*	11:30:08.88	-03:33:45.5	0.05154	1.330	0.856	222.3	27.76	23	75.06	0.92	4
³	2PIGG-n1381*	14:25:37.08	-02:17:49.1	0.05215	0.426	0.468	140.0	8.704	10	12.23	1.25	4
³	2PIGG-n1382	14:06:07.75	00:04:00.8	0.05237	0.673	0.418	255.8	7.173	7	8.709	0.26	3
⁶	2PIGG-n1384	14:19:07.38	-00:08:18.9	0.05305	0.812	0.785	308.3	22.92	11	57.96	1.44	4
¹	2PIGG-n1385*	10:17:28.19	-04:46:24.7	0.05106	0.784	0.705	275.5	18.28	17	41.77	1.45	4
¹	2PIGG-n1394*	10:21:34.44	-01:48:32.7	0.05210	0.583	0.760	75.1	21.35	8	52.44	0.82	4
¹	2PIGG-n1398*	10:52:36.36	-02:26:58.4	0.05255	0.416	0.412	115.0	6.998	5	8.339	0.27	3
³	2PIGG-n1403	11:30:37.40	-02:34:04.5	0.05130	0.366	0.406	219.3	6.837	7	8.003	-0.13	2
⁴	2PIGG-n1404	13:43:09.95	-05:15:13.1	0.05211	0.446	0.777	218.7	22.37	7	56.01	0.29	3
³	2PIGG-n1413*	11:21:18.46	-03:58:43.0	0.05295	0.694	0.800	395.5	23.86	13	61.23	1.08	4
¹	2PIGG-n1416*	10:23:21.85	-02:43:11.3	0.05151	0.547	0.348	401.2	5.218	7	5.043	1.57	4
⁴	2PIGG-n1418	11:38:49.88	-02:18:59.3	0.05364	0.349	0.417	355.6	7.151	5	8.660	0.89	4
⁴	2PIGG-n1423	13:40:34.33	-04:45:17.2	0.05278	0.317	0.280	106.2	3.447	5	2.623	-0.21	1
¹	2PIGG-n1440*	10:15:00.48	-05:46:28.7	0.05390	0.948	0.753	294.5	20.98	20	51.10	0.86	4
³	2PIGG-n1441*	11:15:37.87	-04:11:11.5	0.05313	0.600	0.658	241.8	16.01	15	34.10	0.50	3
³	2PIGG-n1445*	11:22:24.09	-03:41:09.3	0.05283	0.737	0.548	106.6	11.46	8	19.73	1.03	4
⁴	2PIGG-n1449	13:32:37.51	-02:45:17.1	0.05318	0.593	0.370	79.7	5.806	5	6.039	-0.14	1
⁴	2PIGG-n1454	13:37:43.48	-04:32:33.8	0.05366	0.252	0.640	188.1	15.17	5	31.31	0.16	2
⁶	2PIGG-n1457	14:15:17.75	00:32:59.4	0.05194	0.812	1.134	552.8	55.92	30	174.1	1.87	4
¹	2PIGG-n1461*	10:16:13.64	-04:21:26.4	0.05415	0.657	0.394	253.5	6.488	10	7.306	0.45	3
³	2PIGG-n1466	14:01:26.94	-01:25:45.0	0.05292	0.906	0.747	331.9	20.59	17	49.79	0.59	3
²	2PIGG-n1467*	11:08:52.83	-04:11:27.5	0.05414	0.327	0.385	151.9	6.245	5	6.840	0.63	4
³	2PIGG-n1469*	11:39:06.31	-01:58:08.3	0.05429	0.406	0.555	155.1	11.73	6	20.51	0.76	4
⁴	2PIGG-n1472	14:03:23.30	-00:59:32.7	0.05370	0.430	0.589	176.7	13.03	5	24.46	0.70	4
¹	2PIGG-n1475*	10:19:33.68	-01:14:46.9	0.05405	0.295	0.583	252.3	12.81	5	23.79	0.66	4
³	2PIGG-n1476*	11:19:51.61	-03:59:41.7	0.05292	0.888	0.828	204.8	25.76	14	67.93	1.03	4
¹	2PIGG-n1480*	10:13:01.02	-05:22:09.4	0.05368	0.521	0.574	258.9	12.43	13	22.61	0.62	4
³	2PIGG-n1484	13:15:52.05	01:09:57.2	0.05401	0.464	0.314	84.9	4.314	5	3.700	-0.29	1
⁶	2PIGG-n1486	14:05:16.34	-00:42:48.7	0.05393	0.826	0.905	388.5	31.59	23	88.69	1.09	4
⁶	2PIGG-n1488	14:09:19.73	00:11:00.9	0.05398	0.810	0.636	190.5	15.03	9	30.86	0.49	3
²	2PIGG-n1491*	10:07:43.43	-04:44:52.6	0.05618	1.136	1.138	444.2	56.73	48	177.0	1.17	4
⁶	2PIGG-n1494	14:20:27.82	01:01:16.1	0.05389	0.291	0.376	98.1	5.998	5	6.383	0.11	2
¹	2PIGG-n1503*	11:04:23.33	-04:29:00.8	0.05419	0.432	0.400	225.5	6.678	6	7.684	0.38	3
¹	2PIGG-n1510*	10:15:35.24	-05:10:41.2	0.05475	1.003	0.767	253.6	21.84	14	54.13	0.79	4
¹	2PIGG-n1514*	10:18:30.19	-04:13:03.4	0.05433	0.688	0.733	235.7	19.87	17	47.27	1.18	4
⁶	2PIGG-n1522	14:09:21.21	00:43:55.4	0.05450	0.558	0.643	240.6	15.34	10	31.89	0.80	4
³	2PIGG-n1523	14:04:38.91	-02:29:22.8	0.05533	0.412	0.442	289.6	7.916	5	10.35	0.16	2
⁶	2PIGG-n1525	14:05:46.98	-00:21:17.1	0.05295	0.677	0.487	265.6	9.327	11	13.81	1.23	4
⁶	2PIGG-n1528	14:06:45.08	00:09:26.6	0.05363	0.921	0.425	183.8	7.384	9	9.160	0.29	3
³	2PIGG-n1532	13:34:06.07	-03:17:04.2	0.05344	1.133	0.864	127.0	28.33	15	77.10	0.86	4
⁶	2PIGG-n1533	14:07:31.39	-00:04:29.3	0.05399	0.504	0.324	257.5	4.590	5	4.086	0.88	4
³	2PIGG-n1534*	11:39:08.71	-02:34:53.7	0.05501	0.360	0.497	273.8	9.673	5	14.71	0.67	4
³	2PIGG-n1540	14:27:03.55	00:35:26.4	0.05489	1.023	1.138	275.7	56.61	32	176.6	0.79	4
³	2PIGG-n1543*	13:23:17.84	-00:25:09.4	0.05493	0.136	0.413	133.9	7.051	6	8.449	0.07	2
¹	2PIGG-n1556*	10:09:00.67	-05:38:24.9	0.05485	0.478	0.512	128.0	10.17	8	16.06	0.56	3
⁶	2PIGG-n1558	14:07:47.65	-00:52:47.0	0.05426	0.571	0.547	90.7	11.42	7	19.60	0.47	3
⁶	2PIGG-n1572	14:22:58.68	-01:16:30.3	0.05501	0.899	0.733	190.0	19.84	19	47.17	0.87	4
⁴	2PIGG-n1574	14:04:12.43	-03:27:19.1	0.05485	1.017	0.979	269.3	38.31	28	112.4	0.67	4
³	2PIGG-n1584*	14:34:02.76	00:54:18.5	0.05583	0.323	0.421	150.0	7.280	6	8.936	0.70	4
⁴	2PIGG-n1587	11:40:04.46	-02:50:06.3	0.05555	0.406	0.373	92.0	5.924	5	6.249	0.30	3
¹	2PIGG-n1588*	10:19:01.37	-04:42:04.2	0.05444	1.094	1.271	454.4	76.80	71	246.1	1.16	4
²	2PIGG-n1593*	10:17:17.68	-03:39:05.8	0.05635	0.675	0.511	231.2	10.17	9	16.04	0.67	4
⁶	2PIGG-n1597	14:25:07.25	-01:31:58.2	0.05468	1.007	0.883	351.6	29.82	16	82.37	1.07	4
³	2PIGG-n1598*	14:33:19.46	-01:03:40.0	0.05600	0.569	0.606	114.2	13.75	9	26.71	0.55	3
²	2PIGG-n1606*	10:36:15.34	02:04:02.8	0.05612	0.262	0.505	106.4	9.953	7	15.47	0.21	2
²	2PIGG-n1610*	09:51:07.59	-04:54:10.5	0.05615	0.251	0.495	145.1	9.608	10	14.54	0.63	4
⁶	2PIGG-n1622	14:28:45.22	-01:31:48.8	0.05458	0.970	1.017	524.5	42.18	27	126.1	1.22	4
²	2PIGG-n1623*	10:15:52.23	-03:41:41.9	0.05702	0.552	0.367	253.8	5.745	5	5.930	0.86	4
⁴	2PIGG-n1626	11:35:34.50	-05:10:26.9	0.05620	0.238	0.270	190.1	3.196	5	2.350	0.54	3
²	2PIGG-n1630*	14:44:22.06	-03:19:29.5	0.05846	0.538	1.042	370.3	45.02	18	136.1	1.64	4
²	2PIGG-n1637*	09:56:42.39	-04:26:00.7	0.05646	0.379	0.338	112.8	4.951	5	4.621	0.20	2
²	2PIGG-n1648*	11:02:12.89	-03:39:25.1	0.05645	0.387	0.232	37.9	2.304	5	1.500	-0.06	2
⁴	2PIGG-n1671	11:36:30.38	-04:02:25.5	0.05542	1.031	1.299	368.7	81.61	41	262.7	1.29	4
²	2PIGG-n1672*	11:03:57.41	-03:42:14.1	0.05686	0.419	0.321	177.7	4.520	5	3.987	0.16	2

Table 1 — *Continued*

name	RA (B1950)	DEC (B1950)	z	r_{rms} (Mpc)	\hat{R}_{200} (Mpc)	σ (km s ⁻¹)	L_{GROUP} (10 ¹⁰ L _⊙)	N_m	M_{GROUP} (10 ¹² M _⊙)	$\log(1 + \delta_{LSS})$	Env.
² 2PIGG-n1702*	09:51:59.37	-03:51:50.5	0.05738	0.451	0.573	69.7	12.42	9	22.60	0.72	4
² 2PIGG-n1706*	14:47:04.10	-03:25:40.7	0.05781	0.490	0.747	275.3	20.69	7	50.14	1.44	4
² 2PIGG-n1714*	10:33:34.48	-03:46:37.9	0.05760	0.652	0.550	n.a.	11.57	7	20.04	0.78	4
³ 2PIGG-n1721*	12:35:48.75	-04:16:47.8	0.05844	0.881	0.488	128.8	9.400	8	14.00	0.66	4
² 2PIGG-n1746*	14:37:43.57	-03:33:05.7	0.05849	0.520	0.516	191.4	10.34	9	16.53	0.24	3
² 2PIGG-n1829*	10:04:21.96	-05:20:25.4	0.05718	0.905	1.483	691.3	119.5	67	392.0	1.62	4

Note. — Properties of the *ZENS* groups. The first column lists the group ID. Upper-left indices in the IDs identify the observing run during which WFI *B* and *I* imaging was acquired for a given group; see Table C1 in Appendix C. The asterisks identify the 79 first-epoch groups for which the WFI *B* and *I* images have been to date reduced and analyzed, and the resulting structural and photometric measurements presented in Papers II and III, respectively (and already published in the attached catalogue). From left to the right, the other columns in the Table show right ascension and declination of the group, 2dFGRS redshift, 2PIGG r.m.s radius in Mpc, our computation of group size \hat{r}_{200} in Mpc, 2PIGG velocity dispersion σ in km s⁻¹, total group luminosity L_{GROUP} , number of members above the magnitude limit of the survey, total group mass M_{GROUP} , the value of LSS overdensity calculated with our 5th-nearest-group algorithm. The last column lists the overdensity quartile to which the groups belong relative to the global distribution of overdensities in the redshift window $0.035 < z < 0.075$ (with first and fourth quartile indicating respectively regions of lowest and highest environmental density). Definitions for all quantities are given in the text (if not self-explanatory). The IDs follow the original 2PIGG nomenclature: an ‘n’ (2PIGG-nXXXX) identifies groups located in the Northern Galactic Hemisphere; an ‘s’ identifies groups in the Southern Hemisphere.

APPENDIX

A. THE IMPACT OF THE ORIGINAL 2DFGRS MAGNITUDE LIMITS IN OUR STUDY

The 2dFGRS team made available three maps which specify for a given position in the sky θ : a) the extinction-corrected magnitude limit of the survey $b_{j,lim}(\theta)$; b) the redshift completeness $R(\theta)$, - the number of galaxies with measured redshift relative to the parent APM survey catalog, which is the photometric basis of the 2dFGRS; and c) the parameter $\mu(\theta)$ that enters the expression for the magnitude-dependent redshift completeness, $c_z(b_j, \mu(\theta)) = \gamma [1 - \exp(b_j - \mu(\theta))]$, with $\gamma = 0.99$ (Colless et al. 2001). The overall redshift completeness around a given set of celestial coordinates is given by: $C(\theta, b_j) = R(\theta)c_z(b_j, \mu(\theta))/\bar{c}_z(\mu(\theta))$. The factor $\bar{c}_z(\mu(\theta))$ is a normalization constant derived from the average of $c_z(b_j, \mu)$ over the expected apparent magnitude distribution of the survey galaxies (Colless et al. 2001; Norberg et al. 2002; Cole et al. 2005) and can be calculated using equation 7 of Colless et al. (2001).

The 2PIGG catalogue is constructed only from those fields and sectors of the 2dFGRS which have a high number of measured redshifts and during the selection of the *ZENS* groups we furthermore restricted the sample to the most complete ones (i.e. those which have galaxy weights from the 2PIGG catalogue < 1.6). This ensures that the average completeness $R(\theta)$ in the group, defined as the mean of all values at the positions in the sky of the member galaxies, is typically $\sim 90\%$. We thus compute the limiting faint magnitude at which the survey is complete at the 80% level ($< b_j^{0.80} >$) from mean estimates of the limiting magnitude without constraints on completeness ($< b_{j,lim} >$) and by inverting the expression for $C(\theta, b_j)$ given above. In calculating the factor $\bar{c}_z(\mu(\theta))$ we use a bright and faint magnitude limit of $b_j = 14$ and $b_{j,lim}(\theta)$, respectively. Figure A1 shows the derived distribution of $< b_{j,lim} >$ and $< b_j^{0.80} >$. There are small variations, amongst the *ZENS* groups, in the faintest magnitude reached by the original 2dFGRS data. As shown in the Figure, the effect is however small, with only a handful of groups having $< b_j^{0.80} >$ brighter than 19. Most of the *ZENS* groups are complete down to the ($< b_{j,lim} >$) limit. We have checked in all cases that none of our results are affected by this modest field-to-field scatter in completeness in the *ZENS* fields.

We finally applied corrections for spectroscopic completeness. As done in the 2dFGRS studies, these are obtained by assigning to each galaxy a weight w defined as $w = 1/C(\theta, b_j)$, such that the complete number of galaxies N (total, or of a given type) is $N = \sum_i 1/w_i$.

B. IMPACT OF ‘MISSED’ GALAXIES ON OUR ANALYSES

B.1. Searching in the SDSS for galaxies missed by the 2dFGRS

To identify biases in the *ZENS* sample introduced by galaxies ‘missed’ by the 2dFGRS¹², we studied the SDSS DR7 spectroscopic catalogue of Abazajian et al. (2009). About a quarter (42 of 141) *ZENS* groups are located in fields that overlap with the SDSS (16 of which are amongst the 79 first-epoch *ZENS* groups). For each of these 42 groups, the search for missed galaxies was performed on circular projected areas of radius equal to 1.5 times the r.m.s. radius of the group, centered on either the nominal most massive galaxy for the already analyzed, first-epoch groups, or on the 2PIGG original center, for the remainder groups.

To set an operational definition, we considered as plausible missed galaxies in each of these groups galaxies with coordinates within these circular areas, and with redshifts between $z_{min} - \delta < z < z_{max} + \delta$. Here z_{min} and z_{max} are the minimum and maximum redshift of the galaxies in the given 2PIGG group, and δ was set equal to 30% of the

¹² This approach is similar to the one we adopted in Section 3.1.1.1 to search for suitable galaxies in the 2dFGRS which had

not been associated with a given group by the 2PIGG algorithm.

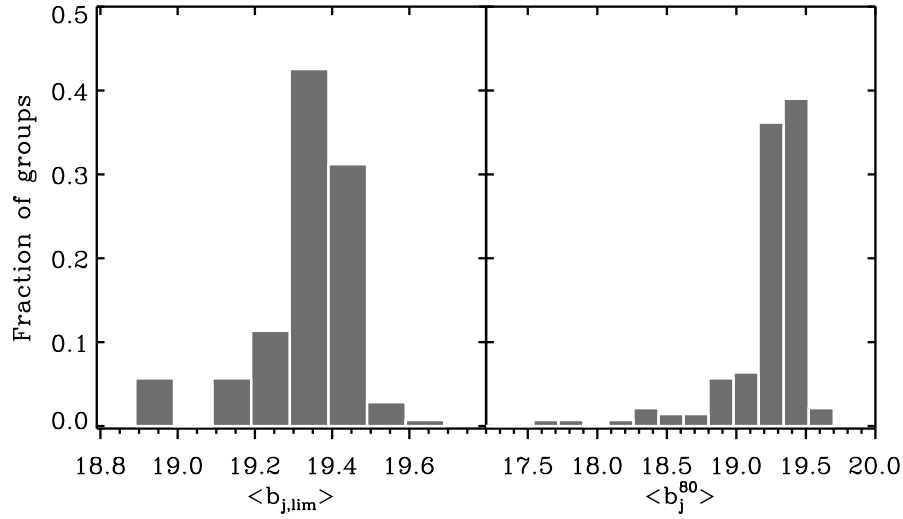


Figure A1. Completeness of the 2dFGRS over the targeted *ZENS* fields. Left: Average value of the limiting magnitude in the 2dFGRS catalog, without constraints on completeness. Right: Mean limiting magnitude for the *ZENS* fields, imposing a 80% completeness level in the 2dFGRS images.

redshift interval spanned by the nominal 2PIGG galaxy members of that group. Adopting $\delta \sim 10\%$ does not alter the results that we report below.

We found a total of 59 ‘extra’ galaxies in the SDSS which satisfied these criteria in 20 of the total 42 *ZENS* groups with SDSS pointings. A summary of the fields with these ‘extra’ galaxies is given in Table B1. As indicated in this Table, only a small fraction of these galaxies have magnitudes below the nominal selection limit of the 2dFGRS (for 25 galaxies we could not find the information on the b_j magnitude; for these we used the relation between b_j and SDSS g magnitudes for those galaxies in which both are available). An analysis of the images shows that fiber collisions should not be a main reason for the absence of these galaxies from the 2dFGRS catalog. Although ultra-compact galaxies could be missed due to a star/galaxy misclassification, generally these galaxies seem simply casualties of the 2dFGRS statistical sampling. In the sample of 16 first-epoch *ZENS* groups in SDSS fields, only 7 had plausible ‘extra’ member candidates in the SDSS catalogue which are not listed as 2dFGRS targets, for a total of 11 such ‘extra’ galaxies, to be compared with a total of 68 nominal 2PIGG members in these 7 groups.

The statistics above suggests that of order $\sim 40 - 50\%$ of the *ZENS* groups and in general of the 2PIGG groups are potentially missing some member galaxies above the 2dFGRS magnitude limit, due to their absence from the parent 2dFGRS catalog. We use this information to assess an order of magnitude estimate for the impact of the plausible extra members on our analyses, including group mass estimates as well as the definition of centrals and satellites.

In Table B1 we show the nominal group masses for these seven groups; even assuming that all missed SDSS galaxies are additional members of the relevant *ZENS* groups changes the group masses by less than 30% in four of them. In two of the remaining the change is 60% and in one the mass would change by a factor of two (see Table B1). These results imply little or no effect on the group mass estimates resulting from these missed potential group members.

We then ran on these 7 groups the algorithm described in Section 3.2.1 for the identification of central and satellite galaxies, this time also including the 11 extra galaxies (using the total stellar masses provided in the MPA/JHU value added catalog for the masses of the extra SDSS galaxies; in Paper III we use a sample in common to show that there are no severe systematics between our estimates for galaxy stellar masses and those of this catalog). Since for the extra SDSS galaxies we do not have information on the full PPDs for their stellar mass, we generated artificial Gaussian PPDs, centered on the galaxy MPA/JHU stellar mass, and with a standard deviation of 0.3 dex. Only in two of these seven groups (2PIGG-n1363 and 2PIGG-n1469) the inclusion of the extra SDSS galaxies results in a possible change in the identification of the central galaxy. One of these two potential ‘SDSS centrals’ has structural, morphological stellar mass and star formation properties very similar to those of the nominal *ZENS* central. In the remaining case, the ‘SDSS central’ is a quiescent E/S0 galaxy, in contrast with the nominal *ZENS* central, which had an intermediate disk morphology and an intermediate SFR (see Paper III for our definitions of quiescent, moderately star-forming and strongly star-forming). While in principle such situation may lead to uncertainties in the analysis of the central and satellite galaxy populations, the global statistics are comforting.

Under the reasonable assumption that the 16 reduced groups with SDSS pointings are representative for the complete 2PIGG sample, we estimate the incompleteness relative to the SDSS as follows. We first assumed that all missed SDSS galaxies are physically associated with the 7 groups in question, and that the true central galaxies in the two aforementioned groups, for which the inclusion of the SDSS extra sample leads to a change in the identification of the central, are indeed the two newly added SDSS galaxies rather than the nominal *ZENS* centrals. Considering all

16 groups for which we know whether they are (or not) missing SDSS galaxies, we then defined (i) the number of centrals that we should have observed, $n_{centrals} = 16$; (ii) the number of centrals that we have correctly identified, $n_{centrals,obs} = 14$; (iii) the number of satellites that we should have observed, $n_{sats} = 123$ (i.e., the total sample of 128 2PIGG members of the 16 groups in question, plus the 11 extra SDSS galaxies found in total for this sample, minus 16, the number of their centrals); (iv) the number of satellites which are misclassified as centrals, $n_{false-cen} = 2$, and, finally, (v) the number of correctly identified satellites $n_{sats,obs} = 112$ (i.e., the total sample of 128 2PIGG members, minus 16 centrals). We then estimate the level of incompleteness due to missing SDSS galaxies in the 2dFGRS sample as, for the central galaxies, $1 - n_{centrals,obs}/n_{central} \sim 10\%$, and, for the satellites, $1 - n_{sats,obs}/n_{sats} \sim 10\%$. This implies a level of contamination of satellites incorrectly identified as centrals of $n_{false-cen}/n_{centrals} \sim 10\%$. All these are upper limits to the fraction of misidentifications, since not all ‘extra’ galaxies identified as described above will be missed group members. We therefore conclude that this specific source of uncertainty in the identification of the central (and thus satellite) galaxy populations is not a dominant one. Such identification remains mostly affected by other factors such as the global impact of the friend-of-friend clustering algorithm used for the identification of bound galaxy groups.

For the two groups with a candidate ‘missed’ central galaxy, we had to decide to which galaxy to assign the rank of central. We maintained the identification of the central galaxies in these two groups with the original centrals found amongst the nominal 2PIGG group members, and checked that this choice (involving only two groups) does not affect any of our conclusions.

B.2. *ZENS* galaxies missed by *ZENS* pointings

Another possible source of error in the estimate of group mass and identification of centrals and satellites are galaxies missed in the WFI observations. For 13 of the 79 first-epoch groups, the WFI pointings did not cover their entire extent, resulting in a total of 68 members for which no *B*– and *I*–band imaging is available. These groups are indicated with an exclamation mark in Figure 9. For 9 groups the fraction of missing members is $< 20\%$ of the true group richness, for other three is between $20 - 30\%$ and only for one massive group (2PIGG-n1377) is as high as 45% . We include in the *ZENS* catalogue these galaxies out-of-WFI-field, setting to null entries all quantities which rely on the WFI photometry except for the galaxy mass. A mass estimate for these galaxies was in fact obtained from the linear relation between the SuperCosmos Survey (Hambly et al. 2001) r_F magnitude (provided in the 2dFGRS data release and corrected for galactic extinction) and the SED inferred galaxy mass, as derived for the *ZENS* galaxies with available *B*– and *I*–band observations. We assumed for the mass probability distribution of these galaxies a Gaussian centered on the mass predicted by the $r_F - M$ relation, and having a deviation equal to 1.5 times the observed scatter of this relation.

Table B1
ZENS groups with extra candidate galaxy members in the SDSS

Name	Nominal members	SDSS candidates	Below $b_{j,lim}$	M_{GROUP}
2PIGG_m1363*	8	2	-	7.781×10^{12}
2PIGG_m1377*	23	1	-	7.506×10^{13}
2PIGG_m1381*	10	3	-	1.223×10^{13}
2PIGG_m1384	11	1	1	5.796×10^{13}
2PIGG_m1418	5	1	-	8.660×10^{12}
2PIGG_m1457	30	9	1	1.741×10^{14}
2PIGG_m1469*	6	1	-	2.051×10^{13}
2PIGG_m1472	5	1	-	2.446×10^{13}
2PIGG_m1486	23	4	-	8.869×10^{13}
2PIGG_m1522	10	2	-	3.189×10^{13}
2PIGG_m1523	5	1	-	1.035×10^{13}
2PIGG_m1525	11	2	-	1.381×10^{13}
2PIGG_m1532	15	1	-	7.710×10^{13}
2PIGG_m1540	32	10	2	1.766×10^{14}
2PIGG_m1543*	6	1	-	8.449×10^{12}
2PIGG_m1572	19	2	-	4.717×10^{13}
2PIGG_m1584*	6	1	-	8.936×10^{12}
2PIGG_m1597	16	4	-	8.237×10^{13}
2PIGG_m1598*	9	2	1	2.671×10^{13}
2PIGG_m1622	27	10	-	1.261×10^{14}

Note. — The *ZENS* groups for which candidate ‘extra galaxy members’ were found in the SDSS DR7 spectroscopic sample, according to the criterion described in Appendix B.1. For each groups we specify the number of original 2PIGG members (column 2), the number of SDSS galaxies which are not in 2dFGRS (column 3), and, amongst these, the number of galaxies whose magnitudes lie below the 2dFGRS selection limits (columns 4). In column 5 we list the fiducial group masses based on the extrapolation of the luminosity function (in units of M_\odot), as sampled by the 2PIGG galaxies (see Section 3.1).

We again asked whether these ‘missed’ galaxies could be the true central galaxies in groups for which we failed to find a self-consistent solution in Section 3.2.1. In the majority of cases, such galaxies that lie beyond the WFI

pointings are small satellites in the outskirts of the groups. In fact, 90% of the galaxies that fall outside our WFI pointings are substantially more than a factor of four less massive than the most massive group member; 60% of these ‘missed’ galaxies have masses below the mass completeness limit of our study. Only for two groups, 2PIGG-s1272 and 2PIGG-n1377, our scheme for the definition of the group center identified one of the galaxies with no B - and I -band WFI imaging as a possible candidate central galaxy. From a statistical perspective, this again a negligible contributor to the misidentification of central and satellite galaxies in our sample.

Again we had to decide on which galaxy to consider the central in these two groups. Given that the uncertainties on the masses for the ‘missed’ galaxies are substantially larger than for the rest of the sample, and that the difference between the mass of these ‘missed’ galaxies and the highest mass in the galaxies imaged by the WFI was marginal, we decided to keep the identification of the central galaxies in these two ‘unrelaxed’ groups with the most massive galaxy imaged in our WFI data. As expected, given that only two groups are involved, this choice does not affect our conclusions.

B.3. Search in the 2dFGRS for potential missed members of the ZENS-2PIGG groups

As mentioned in Section 3.1.1.1, the search for 2dFGRS galaxies not included in a given *ZENS* (i.e. 2PIGG) group but with magnitudes, coordinates and redshifts within ranges that could possibly make them members of this group (according to the criteria listed in Section 3.1.1.1), resulted in a total of 26 galaxies distributed over 11 of the 79 first-epoch *ZENS* groups. Figure B1 shows the spatial (left panels) and velocity (right panels) distributions for these possible candidate members, in relation to the galaxies which compose the *ZENS* group extracted from the 2PIGG catalog. Note that often they cluster both spatially and in velocities. While statistically their identification with independent groups is validated by the comparisons with mock catalogues, it is clear that, on a group-to-group basis, it is not possible to exclude that, at least some of these galaxies, may be missed members of the 2PIGG groups that we study in *ZENS*. The velocity dispersions and masses of these groups would however not change substantially if the potential extra candidate members were added to them, as these groups have already relatively high total masses, as shown in Figure B2 (see also Section 3.1.1.1). Furthermore, none of these extra galaxies would qualify as being the central galaxies in the *ZENS* groups of which they could potentially be extra group members. We therefore neglect these extra galaxies in any future analysis, and restrict the group membership in the *ZENS* groups to the nominal 2PIGG members.

C. PROPERTIES, REDUCTION AND PHOTOMETRIC CALIBRATION OF THE WFI B AND I DATA

Table C1 gives a log of the observing runs for the new ESO/2.2m B and I WFI images. These images were taken with the 4×2 mosaic of $2k \times 4k$ coated CCDs, which provides a scale of $0.238''/\text{pix}$ and covers a total field of view of $34' \times 33'$, well suited to the typical sizes of the *ZENS* groups. Each group was observed with five dithered exposures to remove inter-chip gap effects and cosmic rays events; the single exposure times were 132s for the 2005 runs and 144s for all other runs. All observations were carried out under clear night conditions. For the 79 first-epoch groups, the final seeing after image stacking is typically $\sim 1''$, reaching down for the best runs to $0.7''$ and $0.9''$ in the I - and B -band, respectively, and, in a few worst cases, degrading to $1.5''$ and $1.6''$. Figure C1 gives a summary of the airmass and seeing conditions of the WFI observations.

The *ZENS* detection limits are given by the 1σ background fluctuations in a uniform area of 1 arcsec^2 (18 pixels) and correspond to $\mu(B) = 27.2 \text{ mag arcsec}^2$ and $\mu(I) = 25.5 \text{ mag arcsec}^2$ (AB magnitudes). The depth of the WFI B and I data allow us to robustly quantify the structure of the *ZENS* galaxies out to at least 2 half-light radii, and to detect low surface brightness tidal tails and merger-induced features. At the given depth limits, and with a total sky coverage of 45 deg^2 , *ZENS* is a relatively deep survey on a relatively large area, and thus a valuable dataset also for legacy science.

Table C1
Log of Observing Runs

Run	Date	Exposure Time (sec)	Number of Groups	Program ID	Mode
1	Jan. 5 - Feb. 18, 2005	131.917	20	074.B-0570	Service
2	May 1 - Dec. 23, 2006	143.917	50	177.A-0680(A/B)	Service
3	Feb. 18 - July 14, 2007	143.917	21	177.A-0680(A/B)	Service
4	March 14 - July 31, 2008	143.917	12	177.A-0680(A/B)	Service
5	Oct. 30 - Nov. 5, 2008	143.917	25	177.A-0680(C)	Visitor
6	Mar. 25 - Mar. 28, 2009	143.917	13	177.A-0680(D)	Visitor

Note. — For each set of observations we list the exposure times, the number of observed groups and the program ID and mode. Sequential numbers in the first columns indicate the run ID.

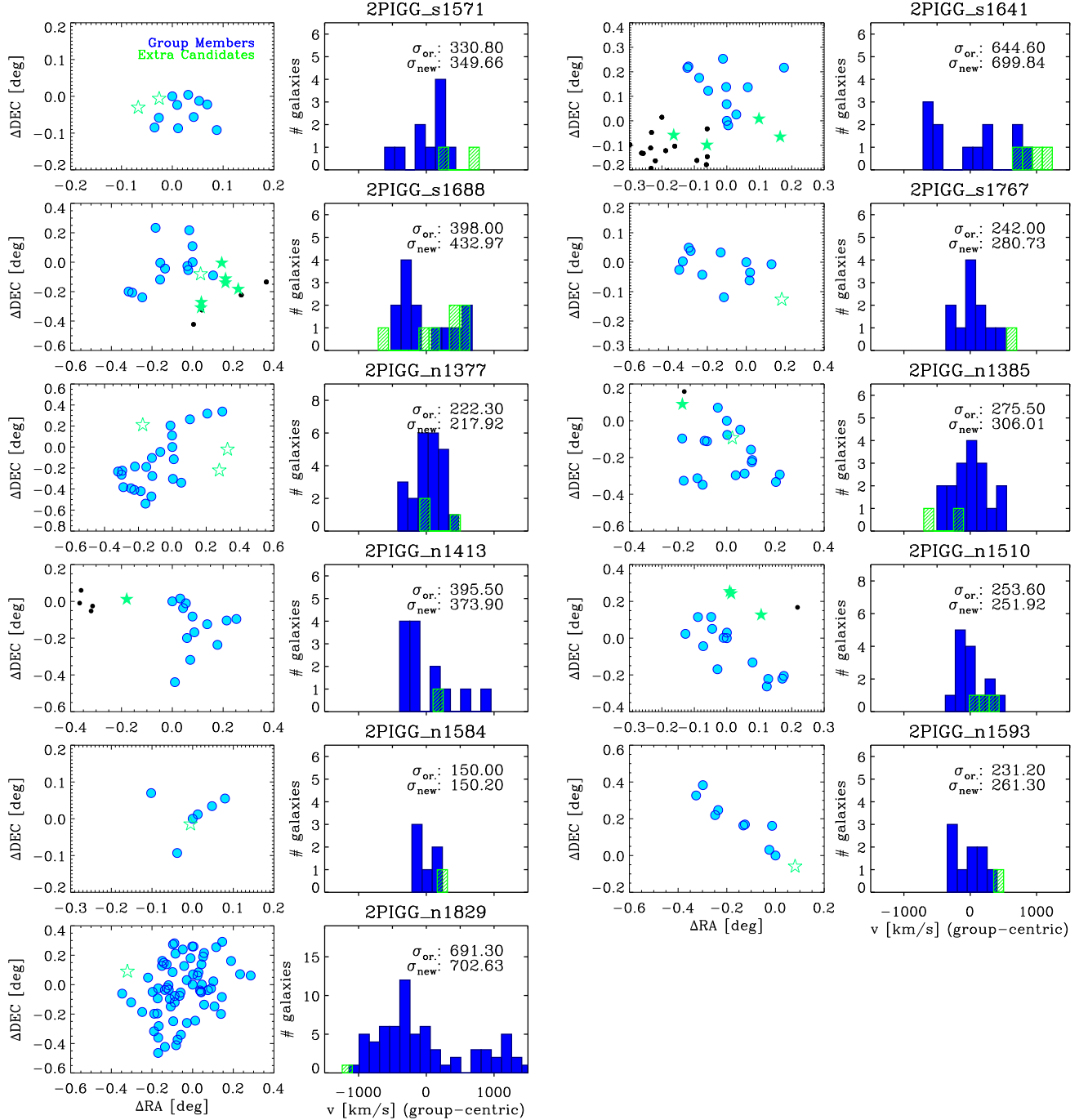


Figure B1. *Left:* The projected spatial distribution, relative to the group central galaxy as defined in Section 3.2.1 (placed at the (0,0) position) of potential group member galaxies in the 2dFGRS catalog, which are not listed as members of the 2PIGG groups that we use in *ZENS*. The nominal 2PIGG member galaxies are shown as filled circles, the potential extra group members as stars. Amongst these potential 'extra' candidate members for a given 2PIGG group, we identify with empty stars galaxies which are not associated with any other 2PIGG group, and with filled stars galaxies which are associated with a different 2PIGG group. We also show as black dots the remaining galaxies members of these other 2PIGG groups to which the filled-star galaxies belong, although these dot-galaxies do not qualify to be potential extra members of our *ZENS* groups, according to the definition discussed in Section 3.1.1.1. *Right:* The corresponding distribution of relative velocities of galaxies with respect to the mean redshift of the group. Solid histograms show the velocities for the original 2PIGG group members, and dashed histograms give the relative velocities of the potential 'extra' candidate members. The values of the velocity dispersion of the groups, computed before and after the inclusion of these potential extra members, are given in the top-right corners of the plots. These velocity dispersions are calculated with the gapper estimator as in Eke et al. (2004a).

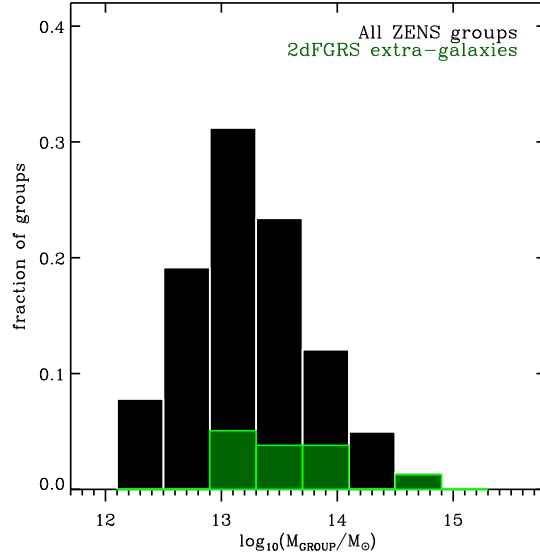


Figure B2. In green we show the distribution of fiducial group masses for the 11 *ZENS* groups for which we have found, in the 2dFGRS catalog, galaxies which are consistent with being additional group members (according to the definition given in Section 3.1.1.1). For comparison, the black histogram shows the distribution of fiducial group masses for the entire *ZENS* sample. The green histogram is normalized to the total number of groups in the *ZENS* sample.

C.1. Data Reduction

The WFI *B* and *I* images were reduced using standard IRAF¹³ routines and in particular the NOAO mosaic software *MSCRED* was used for most of the processing.

The bias subtraction involved two steps: each frame was initially subtracted of a bias level using, for each pixels row, the median value of the overscan pixels in the same row. Remaining large scale features in the bias were further eliminated by subtracting a combined bias image, which was obtained separately for each night by stacking together at least 10 (overscan subtracted) bias frames. Dark current was not subtracted since its value is negligible ($(0.3-0.6) \times 10^{-3} \text{ ADU s}^{-1} \text{ pix}^{-1}$). The images were corrected for pixel-to-pixel variation of the quantum efficiency by dividing them with a twilight flat-field, obtained combining several tens of flat field exposures acquired throughout the different nights of each observing run. The presence of residual large-scale illumination inhomogeneities was removed with a super-flatfield obtained from the science exposures themselves, stacked together with a 3σ -clipping algorithm to remove all bright sources.

The *I*-band images were affected by fringing and required intermediate processing before deriving the super-flat images. All the bias-corrected and flat-fielded *I*-frames were combined to obtain an image of the fringing pattern. The large-scale features of the fringing image were removed by subtracting, from it, a smoothed version of itself; this produced the final fringe template, containing only the signal arising from the fringing itself. The fringing template was then subtracted from the science exposures with an interactive task, allowing us to verify the quality of the correction. These fringing-removed images were finally used to create the super-flatfield for the red filter.

Further reduction steps were made to correct for detector cosmetic effects, such as bad pixels, hot or dead columns. The five individual reduced images of each group in each filter were stacked together to obtain the final science images that we used in our analysis. From the large group frames we extracted postage stamp images for each of the galaxies, of size equal to 3 Petrosian radii. Sky subtraction was performed locally on the cleaned stamps, so as to account for small inhomogeneities in the sky level. Cleaning of the postage stamps involved removing most of the light coming from other galaxies (or from spurious stellar spikes and other contaminations), and substituting to the relevant pixels an iterated value of the average sky level in the stamp. Companion galaxies were identified using SExtractor as sources above 1.5σ of the sky level and the pixels belonging to these objects were replaced with random blank sky regions. All stamps were furthermore visually inspected to verify the quality of the cleaning process.

C.2. Photometric Calibration

Photometric calibration was performed using Landolt (Landolt 1992) standard stars. Several Landolt fields, with at least 5 standard stars, were observed for each night. Aperture magnitudes for these stars were measured with the IRAF task *qphot* and used to derive the photometric zero point (ZP) for the two pass bands.

We used the following calibration equations between the Landolt *B* and *I* and the WFI instrumental magnitudes *b*, *i*: $B = ZP_B + b + \alpha_B(B - V) - k_B X$ and $I = ZP_I + i + \alpha_I(V - I) - k_I X$, respectively. In these calibration equations *X* is the airmass value at the time of observation and *k* is the extinction coefficient. Zero points, color terms and extinction

¹³ IRAF is distributed by the National Optical Astronomy Observatories, which are operated by the Association of Universities

for Research in Astronomy, Inc., under cooperative agreement with the National Science Foundation.

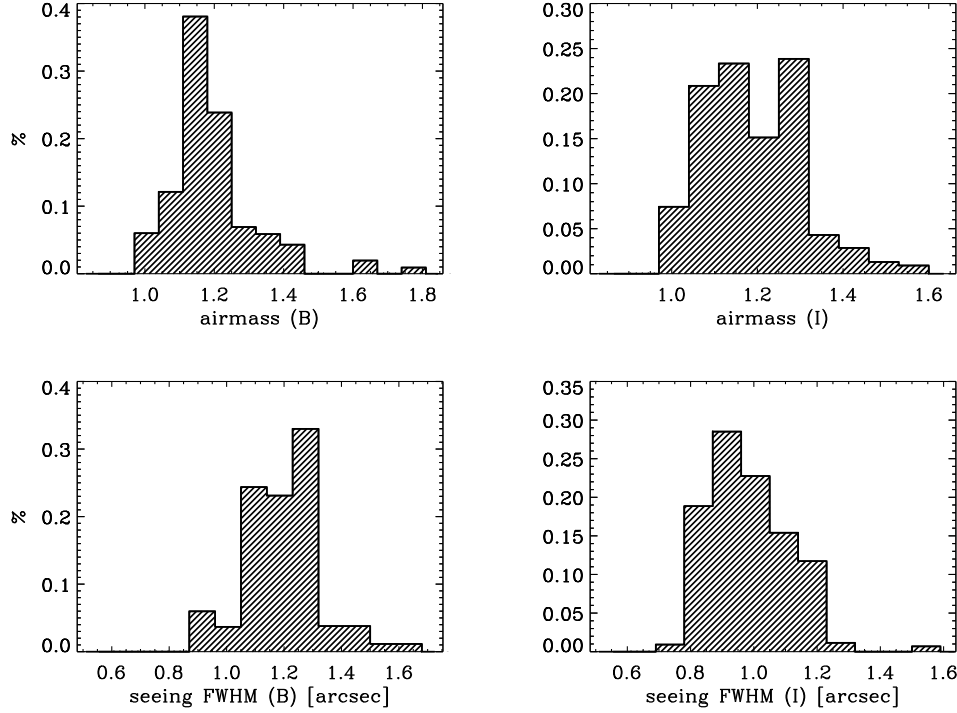


Figure C1. Summary of the observing conditions for the *ZENS* WFI data in the fields of the 79 first-epoch groups. Shown are the distribution of airmass and (instrumental plus atmospheric, i.e., total PSF) seeing values over the targeted fields, for the *B*- (left panels) and *I*-band (right panels), respectively.

coefficients are presented in Table C2. Since our standard stars were not observed at sufficiently differing airmasses to allow for a sensible extinction correction, magnitudes were airmass-corrected by using the extinction coefficients given on the WFI website¹⁴ as a reference. All magnitudes are calibrated onto an extra-atmospherical airmass of zero.

While there is no clear color dependence of the calibration for the *I* filter ($\alpha_I = 0$), it is necessary to correct for a color term ($\alpha_B = 0.215$) in the case of the *B* band. We also found that the ZP points themselves show a shift over the different observing runs, even though the slope of the calibration remains constant (most likely be due to different CCD/ambient conditions during the observations). For this reason, we calibrated each night separately, fixing the slope of the color contribution to the well-established common value for all the nights, while using the night-by-night determined ZPs for each set of observations.

Table C2
Zero points, color terms and extinction coefficients for the WFI B and I filters.

Run	Date	$ZP_B(AB)$	$ZP_I(AB)$	α_B	α_I	k_B	k_I
1	Jan. 5 - Feb. 18, 2005	24.75	23.74	0.215	0	0.22	0
3	May 1 - Dec. 23, 2006	24.75-25.08	23.74-24.0	0.215	0	0.22	0
2	Feb. 18 - July 14, 2007	24.85-24.96	23.81-23.90	0.215	0	0.22	0

Note. — The zero points (in the AB system and for magnitudes in ADUs, a term +0.75 must be added to convert to electrons) and other parameters for the photometric calibrations for those observing runs of Table C1 with finalized data reduction. For each run we list range of measured ZPs. The coefficients α are the color terms in the calibration equations. The airmass extinction coefficients k_B and k_I could not be derived from our own data as the acquired standard stars did not sample a sufficient range of zenith distances. For these quantities we used the latest measurements available on the WFI calibration web page.

The Landolt system is tied to the standard Johnson-Cousin system which uses Vega for reference; we thus converted our magnitudes to the AB system (Oke 1974) through the following procedure. For the B-band, we found the ZP corresponding to an object with zero color in AB in the $ZP - (B - V)$ relation, and used this value as our final calibration factor for the blue filter. As mentioned before, the color term was negligible for the *I* band and thus it was not possible to apply such method. In this case the following transformation was applied: $m_{AB} = m + m_{AB}(Vega)$. We computed the conversion factor using the SYNPHOT IRAF package (see also Fukugita et al. 1995) and found

¹⁴ <http://www.ls.eso.org/lasilla/sciops/2p2/E2p2M/WFI/zeropoints/>

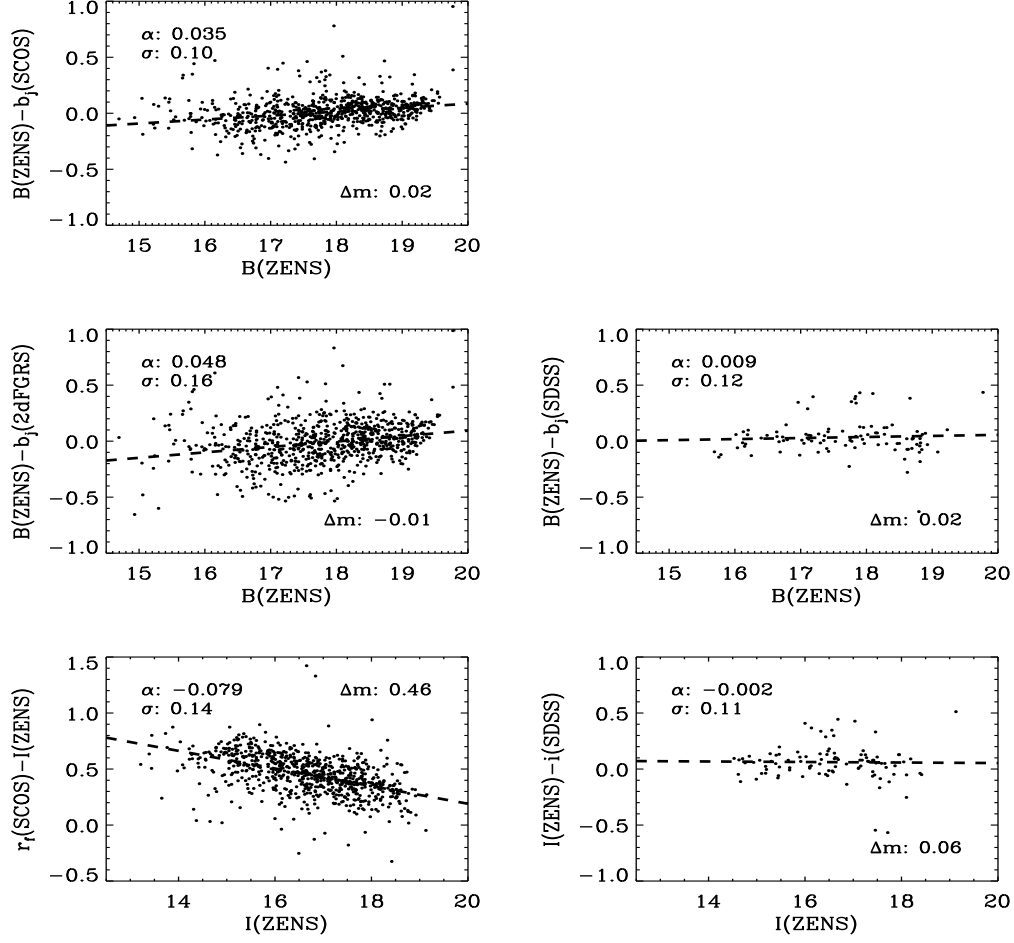


Figure C2. Accuracy of the *ZENS* WFI photometric calibration. Each panel shows the difference between the *ZENS* apparent magnitude in either the *B*- or *I*-band, and relevant magnitudes available from the literature: SuperCosmos Survey b_j , 2dFGRS b_j , SDSS-based b_j , SDSS i , SuperCosmos Survey r_F . The quantities α and σ are the slope of the best linear robust fit to the data and the dispersion around this relation, respectively. Δm is the median difference between each couple of measurements. All magnitudes are corrected for galactic extinction.

it to be $I_{AB}(Vega) = 0.45$. The values for the ZP we find are in good agreement with those reported on the WFI calibration web-page.

We assessed the robustness of our calibration by comparing the magnitudes obtained for (the stars in the *ZENS* fields, as well as for) the *ZENS* galaxies with the others available from the literature. For the *ZENS* galaxies we used the magnitudes obtained with the SExtractor (Source Extractor, Bertin & Arnouts 1996) software and determined from the flux curve of growth inside a Kron-like elliptical aperture (MAG_AUTO in the code). The Kron (1980) aperture radius correspond to 2.5 times the radius of the first image moment. All magnitudes are corrected for galactic absorption using the dust maps of Schlegel et al. (1998) and the Cardelli et al. (1989) dust law. As reference values we consider the 2dFGRS b_j , the SuperCosmos Survey b_j and r_F (Hambly et al. 2001) and the SDSS i and b_j magnitudes (Abazajian et al. 2009). The latter is derived as in Norberg et al. (2002) using the relation $b_j = g + 0.155 + 0.152 \times (g - r)$.

We show in Figure C2 the comparison between the derived *ZENS* magnitudes and the published ones. We have a good agreement with the SuperCosmos values (within a standard deviation of $\sigma = 0.1$ mag), which is better than with the 2dFGRS one ($\sigma = 0.16$ mag). This is very consistent with the quoted photometric errors of the 2dFGRS (b_j magnitudes, 0.15 mag) and SuperCosmos magnitudes (0.1 mag). We mention that our *B* measurements show a small non-linearity with respect to both the SuperCosmos data and 2dFGRS b_j magnitudes. This non-linearity is however absent when we compare with SDSS photometry, which is available for a subset of our galaxies. With the exception of the expected shift between the SuperCosmos r passband ($r_F(SCOS)$) and the *ZENS* *I* passband, the median magnitude offsets in the relevant comparisons are small at the level of $\sim 2\%$.

We remark that in deriving galaxy stellar masses and other photometry-inferred parameters in Paper III, the ZEBRA+ software was first run in “photometry-check mode”, to detect residual offsets from the individual passbands; no offsets were found for the WFI *B* and *I* passbands (see Paper III).

D. TEST ON THE ROBUSTNESS OF THE FIDUCIAL LSS DENSITY ESTIMATES

As discussed in Section 3.3, we adopted a *Nth*-nearest *group* neighbor algorithm to compute our fiducial LSS densities at the location of the *ZENS* fields. The volume-limited sample of 2PIGG *groups* used in the construction of the density field and the imposed minimum luminosity are plotted in Figure D1.

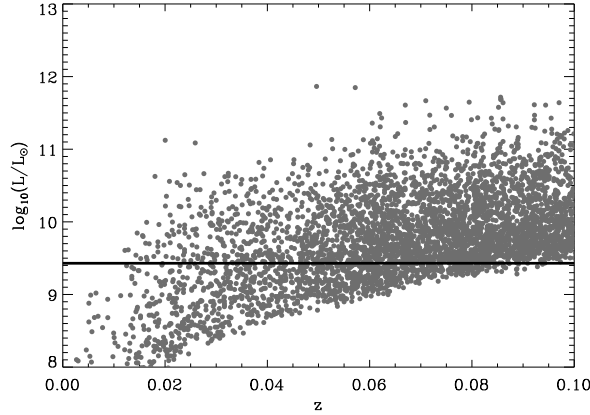


Figure D1. Luminosity of the 2PIGG groups and isolated galaxies used to derive the *Nth*–*group*–*neighbor* LSS density field (see Section 3.3). The solid line shows the minimum group luminosity considered in the computation, i.e., $L = 10^{9.43} L_{\odot}$; this corresponds to the total (i.e. integrated to zero) luminosity of a $b_j = 19.1$ individual galaxies at $z = 0.07$. Densities at each group location are calculated considering all other groups in the 2PIGG catalog, plus the remaining ‘isolated’ galaxies in the 2dFGRS, within a redshift range of $\Delta z = \pm 0.1$ from the given group. Only one every ten points is plotted for clarity.

D.1. The role of the isolated galaxies

As explained in the main text, we investigated whether the fiducial LSS density values for the *ZENS* groups are affected by the addition or removal of isolated galaxies in the 2dFGRS. This is shown in Figure D2. There is a good correlation between the two measurements of LSS density: in only $\sim 10\%$ of the cases the difference between the overdensities derived with and without the isolated galaxies is larger than 0.5 dex. We conclude that considering or neglecting the isolated galaxies does not alter significantly our LSS density measurements, and thus the trends with such density that we investigate in our study.

D.2. A comparison with standard *Nth* nearest galaxy neighbors density estimates

Many studies in the past few years have adopted a *Nth*-nearest *galaxy* neighbor approach to derive an estimate for the LSS density field. In our case, we opted instead for the use of the groups as the density tracers, rather than the galaxies, to avoid the drawback of switching from a density within the groups, for groups with richness $> N$, to a density outside of the groups, for groups with richness $< N$. We highlight below this shortfall of the *Nth*-nearest galaxy neighbor density field, which we also computed (but never used in our analyses, for the reason above).

Similarly to what is customarily done (e.g. Gómez et al. 2003; Balogh et al. 2004; Baldry et al. 2006; Kovač et al. 2010b), we computed the *Nth*-nearest *galaxy* field using a volume-limited sample of galaxies, in our case, with $M_{b_j} < -18.3 - z$ in the Vega system. This brightness limit corresponds to the absolute magnitude of a galaxy having a $b_j = 19.1$ at the maximum redshift of the *ZENS* sample. This was chosen such as to have a uniform depth/completeness over the bulk of the *ZENS* groups (see Figure A1), and yet to provide an adequate number of tracers. Neighbor galaxies were searched within a velocity range of $\pm 1000 \text{ km s}^{-1}$ centered at the given galaxy redshift; galaxies were weighted for spectroscopic incompleteness during the computation.

The distribution of typical distances to the *Nth* nearest galaxy neighbor, with $N=3, 5$ or 10 , is shown in the left panel of Figure D3. The distances to the 3rd and 5th nearest galaxy neighbors peak at $\sim 0.5 - 1 \text{ Mpc}$, a separation which is comparable to the typical radius of many of the *ZENS* groups. This is not surprising given that the *ZENS* groups have at least 5 members; at these distance scales, the *Nth* nearest galaxy neighbor density estimates mostly probe the variation of density within the group themselves. Also the 10th nearest galaxy neighbor densities, at high richness values, will probe the environment inside massive groups rather than be a genuine proxy for the LSS density field. We note that, given the luminosity limit discussed above to ensure a uniform completeness and depth, the density field that we calculate using the *Nth* nearest galaxy neighbor density field uses a sub-sample of the 2PIGG galaxies (and hence of the galaxies used for the definition of the *ZENS* groups). Thus, also for the *ZENS* groups with five members, a partial contamination from interlopers is in principle possible when using the 5th nearest galaxy neighbor approach. From the number of galaxies in the *ZENS* sample which are below the limit of $M_{b_j} < -18.3 - z$, we estimate this contamination to be about $20\% - 25\%$. The corresponding distributions of overdensities for the *Nth* nearest galaxy neighbor realizations with $N=3, 5$ or 10 , are shown in the right panel of Figure D3. As commented in the main text,

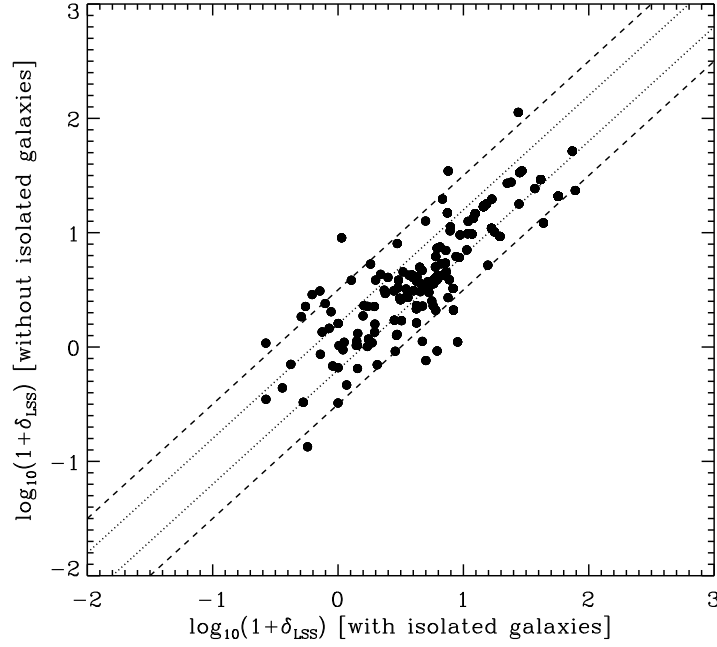


Figure D2. Comparison between the fiducial N th-group-neighbor LSS overdensities for the *ZENS* groups, and those obtained excluding the isolated galaxies in the 2dFGRS. Dotted and dashed lines highlight differences of 0.2 dex and 0.5 dex, respectively.

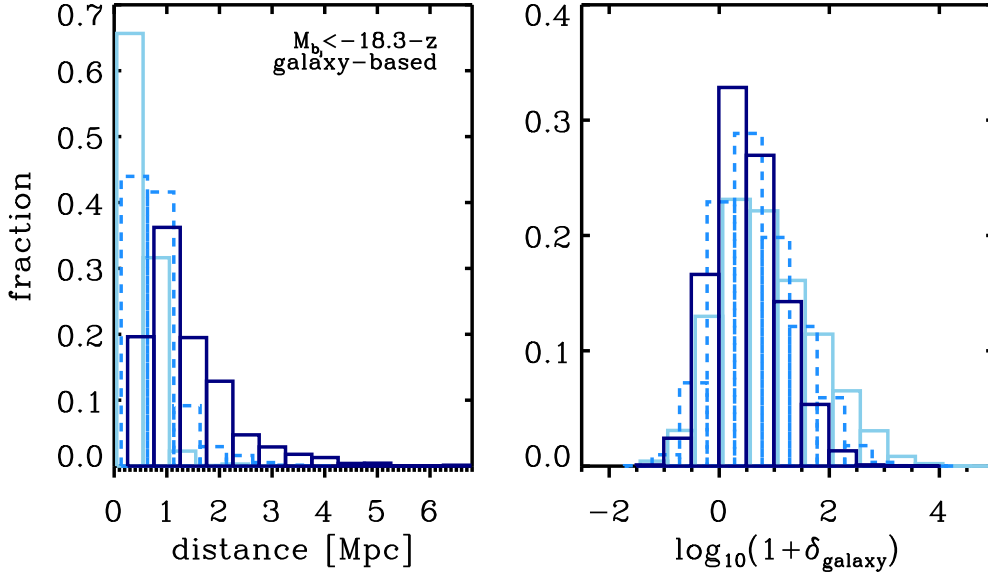


Figure D3. The distribution of distances (left) and densities (right) resulting from a 3rd (solid, light blue), 5th (dashed, blue) and 10th (solid, dark blue) nearest galaxy neighbor computation of the LSS field. We stress that we do not use these densities values in our analysis, since we prefer the adoption of our fiducial LSS density estimates that are based on using the groups instead than the galaxies as tracers of the LSS density field.

and as a consequence of galaxy-galaxy ‘clustering’ within the groups, a tail at high densities is observed, which is not present in our fiducial 5th nearest *group* neighbor computation of the LSS density field.

D.3. The negligible impact of the choice for N when using the groups as density tracers

In Figure D4 we show the comparison between the overdensities calculated using the distance to the third, fifth and tenth nearest neighbors. Upper and lower panels show respectively the density calculated using as tracers the volume

limited sample of $M_{bj} < -18.3 - z$ galaxies from the 2dFGRS and the densities obtained using as tracers the groups in the 2PIGG catalogue with $L > 10^{9.43} L_{\odot}$. The grey areas are the values for the all galaxies or groups in the 2dFGRS with $0.035 < z < 0.075$; the red contours are for the *ZENS* sample. In all cases the *ZENS* galaxies or groups are slightly shifted towards higher density, reflecting the selection of our *ZENS* sample. The figure shows (again) that the densities obtained with the volume limited sample of galaxies show an extended tail below the identity line at $\log(1 + \delta) \sim 2$, which is the signature that densities obtained with small apertures tend to be biased by local density peaks within halos. The Figure also shows that density estimates that use the groups to trace the potential are less sensitive to the choice of N than the estimates that use the galaxies.

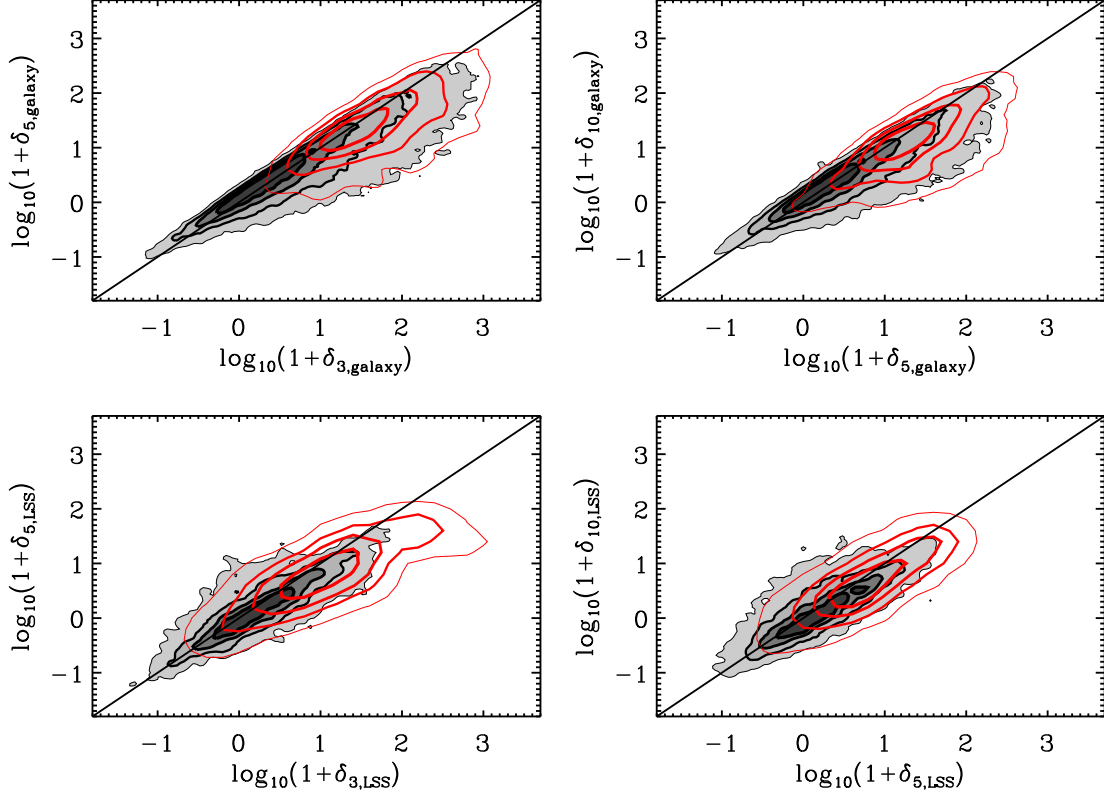


Figure D4. *Top:* Comparison between the overdensities calculated using the distance to the third (δ_3), fifth (δ_5) or tenth (δ_{10}) nearest neighbor. The upper panels are for the density calculated using as tracers the volume limited sample of galaxies from the 2dFGRS with $M_{bj} < -18.3 - z$; the lower panels show the densities obtained using the groups in the 2PIGG catalogue with $L > 10^{9.43} L_{\odot}$ as tracers. The grey areas are the values for the all galaxies or groups in the 2dFGRS with $0.035 < z < 0.075$; the red contours are for the *ZENS* sample.

E. THE README FILE OF THE ENCLOSED *ZENS* CATALOG

We finally list below, for each galaxy in the sample, the structural and photometric measurements presented in Paper II and III, and the environmental diagnostics discussed in this paper. Table E1 matches the *readme* file that accompanies the *ZENS* catalogue which we publish in this paper.

Table E1
The readme file for the *ZENS* catalog of structural, photometric and environmental properties for the sample galaxies

Column	Format	Units	Label	Comments
1	a11	–	GroupID	Group identification
2	a10	–	Gal2dFID	Galaxy 2dFGRS identification
3	a17	–	GalZENSID	Galaxy identification in ZENS
4	f7.5	–	groupz	Group redshift
5	f11.6	deg	RAdeg	RA in decimal degrees (J2000)
6	f11.6	deg	DEdeg	DEC in decimal degrees (J2000)
7	f7.5	–	galz	Galaxy 2dFGRS heliocentric redshift
8	f5.3	–	wComp	Galaxy completeness weight (1)

Table E1 — Continued

Column	Format	Units	Label	Comments
9	f5.3	Mpc	RmsRad	Group r.m.s. radius from 2PIGG catalog
10	f5.3	Mpc	R200	Group R_{200} radius (2)
11	f6.1	km/s	Sigma	Group velocity dispersion from 2PIGG catalog
12	e10.4	L_{\odot}	Lgroup	Group luminosity as in Eke et al. 2004
13	i3	—	Nmemb	Group richness from 2PIGG catalog
14	e10.4	M_{\odot}	Mgroup	Group mass M_{GROUP}
15	f6.3	—	DeltaLSS	Large scale overdensity δ_{LSS} (3)
16	i1	—	qLSS	Quartile large scale overdensity (4)
17	i1	—	relaxFlag	Group dynamical status (5)
18	i1	—	cenFlag	Flag identifying central galaxy and group center (6)
19	f6.3	R200	dR200	Galaxy distance from group center in units of R200
20	e11.4	M_{\odot}	MassBest	Galaxy mass from ZEBRA+ best-fit template (7)
21	e11.4	M_{\odot}	ll_MassBest	Lower limit on MassBest (8)
22	e11.4	M_{\odot}	ul_MassBest	Upper limit on MassBest (8)
23	e11.4	M_{\odot}	MassMedian	ZEBRA+ median likelihood galaxy mass
24	e11.4	M_{\odot}	MassP16	16th percent. of galaxy stellar mass likelihood distribution
25	e11.4	M_{\odot}	MassP84	84th percent. of galaxy stellar mass likelihood distribution
26	e11.4	M_{\odot}	maxLMass	ZEBRA+ maximum likelihood galaxy mass
27	i3	—	MType	Morphological type (9)
28	i3	—	MergerFlag	Merger flag (10)
29	f6.2	—	nI	Galaxy GIM2D I-band raw Sersic index
30	f6.2	—	le_nI	GIM2D formal 99% confidence lower error on nI
31	f6.2	—	ue_nI	GIM2D formal 99% confidence upper error on nI
32	f6.2	—	nB	Galaxy GIM2D B-band raw Sersic index
33	f6.2	—	le_nB	GIM2D formal 99% confidence lower error on nB
34	f6.2	—	ue_nB	GIM2D formal 99% confidence upper error on nB
35	f6.2	—	nICorr	Galaxy GIM2D I-band corrected Sersic index (11)
36	f6.2	—	nBCorr	Galaxy GIM2D B-band corrected Sersic index (11)
37	f7.3	kpc	gReI	Galaxy GIM2D I-band raw half-light semi-major axis
38	f7.3	kpc	le_gReI	GIM2D formal 99% confidence lower error on gReI
39	f7.3	kpc	ue_gReI	GIM2D formal 99% confidence upper error on gReI
40	f7.3	kpc	Delta_gReI	Single vs double component scatter on I-band half-light semi-major axis (12)
41	f7.3	kpc	gReB	Galaxy GIM2D B-band raw half-light semi-major axis
42	f7.3	kpc	le_gReB	GIM2D formal 99% confidence lower error on gReB
43	f7.3	kpc	ue_gReB	GIM2D formal 99% confidence upper error on gReB
44	f7.3	kpc	Delta_gReB	Single vs double component scatter on B-band half-light semi-major axis (12)
45	f7.3	kpc	gReICorr	Galaxy GIM2D I-band corrected half-light semi-major axis (11)
46	f7.3	kpc	gReBCorr	Galaxy GIM2D B-band corrected half-light semi-major axis (11)
47	f7.3	—	gEllipI	Galaxy GIM2D I-band raw ellipticity
48	f7.3	—	le_gEllipI	GIM2D formal 99% confidence lower error on gEllipI
49	f7.3	—	ue_gEllipI	GIM2D formal 99% confidence upper error on gEllipI
50	f7.3	—	gEllipB	Galaxy GIM2D B-band raw ellipticity
51	f7.3	—	le_gEllipB	GIM2D formal 99% confidence lower error on gEllipB
52	f7.3	—	ue_gEllipB	GIM2D formal 99% confidence upper error on gEllipB
53	f7.3	—	gEllipICorr	Galaxy GIM2D I-band corrected ellipticity (11)
54	f7.3	—	gEllipBCorr	Galaxy GIM2D B-band corrected ellipticity (11)
55	f7.3	kpc	diskhI_tot	Galaxy GIM2D I-band pure exponential disk scale-length (semi-major axis) (13)
56	f7.3	kpc	le_diskhI_tot	GIM2D formal 99% confidence lower error on diskhI_tot
57	f7.3	kpc	ue_diskhI_tot	GIM2D formal 99% confidence upper error on diskhI_tot
58	f7.3	kpc	diskhB_tot	Galaxy GIM2D B-band pure exponential disk scale-length (semi-major axis) (13)
59	f7.3	kpc	le_diskhB_tot	GIM2D formal 99% confidence lower error on diskhB_tot
60	f7.3	kpc	ue_diskhB_tot	GIM2D formal 99% confidence upper error on diskhB_tot
61	i3	—	tDecompI	GIM2D vs. Galfit Flag for I-band decomposition (14)
62	i3	—	tDecompB	GIM2D vs. Galfit Flag for B-band decomposition (14)
63	f8.4	—	BTI	I-band bulge-to-total ratio (15)
64	f8.4	—	le_BTI	Formal 99% confidence lower error on BTI
65	f8.4	—	ue_BTI	Formal 99% confidence upper error on BTI
66	f8.4	—	BTB	B-band bulge-to-total ratio (15)
67	f8.4	—	le_BT B	Formal 99% confidence lower error on BTB
68	f8.4	—	ue_BT B	Formal 99% confidence upper error on BTB
69	f7.3	kpc	bulgeRe_I	I-band bulge half-light semi-major axis (15)
70	f7.3	kpc	le_bulgeRe_I	Formal 99% confidence lower error on bulgeRe_I
71	f7.3	kpc	ue_bulgeRe_I	Formal 99% confidence upper error on bulgeRe_I
72	f7.3	kpc	bulgeRe_B	B-band bulge half-light semi-major axis (15)
73	f7.3	kpc	le_bulgeRe_B	Formal 99% confidence lower error on bulgeRe_B
74	f7.3	kpc	ue_bulgeRe_B	Formal 99% confidence upper error on bulgeRe_B
75	f7.3	kpc	diskh_I	I-band disk scale-length (semi-major axis) (15)
76	f7.3	kpc	le_diskh_I	Formal 99% confidence lower error on diskh_I
77	f7.3	kpc	ue_diskh_I	Formal 99% confidence upper error on diskh_I
78	f7.3	kpc	diskh_B	B-band disk scale-length (semi-major axis) (15)
79	f7.3	kpc	le_diskh_B	Formal 99% confidence lower error on diskh_B
80	f7.3	kpc	ue_diskh_B	Formal 99% confidence upper error on diskh_B
81	f7.3	—	nBulge_I	I-band bulge Sersic index (15)
82	f7.3	—	le_nBulge_I	Formal 99% confidence lower error on nBulge_I
83	f7.3	—	ue_nBulge_I	Formal 99% confidence upper error on nBulge_I
84	f7.3	—	nBulge_B	B-band bulge Sersic index (15)

Table E1 — *Continued*

Column	Format	Units	Label	Comments
85	f7.3	–	le_nBulge_B	Formal 99% confidence lower error on nBulge_B
86	f7.3	–	ue_nBulge_B	Formal 99% confidence upper error on nBulge_B
87	f7.3	–	ellBulge_I	I-band bulge ellipticity (15)
88	f7.3	–	le_ellBulge_I	Formal 99% confidence lower error on ellBulge_I
89	f7.3	–	ue_ellBulge_I	Formal 99% confidence upper error on ellBulge_I
90	f7.3	–	ellBulge_B	B-band bulge ellipticity (15)
91	f7.3	–	le_ellBulge_B	Formal 99% confidence lower error on ellBulge_B
92	f7.3	–	ue_ellBulge_B	Formal 99% confidence upper error on ellBulge_B
93	f7.3	deg	diskInclination_I	I-band disk inclination (15)
94	f7.3	deg	le_diskInclination_I	Formal 99% confidence lower error on diskInclination_I
95	f7.3	deg	ue_diskInclination_I	Formal 99% confidence upper error on diskInclination_I
96	f7.3	deg	diskInclination_B	B-band disk inclination (15)
97	f7.3	deg	le_diskInclination_B	Formal 99% confidence lower error on diskInclination_B
98	f7.3	deg	ue_diskInclination_B	Formal 99% confidence upper error on diskInclination_B
99	f7.3	kpc	ReI_decomp	I-band global galaxy half-light semi-major axis from bulge+disk decomposition (16)
100	f7.3	kpc	ReB_decomp	B-band global galaxy half-light semi-major axis from bulge+disk decomposition (16)
101	f7.3	kpc	zReI	ZEST+ I-band raw half-light semi-major axis
102	f7.3	kpc	zReB	ZEST+ B-band raw half-light semi-major axis
103	f7.3	kpc	zReIcorr	ZEST+ I-band corrected half-light semi-major axis (11)
104	f7.3	kpc	zReBcorr	ZEST+ B-band corrected half-light semi-major axis (11)
105	f7.3	–	zEllipI	SEXTRACTOR/ZEST+ I-band raw ellipticity
106	f7.3	–	zEllipB	SEXTRACTOR/ZEST+ B-band raw ellipticity
107	f7.3	–	zEllipIcorr	SEXTRACTOR/ZEST+ I-band corrected ellipticity (11)
108	f7.3	–	zEllipBcorr	SEXTRACTOR/ZEST+ B-band corrected ellipticity (11)
109	f6.2	–	CI	ZEST+ I-band raw Concentration index
110	f6.2	–	CB	ZEST+ B-band raw Concentration index
111	f6.2	–	CIcorr	ZEST+ I-band corrected Concentration index (17)
112	f6.2	–	CBcorr	ZEST+ B-band corrected Concentration index (17)
113	f6.2	–	GiniI	ZEST+ I-band raw Gini index
114	f6.2	–	GiniB	ZEST+ B-band raw Gini index
115	f6.2	–	GiniIcorr	ZEST+ I-band corrected Gini index (17)
116	f6.2	–	GiniBcorr	ZEST+ B-band corrected Gini index (17)
117	f6.2	–	M20I	ZEST+ I-band raw M_{20} index
118	f6.2	–	M20B	ZEST+ B-band raw M_{20} index
119	f6.2	–	M20Icorr	ZEST+ I-band corrected M_{20} index (17)
120	f6.2	–	M20Bcorr	ZEST+ B-band corrected M_{20} index (17)
121	f8.4	–	AsymI	ZEST+ I-band raw asymmetry index
122	f8.4	–	AsymB	ZEST+ B-band raw asymmetry index
123	f8.4	–	SI	ZEST+ I-band raw smoothness index
124	f8.4	–	SB	ZEST+ B-band raw smoothness index
125	f7.3	kpc	RpI	SEXTRACTOR I-Band petrosian radius (semi-major axis) (18)
126	f7.3	kpc	RpB	SEXTRACTOR B-Band petrosian radius (semi-major axis) (18)
127	f7.3	kpc	RkI	SEXTRACTOR I-band Kron aperture (semi-major axis) (19)
128	f7.3	kpc	RkB	SEXTRACTOR B-band Kron aperture (semi-major axis) (19)
129	i3	–	BarType	Bar Flag (20)
130	f7.3	kpc	aBar	Bar semi-major axis
131	f6.2	–	fBar	Bar strength
132	i3	–	SpType	Spectral type (21)
133	i3	–	DustFlag	Dusty, star-forming flag (22)
134	f8.4	M_{\odot}/yr	SFRBest	Star-formation rate from ZEBRA+ best-fit template (23)
135	f8.4	M_{\odot}/yr	llSFRBest	Lower limit on SFRBest (8)
136	f8.4	M_{\odot}/yr	ulSFRBest	Upper limit on SFRBest (8)
137	f8.4	M_{\odot}/yr	SFRMedian	ZEBRA+ median likelihood SFR
138	f8.4	M_{\odot}/yr	SFRP16	16th percentile of the ZEBRA+ SFR likelihood distribution
139	f8.4	M_{\odot}/yr	SFRP84	84th percentile of the ZEBRA+ SFR likelihood distribution
140	f8.4	M_{\odot}/yr	maxLSFR	ZEBRA+ maximum likelihood SFR
141	e11.4	yr^{-1}	sSFRBest	Specific star-formation rate from ZEBRA+ best-fit template (23)
142	e11.4	yr^{-1}	llsSFRBest	Lower limit on sSFRBest (8)
143	e11.4	yr^{-1}	ulsSFRBest	Upper limit on sSFRBest (8)
144	e11.4	yr^{-1}	sSFRMedian	ZEBRA+ median likelihood specific star-formation rate
145	e11.4	yr^{-1}	sSFRP16	16th percentile of the ZEBRA+ sSFR likelihood distribution
146	e11.4	yr^{-1}	sSFRP84	84th percentile of the ZEBRA+ sSFR likelihood distribution
147	e11.4	yr^{-1}	maxLSsSFR	ZEBRA+ maximum likelihood sSFR
148	f8.4	mag	kcorr-B	ZEBRA+ B-band k-correction
149	f8.4	mag	kcorr-I	ZEBRA+ I-band k-correction
150	f8.3	mag	oBmag	Galaxy Petrosian apparent B-band magnitude (observer-frame) (24)
151	f8.3	mag	rBmag	Galaxy Petrosian apparent B-band magnitude (rest-frame) (24)
152	f8.3	mag	e_rBmag	Error on rBmag
153	f8.3	mag	BMag	Absolute galaxy petrosian B-band magnitude
154	f8.3	mag	oImag	Galaxy Petrosian apparent I-band magnitude (observer-frame) (24)
155	f8.3	mag	rImag	Galaxy Petrosian apparent I-band magnitude (rest-frame) (24)
156	f8.3	mag	e_rImag	Error on rImag
157	f8.3	mag	IMag	Absolute galaxy Petrosian I-band magnitude
158	f8.3	mag	BmagKron	Galaxy Kron apparent B-band magnitude (rest-frame) (25)
159	f8.3	mag	e_BmagKron	Error on BmagKron

Table E1 — *Continued*

Column	Format	Units	Label	Comments
160	f8.3	mag	ImagKron	Galaxy Kron apparent I-band magnitude (rest-frame) (25)
161	f8.3	mag	e.ImagKron	Error on ImagKron
162	f8.3	mag	B-I	Galaxy Petrosian rest-frame (B-I) color
163	f8.3	mag	b_j	Galaxy 2dFGRS b_j magnitude (Vega) (26)
164	f8.3	mag	r_F	Galaxy 2dFGRS/SCOS r_F magnitude (Vega) (26)
165	f8.3	mag	FUVmag	Galaxy apparent FUV magnitude (rest-frame) (24,27)
166	f8.3	mag	e.FUVmag	Error on FUVmag
167	f8.3	mag	NUVmag	Galaxy apparent NUV magnitude (rest-frame) (24,27)
168	f8.3	mag	e.NUVmag	Error on NUVmag
169	f8.3	mag	NUV-I	NUV-I color (rest-frame)
170	f8.3	mag	NUV-B	NUV-B color (rest-frame)
171	f8.3	mag	FUV-NUV	FUV-NUV color (rest-frame)
172	f8.3	mag	umag	Galaxy apparent SDSS u magnitude (rest-frame) (24,27)
173	f8.3	mag	e.umag	Error on umag
174	f8.3	mag	gmag	Galaxy apparent SDSS g magnitude (rest-frame) (24,27)
175	f8.3	mag	e.gmag	Error on gmag
176	f8.3	mag	rmag	Galaxy apparent SDSS r-magnitude (rest-frame) (24,27)
177	f8.3	mag	e.rmag	Error on rmag
178	f8.3	mag	imag	Galaxy apparent SDSS i-magnitude (rest-frame) (24,27)
179	f8.3	mag	e.imag	Error on imag
180	f8.3	mag	zmag	Galaxy apparent SDSS z-magnitude (rest-frame) (24,27)
181	f8.3	mag	e.zmag	Error on zmag
182	f8.3	mag	Jmag	Galaxy apparent 2MASS J-magnitude (rest-frame) (24,27)
183	f8.3	mag	e.Jmag	Error on Jmag
184	f8.3	mag	Hmag	Galaxy apparent 2MASS H-magnitude (rest-frame) (24,27)
185	f8.3	mag	e.Hmag	Error on Hmag
186	f8.3	mag	Kmag	Galaxy apparent 2MASS K-magnitude (rest-frame) (24,27)
187	f8.3	mag	e.Kmag	Error on Kmag
188	f7.3	mag	BmagSer	Total galaxy B-band magnitude from GIM2D Sersic fit (rest-frame)
189	f7.3	mag	le_BmagSer	GIM2D formal 99% confidence lower error on BmagSer
190	f7.3	mag	ue_BmagSer	GIM2D formal 99% confidence upper error on BmagSer
191	f7.3	mag	ImagSer	Total galaxy I-band magnitude from GIM2D Sersic fit (rest-frame)
192	f7.3	mag	le_ImagSer	GIM2D formal 99% confidence lower error on ImagSer
193	f7.3	mag	ue_ImagSer	GIM2D formal 99% confidence upper error on ImagSer
194	f7.3	mag	BmagSer_corr	Corrected total galaxy B mag from single Sersic fit (rest-frame)
195	f7.3	mag	ImagSer_corr	Corrected total galaxy I mag from single Sersic fit (rest-frame)
196	f7.3	mag	BmagExp	Total galaxy B-band magnitude from GIM2D pure exponential fit (rest-frame)
197	f7.3	mag	le_BmagExp	GIM2D formal 99% confidence lower error on BmagExp
198	f7.3	mag	ue_BmagExp	GIM2D formal 99% confidence upper error on BmagExp
199	f7.3	mag	ImagExp	Total galaxy I-band magnitude from GIM2D pure exponential fit (rest-frame)
200	f7.3	mag	le_ImagExp	GIM2D formal 99% confidence lower error on ImagExp
201	f7.3	mag	ue_ImagExp	GIM2D formal 99% confidence upper error on ImagExp
202	f7.3	mag	oBmagBulge	Bulge observer-frame B-band magnitude
203	f7.3	mag	le_oBmagBulge	Formal 99% confidence lower error on oBmagBulge (28)
204	f7.3	mag	ue_oBmagBulge	Formal 99% confidence upper error on oBmagBulge (28)
205	f7.3	mag	oImagBulge	Bulge observer-frame I-band magnitude
206	f7.3	mag	le_oImagBulge	Formal 99% confidence lower error on oImagBulge (28)
207	f7.3	mag	ue_oImagBulge	Formal 99% confidence upper error on oImagBulge (28)
208	f7.3	mag	rBmagBulge	Bulge rest-frame B-band magnitude (29)
209	f7.3	mag	rImagBulge	Bulge rest-frame I-band magnitude (29)
210	f7.3	mag	oBmagDisk	Disk observer-frame B-band magnitude
211	f7.3	mag	le_oBmagDisk	Formal 99% confidence lower error on oBmagDisk (28)
212	f7.3	mag	ue_oBmagDisk	Formal 99% confidence upper error on oBmagDisk (28)
213	f7.3	mag	oImagDisk	Disk observer-frame I-band magnitude
214	f7.3	mag	le_oImagDisk	Formal 99% confidence lower error on oImagDisk (28)
215	f7.3	mag	ue_oImagDisk	Formal 99% confidence upper error on oImagDisk (28)
216	f7.3	mag	rBmagDisk	Disk rest-frame B-band magnitude (29)
217	f7.3	mag	rImagDisk	Disk rest-frame I-band magnitude (29)
218	e11.4	M_\odot	BulgeMass	Bulge stellar mass (30)
219	e11.4	M_\odot	BulgeMassP16	16th percentile bulge mass (30)
220	e11.4	M_\odot	BulgeMassP84	84th percentile bulge mass (30)
221	e11.4	M_\odot	DiskMass	Disk stellar mass (30)
222	e11.4	M_\odot	DiskMassP16	16th percentile disk mass (30)
223	e11.4	M_\odot	DiskMassP84	84th percentile disk mass (30)
224	f7.3	mag	d(B-I)/dlogr_v	(B-I) color gradient from Voronoi tessellated color maps
225	f7.3	mag	e.d(B-I)/dlogr_v	Error on (B-I)grad.v
226	f7.3	mag	corr_d(B-I)/dlogr_v	Corrected (B-I) color gradient from Voronoi tessellated color maps (31)
227	f7.3	mag	(B-I)Re_v	(B-I) color at half-light radius from Voronoi tessellated color maps (rest-frame)
228	f7.3	mag	e.(B-I)Re_v	Error on (B-I)Re.v (32)
229	f7.3	mag	corr(B-I)Re_v	Corrected (B-I) color at $r_{1/2}$ from Voronoi color maps (rest-frame) (31)
230	f7.3	mag	(B-I)rms	Dispersion around best fit color profile from Voronoi color maps
231	f7.3	mag	d(B-I)/dlogr_g	(B-I) color gradient from GIM2D best fits
232	f7.3	mag	e.d(B-I)/dlogr_g	Error on (B-I)grad.g
233	f7.3	mag	(B-I)Re_g	(B-I) color at half-light radius from GIM2D best fits (rest-frame)
234	f7.3	mag	e.(B-I)Re_g	Error on (B-I)Re.g (33)

Table E1 — *Continued*

Column	Format	Units	Label	Comments
235	e11.4	M_{\odot}	FlagBadSFR	Flag for ZEBRA+ template limited to a star forming model (34)
236	i3	—	cFlag	Contamination flag (35)

Note (0): Projected sizes are converted into physical units assuming the following cosmological parameters: $h=0.7$, $\Omega_m=0.3$, $\Omega_{\Lambda}=0.7$. Parameters which are not available are listed as: -99 entries for definite positive parameters, and +99 for definite negative parameters. For merging galaxy pairs we list parameters for both the primary and secondary galaxy, when available. Unless specified differently, all magnitudes and colors are in the AB system. For galaxies out of the WFI FOV all galactic parameters, except the stellar masses, are given as -99 entries.

Note (1): Galaxy weight accounting for 2dFGRS redshift incompleteness calculated as described in Section A.

Note (2): R_{200} akin radius, derived from the group mass (see text)

Note (3): Defined as $\log(1 + \delta_{LSS})$ where δ_{LSS} is calculated to the fifth nearest 2PIGG group (see text).

Note (4): 1=group located in first quartile of the distribution of $\log(1 + \delta_{LSS})$; 2=second quartile; 3=third quartile; 4=fourth quartile.

Note (5): 0=relaxed, nominal best-fit most massive galaxy is identified as “central” (and group center); 1=relaxed, central galaxy satisfying criteria of Section 3.2.1 is identified, but it is not the nominal best-fit most massive galaxy; 2=unrelaxed, no galaxy in the group satisfies the criteria of Section 3.2.1 to be a central, but nevertheless the nominal best-fit most massive galaxy is labelled as “central” and used as the group center.

Note (6): 0=satellite, 1=central.

Note (7): For galaxies out of the WFI FOV the masses are inferred from the mass vs r_F magnitude relation as described in text

Note (8): Lower and upper limits corresponding to an increase of 50% of the best-fit χ^2 , derived from the distribution of χ^2 for all templates used in the ZEBRA+ SED fitting.

Note (9): 0=elliptical; 1=S0; 2=bulge-dominated spiral; 3=intermediate disk; 4=late-type disk; 5=Irregular

Note (10): 1=merger; 0=not merging.

Note (11): the parameter is corrected for observational biases as described in Paper II.

Note (12): Together with the formal GIM2D errors we also provide an additional error which is obtained by the half difference between the single and double component half-light radii.

Note (13): Disk scale length from pure exponential GIM2D fit for the entire galaxy. This scale length is only available for late type disks (Mtype=4).

Note (14): 0=GIM2D; 1=GALFIT. This is due to the fact that GIM2D failed to provide some decompositions, which were successfully re-computed using the GALFIT software package.

Note (15): -99 if no reliable decomposition is available or galaxy is a single-component structure with elliptical morphology and Sérsic index $n > 3$; -98 if galaxy has a late-type morphology and is described by a single component Sérsic fit with $n < 1.5$.

Note (16): Obtained by integration to infinity of the bulge+disk surface brightness profiles

Note (17): Non parametric structural index corrected for PSF and observational biases as described in Paper II.

Note (18): This is the actual Petrosian radius, not the default SEXTRACTOR Petrosian aperture which is 2.5 the Petrosian radius.

Note (19): Default SEXTRACTOR Kron aperture equal to 2.5 times R_{Kron}

Note (20): 0=not barred, 1=barred.

Note (21): 0=quiescent, 1=moderately star-forming, 2=strongly star-forming.

Note (22): 0=the galaxy has an strongly star-forming spectrum and satisfies color-color criteria (see Paper III); 1=the galaxy has an actively star-forming spectrum but has red optical-UV colors (see Paper III)

Note (23): The SSFR for galaxies for which the best fit SED result in a $SFR < 10^{-4} M_{\odot} \text{yr}^{-1}$ is set equal to $sSFR=10^{-14} \text{yr}^{-1}$. Likewise $SFR < 10^{-4} M_{\odot} \text{yr}^{-1}$ are set to $SFR=10^{-4} M_{\odot} \text{yr}^{-1}$.

Note (24): Magnitude computed in an elliptical aperture equal to 2 times the Petrosian radius. This data is used in the derivation of stellar masses.

Note (25): Sextractor MAG_AUTO

Note (26): These are the original b_j and r_F magnitudes, as released by the 2dFGRS team. The b_j magnitude is corrected for galactic extinction, but is not at the rest-frame. The r_F is not corrected for galactic extinction and is not at the rest-frame. Both the r_F and b_j magnitudes are in the Vega system.

Note (27): 999=undetected, -99= not available.

Note (28): Sum in quadrature of the magnitude errors deriving from the formal GIM2D uncertainty on the flux and on the bulge-to-total ratio. Bulge lower magnitudes errors are set to 99 if $\text{le_BT}=0$. Disk upper magnitudes errors are set to 99 if $\text{ue_BT}=1$.

Note (29): For the bulge and disk components the k-corrections are obtained from the observed colors and the relation between the k-correction and color as derived for the entire galaxies (see Paper III).

Note (30): -99 if no reliable B+D decompositions are available in both B - and I -band or color cannot be reproduced by synthetic spectral library.

Note (31): color gradients and color at the half-light radius corrected for observational biases as described in Paper III.

Note (32): This error reflects the S/N ratio obtained in the Voronoi bins at the galaxy half-light radius. It is set to 99 if tessellated map does not reach the half-light radius.

Note (33): Quadratic sum of the B -, I -surface brightnesses errors on a single pixel at the galaxy half-light radius. It is set to 99 if surface brightness in one of the two bands is below rms value of the sky.

Note (34): For a few galaxies classified as moderately- or strongly star-forming from their spectral features or location on the NUV-optical color-color diagram, the unconstrained ZEBRA+ fits give inconsistently low SFR and sSFR values. For these galaxies ZEBRA+ was re-run imposing a star-forming template model. The flag in this column identifies such galaxies and is set equal to the “incorrect” galaxy stellar mass from the unconstrained ZEBRA+ fits for the re-fitted galaxies, and to -99 for all other galaxies (see Paper III for details).

Note (35): 1=no bright star/companion within Petrosian radius; 1=galaxy lies close to a bright star, the parameters for this galaxy may be subject to large uncertainties; 2=companion within the galaxy Petrosian radius; 3=bright clump/star-clusters within Petrosian radius.